Design and Synthesis of Fluorogenic and Chromogenic Probes for the Detection of Ionic Guests in Solution and Biological Medium

A Dissertation

Submitted in partial fulfillment for the degree of

Doctor of Philosophy

Barun Kumar Datta

(Roll No. 11612226)

Thesis Supervisor: Prof. Gopal Das

Department of Chemistry

Indian Institute of Technology Guwahati

Assam-781039, India

Dedicated to

my parents

INDIAN INSTITUTE OF TECHNOLOGY GUWAHATI

Department of Chemistry

STATEMENT

I do hereby declare that the matter embodied in this thesis is the result of investigations carried out by me in the Department of Chemistry, Indian Institute of Technology Guwahati, India, under the guidance of Prof. Gopal Das, Department of Chemistry, Indian Institute of Technology Guwahati, India.

In keeping with the general practice of reporting scientific observations, due acknowledgements have been made wherever this work is based on the findings of other investigators.

2nd February, 2016
IIT Guwahati

Barun Kumar Datta

INDIAN INSTITUTE OF TECHNOLOGY GUWAHATI

Department of Chemistry

CERTIFICATE

This is to certify that Mr. Barun Kumar Datta has been working under my supervision since January, 20011 as a regular registered Ph. D. student. His thesis entitled **"Design and synthesis of Fluorogenic and Chromogenic probes for the Detection of Ionic Guests in Solution and Biological medium"** is authentic record of the results obtained from the research work carried out under my supervision in the Department of Chemistry, Indian Institute of Technology Guwahati, Assam, India. I am forwarding his thesis to submit for the award of degree of Doctor of Philosophy, from this institute. I hereby certify that he has fulfilled all the requirements, according to the rules of this institute regarding the investigations embodied in his thesis and this work has not been submitted elsewhere for a degree.

Prof. Gopal Das
(Thesis Supervisor)
Professor
Department of Chemistry
IIT Guwahati
Assam - 781039, India

Acknowledgement

At this final stage of truly memorable journey towards my intellectual destination, it is really hard to list all the people who sincerely helped me and I would like to thank all of them who have made this thesis possible. I would like to express my deepest gratitude to my father Biswanath Datta and mother Pratima Datta, two people with irrational and unbreakable belief on me. Their unconditional love and support made me reach this stage of my life. I am highly indebted to my thesis supervisor Prof. Gopal Das for his kind support, insightful advice and encouragement. I earnestly thank him for his nice guidance, freedom to work, encouragement and inspiration which helped me to enrich myself.

Besides my supervisor, I would also like to give sincere gratitude to my doctoral committee members, Dr. Lal Mohan Kundu, Dr. Sandip Paul and Dr. Subhash Pan for their advices and valuable suggestions. I shall always be obliged to Prof. Aiyagari Ramesh for his admirable support throughout my research work. I also wish to thank staff members of chemistry department. I would also thank Dr. BLD for the help he has rendered through these years. My sincere thanks to the staffs of central instrument facility, for their help and in hand guidance to several analytical instruments, required during my research work.

Alongside I have always felt lucky that I got wonderful seniors like Bedo da, Sandeep da, Arghya da, Chirantan da, Jiban da and extraordinary associates like Md Najbul, Romen, Abhijit, Barun, Soham, Nilotpal, Rupinder, Utsab, Biswajit and Madhurima. It was great to work and spend times with these interesting human beings and I will always cherish the memories of their jokes, laughter and humor throughout my life. My days in these few years never started without having the morning tea with you people, you are real friends and fellow warrior. Keep up the fight. I am always a phone call away. I shall always be obliged to Arghya da and Chirantan da, they were my guru and comrade who taught me the basics of lab techniques, without your support I would have given this up a long time ago.

I also owe my obligations to my other seniors, batch mate and juniors of PhD fraternity of chemistry department for their help and support.

I take this opportunity to thank my Lab members and friends, Bedo da, Bimlesh da, Sandeep da, Arghya da, Jiban, Chirantan da, Najbul, Romen, Abhijit, Soham, Nilotpal, Rupinder, Utsab, Biswajit and Madhurima for their co-operation and inspiration in my research work, without which it would not been easy to complete the PhD thesis. It was great to work and spend times with these interesting human beings and I will always cherish the memories of their jokes, laughter and humor throughout my life. I wish them great success in every aspects of their life.

I also owe my obligations to my other seniors, batch mates and juniors of PhD fraternity of the chemistry department for their help and support.

In context to the thesis work, I had opportunity to mingle with friends of Biosciences & Bioengineering, IIT Guwahati. I owe my gratitude to Manab da, Thiyagaranjan, Sandipan for their unconditional support and all the help they extended from time to time whenever required.

I take this opportunity to thank my friend Ashraful, Chanky, Anupam (mole), Param, Partha, Arnab, Somnath, Sudip, kaka, Vaipo, Satavisha, Gora, Tapas, Sanjib, Arpan, Ashta, Mainak and all others for

being a source of my encouragement and love through this time. Also big thanks to Samir, Utpal, Soumendra, for supporting me in countless occasions. I would also like to thank Chandani di and Moumita di (IIT Kharagpur) for their assistance and well-wishing.

No words would suffice to express my feelings for my teachers to whom I owe debt for their kindness and benevolence; Nimai babu, Sisir babu, Manas babu, Subhasis Babu and kakima, Ashis babu, Asim Basu, Arin sir, Kallol babu, Bhakta Babu, Anup sir, Rupendu sir, Mahadev sir, Goda da, kali da, Sushovan da, Deba da, krishno da, and many others from my school, college and university who gave me the direction and insightful informations to march forward in this field. I have the rare opportunity to come in touch with some extraordinary personalities like Pranab da, Asim Da, Gourav da, Pranesh da, Bidhan da, Uday da, Alaka da and the Visva-bharati fraternity. They are so humble, so kind, so helpful, so inspirational that sometimes we felt ashamed of our own behavior. It's unbelievable to expect that kind of humble behavior from a professor.

Finally, I would like to thank the Microsoft Corporation for presenting the MS word, from grammar check to synonyms, from equation to symbols without this software, the thesis would have taken another five years.

Still many names are missing whose contribution and help is worth mentioning.

Barun

Synopsis

The contents of this thesis entitled "**Design and synthesis of Fluorogenic and Chromogenic probes for the Detection of Ionic Guests in Solution and Biological medium**" have been divided into six chapters based on the results of experimental work performed during the research period.

Chapter 1: Introduction

Ionic species especially metal ions and anions have immense importance in chemistry, biology and environment. In the last few decades selective and specific detection of those ionic species has become a significant field in chemistry and biochemistry. There is a great demand for the development of selective, sensitive and easy techniques to detect biologically and environmentally important ions. Sensing of target ions by chromogenic and florigenic probes have been established as a prominent technique among other methods. Optical chemosensors are becoming popular increasingly due to their ability to work in a relaxed condition, high sensitivity, and low detection limit. A chemosensor with fluorescence turn ON/OFF response upon interaction with ionic guests is of immense importance. Hence, designing of selective chemosensor is of paramount importance. Chemosensors which can work in aqueous medium or in physiological condition are even better than those who have the limitation of performing in physiological condition, as these probes can be applied for biological studies. Thus, the development of new small organic sensor molecules for specific ions which can work in physiological condition, have ultra-sensitivity, have emission in the higher wavelength is highly desirable.

Chapter 2: Experimental methods and characterization

This chapter explains comprehensive information about the various materials used in the synthesis of the receptors/probes, detail synthetic techniques, crystallization details, binding studies; specifications of instruments used for the characterization of the synthesized compounds were discussed.

Chapter 3: Selective Detection of Zn^{2+} and PPi in Physiological Conditions and Application in Bacterial Cell Number Estimation

This chapter describes the thorough investigation of the binding properties of a diformyl-quinoline based receptor (**L_1**) which exhibits selective colorimetric and fluorometric sensing of

Zn^{2+} in aqueous medium at pH 7.4 based on ICT process. The *in situ* formed phenoxo-bridged complex, $\mathbf{L_1}$.2Zn can selectively and specifically sense PPi among all the other biologically important anions including ATP through reversible binding. The detection limit for Zn^{2+} and PPi were found to be approximately 56 ppb and 2 ppb respectively. The unique selectivity of the PPi by $\mathbf{L_1}$-Zn ensemble could be used as an analytical tool to probe PPi generation in a prototype PCR setup and track DNA amplification with higher sensitivity as compared to conventional agarose gel electrophoresis. Interestingly, the principle of PPi estimation in PCR rendered rapid estimation of bacterial cell numbers with a limit of detection of 10 CFU of *E.coli* MTCC 433 in as early 10 PCR cycles. The proposed method of PPi sensing offers interesting application potential in PCR-based rapid diagnostics for pathogenic agents and microbiological quality control.

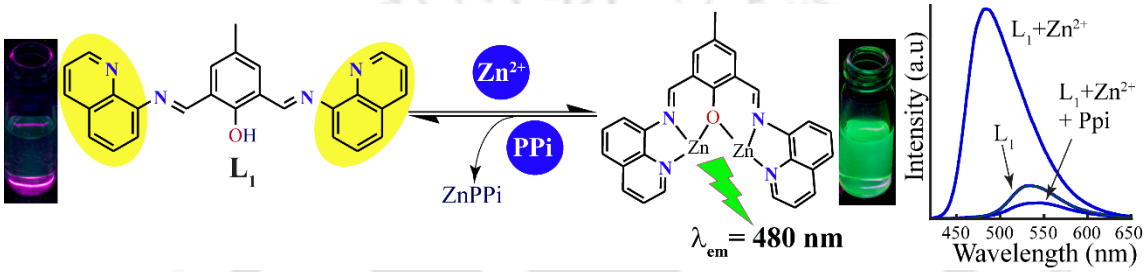

Scheme 1. A comprehensive representation of the research work included in chapter 3.

Chapter 4: A novel chemosensor with visible light excitability for sensing Zn^{2+} in physiological medium and in HeLa cells

In this chapter a imine-hydrazone based fluorescent chemosensor ($\mathbf{L_2}$) have been designed which was used for efficient and selective sensing of Zn^{2+} over other biologically important metal ions in physiological conditions is reported. Enhancement in fluorescence emission intensity of the developed probe with a red shift of ~25 nm was observed with Zn^{2+}, whereas other metal ions failed to reveal any significant change in the emission spectra. Interestingly, the receptor functioned in completely physiological condition (99.7% HEPPES buffer) and has visible light excitability. Sensing of Zn^{2+} was investigated in detail through absorption spectroscopy, emission spectroscopy, DFT calculation, ^{1}H-NMR titration experiment and ESI-MS experiment. Association constant between $\mathbf{L_2}$ and Zn^{2+} was found to be 5.58×10^5 M^{-1}. The receptor could detect as low as 69 ppb Zn^{2+}. Sensing of Zn^{2+} is proposed through switch-on of intramolecular charge transfer (ICT) and chelation enhanced fluorescence (CHEF) process after the introduction of Zn^{2+} to the free ligand. The developed receptor was non-toxic and rendered intracellular sensing of Zn^{2+} in HeLa cells through fluorescence imaging studies.

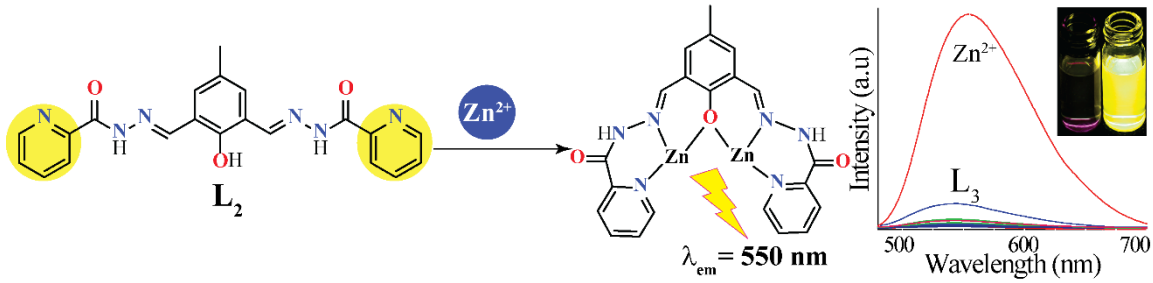

Scheme 2. A comprehensive representation of the research work included in chapter 4.

Chapter 5: A lab-on-a-molecule: Traffic signal like sensing of Al^{3+}, Zn^{2+} and F^{-}

This chapter gives detailed information about a novel dialdehyde-based multi-analyte sensor (**L_3**) which renders distinctive emission spectra for Al^{3+}, Zn^{2+} and F^{-} ions. The ligand exhibited different types of interactions with these three different ions resulting into the enhancement of fluorescence intensity at three different wavelengths. All the sensing processes were studied in details by absorption spectroscopy, emission spectroscopy and 1H-NMR titration experiment. The ligand has the working ability in a wide pH range including the physiological pH. The ligand is non-toxic and amicable for sensing intracellular Al^{3+} and Zn^{2+} in live Hela cells.

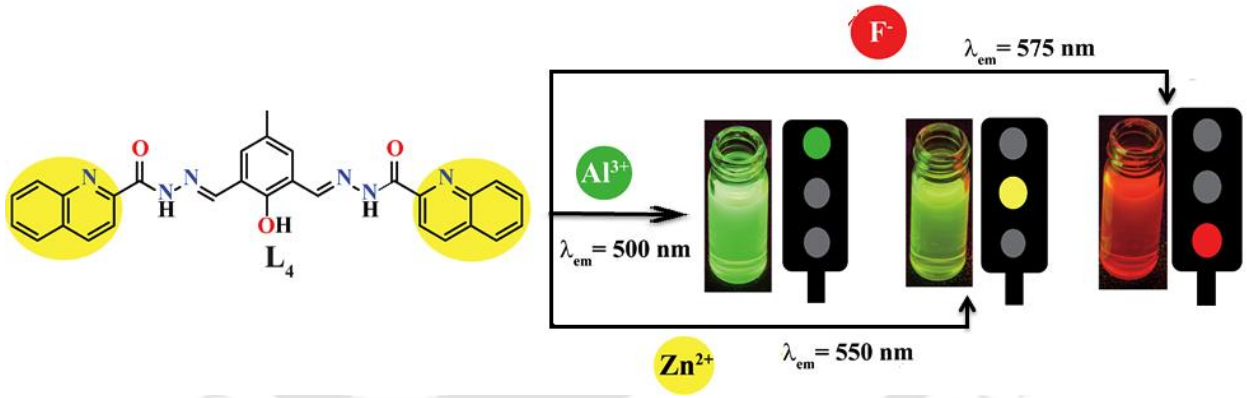

Scheme 3. A comprehensive representation of the research work included in chapter 5.

Chapter 6: A Near-Infrared (NIR) emissive Al^{3+} sensing platform for specific detection in solution, cells and probing DNase activity

The final chapter describes a new tricarbocyanine-based chemosensor **(L_4)** which exhibited a dramatic Al^{3+}-specific fluorescence turn-on response in the Near-Infrared (NIR) region. The receptor was found to be highly selective towards Al^{3+} over other metal ions in physiological condition. The sensor was also capable to sense Al^{3+} in complex medium like environment samples (tap water, lake water and river water). The sensor was non-toxic and could thus be employed as an imaging probe for detecting intracellular Al^{3+} in live cells. Interestingly, upon interaction with DNA in solution, the **L_4**-Al^{3+} ensemble rendered tracking of DNase activity in solution through a systematic reduction in the fluorescence emission intensity.

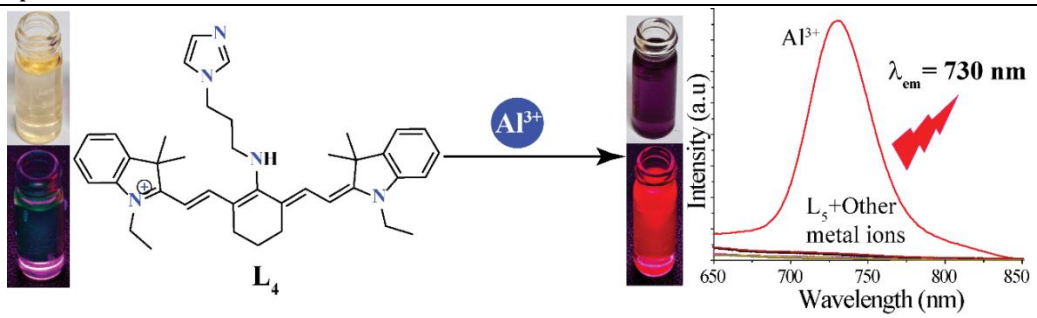

Scheme 4. Schematic illustration of the research work incorporated in chapter 6.

Conclusion and future perspective

In conclusion, the overall thesis elucidates some important results in the field of chemosensor for biologically and environmentally important analytes in solution and in biological medium. We have designed, synthesized and investigated some unique receptor systems (**L_1-L_4**) ranging from simple to complex structures and also spectral responses ranging from UV-region to near-IR region which can detect various analytes in aqueous solution and inside living cells.

Receptor **L_1** can selectively sense Zn^{2+} in physiological condition with a turn-on (green fluorescence) response. The *in situ* formed complex, **L_1**.2Zn can selectively and specifically sense PPi among all the other biologically important anions. The unique selectivity of the PPi by **L_1**-Zn ensemble could be used as an analytical tool to probe PPi generation in a prototype PCR setup and track DNA amplification with higher sensitivity as compared to conventional agarose gel electrophoresis. Interestingly, the principle of PPi estimation in PCR rendered rapid estimation of bacterial cell numbers of *E.coli* MTCC 43. Receptor **L_2** can also specifically sense Zn^{2+} in complete physiological medium with a turn-on response (yellow fluorescence). The receptor was non-toxic and sense Zn^{2+} in HeLa cells. **L_3** can sense Al^{3+}, Zn^{2+} and F^- ions (green, yellow and orange fluorescence respectively) with three distinctive emission spectra. The ligand can work in a wide pH range including the physiological pH and was also applied for sensing intracellular Al^{3+} and Zn^{2+} in live HeLa cells. In chapter 6, we have discussed about **L_4** which can selectively and specifically recognize Al^{3+} among all other cations with turn-on responses (red fluorescence). Both the absorption (710 nm) and emission (730 nm) responses were in the NIR region. Interestingly, upon interaction with DNA in solution, the **L_4**-Al^{3+} ensemble rendered tracking of DNase activity in solution through a systematic reduction in the fluorescence emission intensity.

Contents

Chapter 4

A novel chemosensor with visible light excitability for sensing Zn^{2+} in physiological medium and in HeLa cells

Chapter 5

A lab-on-a-molecule: Traffic signal like sensing of Al^{3+}, Zn^{2+} and F^-

Chapter 6

Chapter 1

Introduction

Chapter 1

1.1. Fluorogenic Chemosensors: An Introduction

Luminescence, a stunning and bewildering phenomena among many other amazing Natural wonders. Luminescence (Latin: Lumen = light), whether man-made or created by Nature itself, is the only phenomenon that lightens up "life", besides the visible radiation from combustion and photon emission as a consequence of nuclear fusion of hydrogen by the yellow dwarf star (G2V) that shines on our planet. Interestingly, a photon produced in the core of the sun will take thousands of years to travel from the core to the surface, but only 8 minutes to reach our planet. Commonly, people identify at least two types of luminescence: fluorescence and phosphorescence. However, luminescent processes comprise a large group of related phenomena that have purely physical, chemical, and/or biological/biochemical origins.[1.1]

Among many dramatic visual phenomenon occurring within the laboratory, switching of luminescence of chemosensors by specific analytes became more famous among scientists from different fields. The past two or three decades offer plenty of indications that this spectacle continues to amuse scientists in laboratories around the world in good numbers. It was not surprising that such an inexpensive and feasibly practical indicator will be employed for the noble use in the quantification of chemical species of various kinds, that is, chemosensors serve real-life needs in the wider world. The need of organic chemistry is crucial behind all these creativity, because design, synthesis and characterization of small organic molecules leads the demonstration of luminescence switching.[1.2]

Generally, chemosensors are abiotic molecules which can specifically and selectively bind the target analyte of interest in a reversible manner with a consequential alteration in one or more properties of the system, such as redox potentials, absorption or fluorescence spectra [1.3, 1.4]. In general, two different processes are occurring simultaneously during analyte detection, i.e. molecular recognition and signal transduction. So, chemosensors can be constructed with three possible different constituents (Fig. 1.1): (i) a receptor, (ii) a fluorophore and, (iii) a mechanism for communication between the two former moieties. [1.5]

Fluorescent chemosensors have their own advantages over other chemosensors such as: fluorescence measurements are usually very sensitive (single molecule detection is possible),

inexpensive, easy to execute, and adaptable, very low detection limit with submicron visualisation and high sensitivity [1.3, 1.4]. Moreover, the photophysical properties of a fluorophore can be modified by introducing different processes such as proton-, energy- and electron-transfer processes, the presence of heavy-atom effects, changes of electronic density, and the destabilisation of a non-emissive nπ* excited state [1.3]. So, by just altering a simple process, different efficient chemosensors can be designed and developed. The signal transduction of a chemosensor after binding with the target analyte offers the possibility to monitor analyte concentration in real-time and real space. Chemosensors are receiving fascination and attention in the scientific community, especially from chemists, biologists, physicists and material scientists. In biochemistry, clinical and medical sciences, and cell biology, freely mobile sensor molecules are employed extensively in microscopy, a use that offers the possibility of performing real-space measurements. There is a massive necessity for developing the real time detection toolkits in analytical chemistry and environmental sciences. These tools has stretched the opportunity of carrying out remote real-time measurements with optical sensors (optodes) by observing variations in the absorption or luminescence spectra of chromogenic or fluorescent compounds immobilized on polymer matrix on the tip of a fibre. So, with the help of a micro sized optical fibre, detection and analysis of a specific analyte is possible at almost any location at any time instantly.[1.6]

The field of chemosensors started to bloom only after the late 1970s when Pedersen, Cram and Lehn developed the revolutionary supramolecular chemistry. On the other hand, the improvement of photochemistry provided the foundation for designing systems which can produce changes in absorbance or fluorescence spectra after binding with the analyte. Developing chemosensors for metal ions got special interest from the scientific community, because metals are required for almost all the living organisms, as metals play crucial roles in fundamental processes, including osmotic regulation, catalysis, metabolism, bio-mineralization, and signalling. Group I and II metals (alkali and alkaline earth metals) are highly abundant in most biological organisms. Gradients of group I and II metals across membranes represent a classical way to store potential energy, and these ions play roles in osmotic regulation, generation of action potentials, and signalling. Transition metals especially iron, zinc, copper, manganese, cobalt, nickel, molybdenum, tungsten, chromium, and vanadium play significant roles in several biological processes. [1.7] These are termed as the trace elements because of their small abundance in the biological organisms compared to the group I and II metals although iron and zinc are often found in substantial amounts. On the other hand, anions also play fundamental roles in a wide range of chemical and biological processes.[1.8]

The signal transduction of a fluorophore may undergo through various mechanisms such as ICT (internal charge transfer), PET (photoinduced electron transfer), EET (electronic energy transfer) FRET (Fourier resonance energy transfer), CHEF (chelation-enhanced fluorescence), monomer-excimer formation and many more. Among them, ICT, PET, CHEF, MEF are the most extensively studied processes which are used for signal transduction.[1.2] Several scientific papers have been published concerning fluorescence or colorimetric sensors for metal ions and anions with the help of the above mentioned mechanisms.[1.99–1.16] In general, (1) Protonation-deprotonation; (2) complexation (direct complexation and competitive displacement complexation); (3) cleavage and formation of covalent bonds; and (4) redox reaction, are the common approaches used for the analyte detection. Among all these approaches, complexation (direct complexation and competitive displacement complexation) dependent sensor molecules have been designed, synthesized and their properties have been investigated in details in this thesis. Some examples from the literature have been shown in the next two sections.

1.2. Different Design Strategies

Complexation based chemosensors can be divided into two different sections, one is direct complexation and the other is competitive displacement complexation. In the first case, a spacer connects the binding site with the signalling unit. The target analyte binds with the binding unit via any of the following ways: coordination, electrostatic interaction, or hydrogen bonding rendering the signal transduction of the signalling unit. This is one of the most extensively used strategy for the development of chromogenic and fluorogenic probes which have the advantages of rapid spectroscopic response and excellent reversibility which again benefits real time detection of a specific analyte easily in no time.

Unlike the first approach, in displacement approach the binding site and the signalling subunit are not attached covalently rather they form a coordination complex (one part of the host-indicator assembly that is used in indicator displacement).[1.17] The indicator is replaced from the binding site by the target analyte, ensuing a change from a coordinated to non-coordinated state. Generally, the spectroscopic characteristics of the signalling subunit in a coordinated state are different from the non-coordinated state. So, the analyte binding process is coupled to a signal modulation. Thus, it can be assumed that the stability constant of the complex formed between the binding site and the analyte should be higher than the complex formed between binding site and the signalling unit. The displacement approach has great advantages like no need to incorporate the signalling unit into the structures of receptor or analyte, high reversibility, recyclable, exchangeable indicators. Also, the detection mechanism of this method is independent of the analyte structure.[1.18]

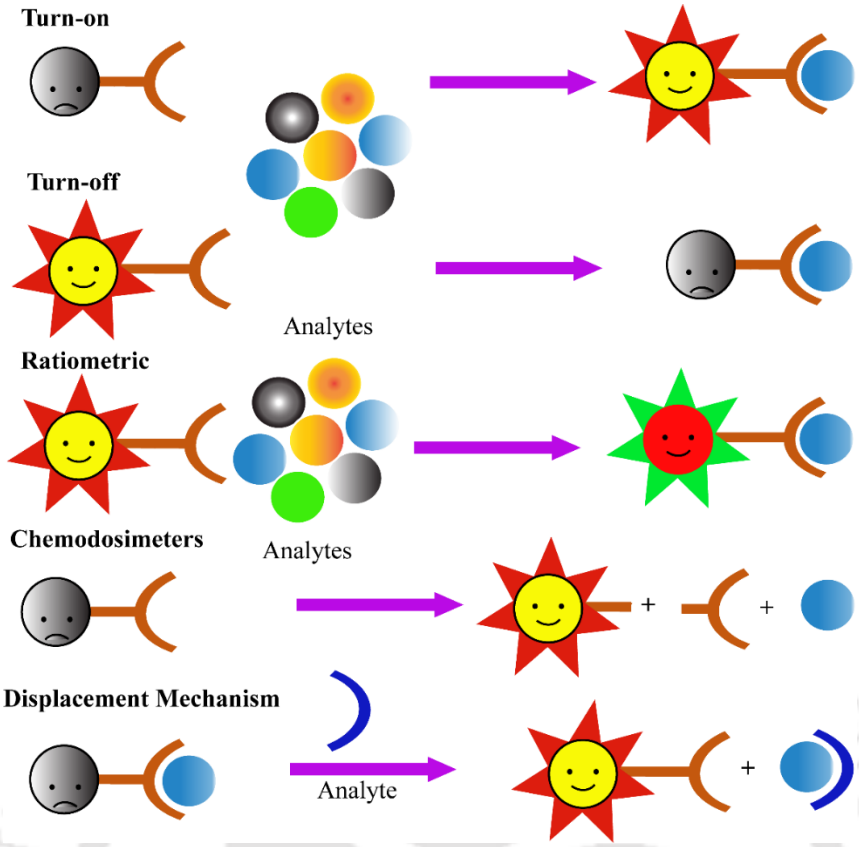

Figure 1.1. Different types of design strategies for chemosensors.

1.3. Recent Developments in Chemo-sensing arena

Suzuki *et al.* has reported a near-infrared fluorescent probe (**1**) for calcium[1.19] (Fig. 1.2.). The probe was composed of two moieties, a fluorescent moiety and a Ca^{2+} binding moiety. The probe has excellent spectroscopic properties such as sharp fluorescence spectra (in NIR region) with high extinction coefficients and high quantum yields, as well as the fine-tuning ability of the absorption/emission spectral bands in the visible-NIR region and applicable for real-time dual-color intracellular Ca^{2+} imaging. They have used the well-known Ca^{2+} chelator, BAPTA (O, O'-bis(2-aminophenyl) ethyleneglycol-N,N,N',N'- tetra acetic acid) as the and binding site for Ca^{2+}. The PET (photoinduced electron transfer) from the electron-rich ion chelating moiety to the fluorescent dye moiety quenches the fluorescence of the whole system. As soon as Ca^{2+} was introduced, the PET process was prohibited which resulted into enhancement in the emission intensity of the probe.

Mallet and coworkers had developed a new visible-light red-emitting receptor (**2**) for Ca^{2+} (Fig. 1.2.).[1.20] The large molar extinction, high quantum yield, high photostability and large red shift of the receptor ranks this receptor among the brightest red-fluorescent Ca^{2+}-sensitive dyes. With its spectral properties, they respond to the demands of many biological multicolor fluorescence

applications, specifically when imaging cells expressing enhanced green fluorescent protein (EGFP).

Watkinson and coworkers have reported two cyclam-based macrocyclic sensors which were prepared using click chemistry to link fluorophores to the macrocyclic receptors (Fig. 1.2.)[1.21]. These sensor molecules exhibited high selectivity for Zn(II) over a other important metal ions with turn-on responses in the emission spectra over a wide pH range. The sensor molecules can access biologically available zinc in mammalian cells, sensing the Zn(II) flux that exists during apoptotic cell death.

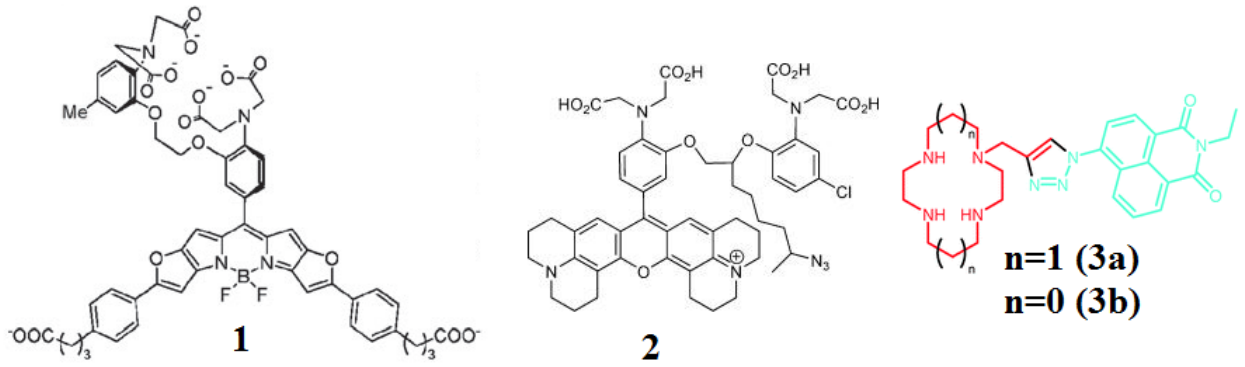

Figure 1.2. Structures of probe **1**, **2** and **3a, 3b**.

Hong and co-workers have developed a naphthalene-based fluorescent sensor, **4**[1.22]. The Zn-complex of this ligand selectively detects PPi with high affinity in aqueous solution over a wide pH range (Fig. 1.3). Their system showed remarkable selectivity for PPi over other anions, including strong competitors such as HPO_4^{2-} and ATP. The zinc complex had low fluorescence in solution but after the addition of PPi its fluorescence enhances drastically due to the release of zinc as Zn-PPi complex resulting in the free ligand.

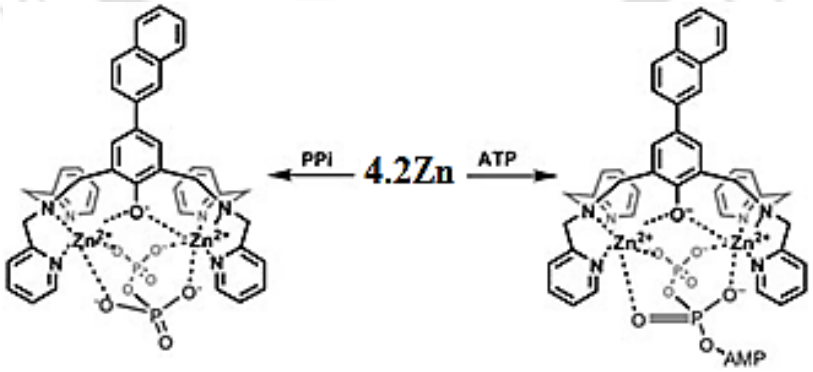

Figure 1.3. Response of probe **4.2Zn** towards PPi and ATP.

Kim and coworkers have reported a zinc(II) complex with a two-dipicolylamine-substituted 1,8-naphthalimide (Fig. 1.4.) for recognition of PPi with ratiometrical fluorescence changes in aqueous solution[1.23]. They have also monitor the intracellular PPi by the observation that the

fluorescence of **5** was enhanced by the presence of the Zn^{2+} ion and was quenched by addition of PPi.

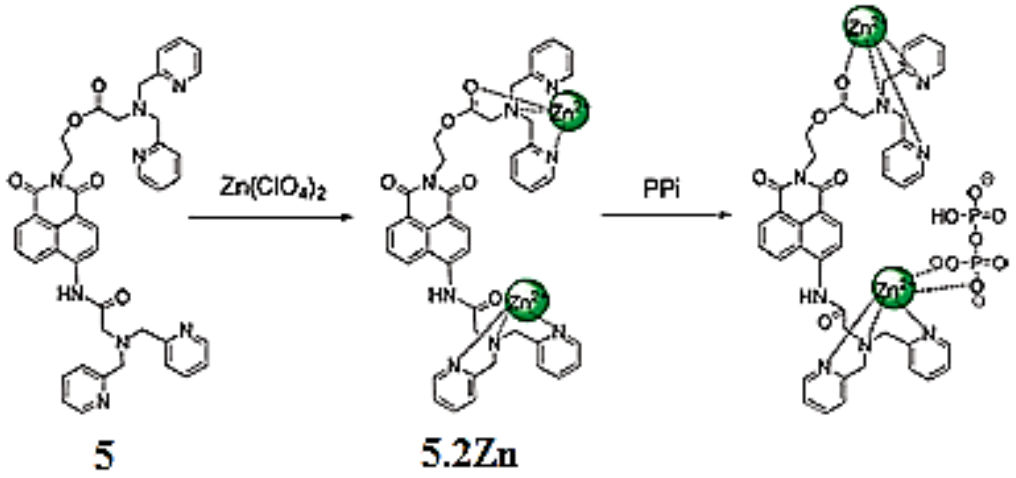

Figure 1.4. Sequential sensing of Zn^{2+} and PPi by probe **5**.

Yoon, Park and coworkers devised a simple method for detecting CN^- ion in aqueous solution at pH 7.4[1.24]. The fluorescent probe **6** displays a fluorescence quenching effect with Cu^{2+}, which shows fluorescence ON upon the addition of CN^- ion (Fig. 1.5). This sensing system has been incorporated into a microfluidic platform, in which the fluorescent sensor 6-Cu^{2+} displays green fluorescence upon the addition of CN^- ion. Finally, studies of biological applications using Caenorhabditis elegans demonstrated that their system can be employed for the *in vivo* imaging of cyanide.

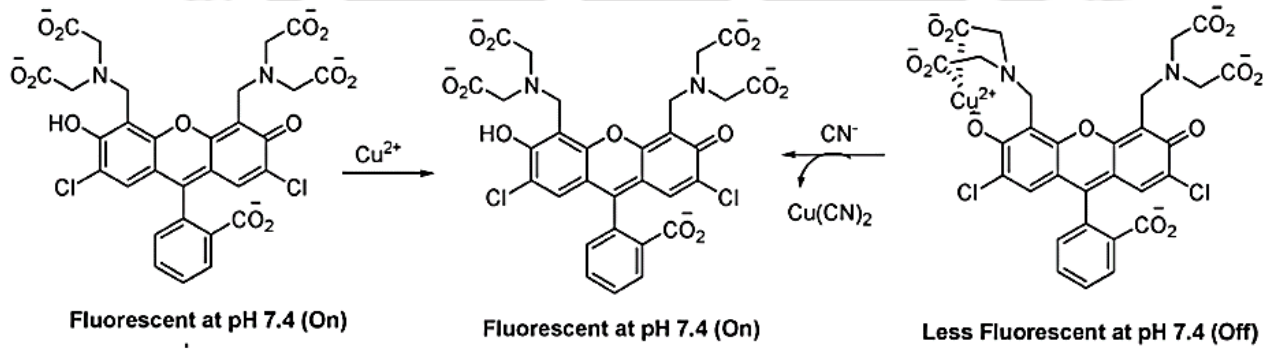

Figure 1.5. Sequential sensing of Cu^{2+} and CN^- by probe **6**.

Jiang et.al had designed one selective Ag^+ sensor (**7**) using a quinaldine moiety as fluorophore attached with an azacrown[1.25]. It provides ratiometric measurements for Ag^+ with high sensitivity and selectivity in aqueous solution (Fig. 1.6). Keeping in mind about the low solubility product of

AgX (X -halide) in water they had used the in situ formed Ag complex for the sensing of I- through sequestrating Ag^+ from the complex via formation of AgI precipitates in aqueous media.

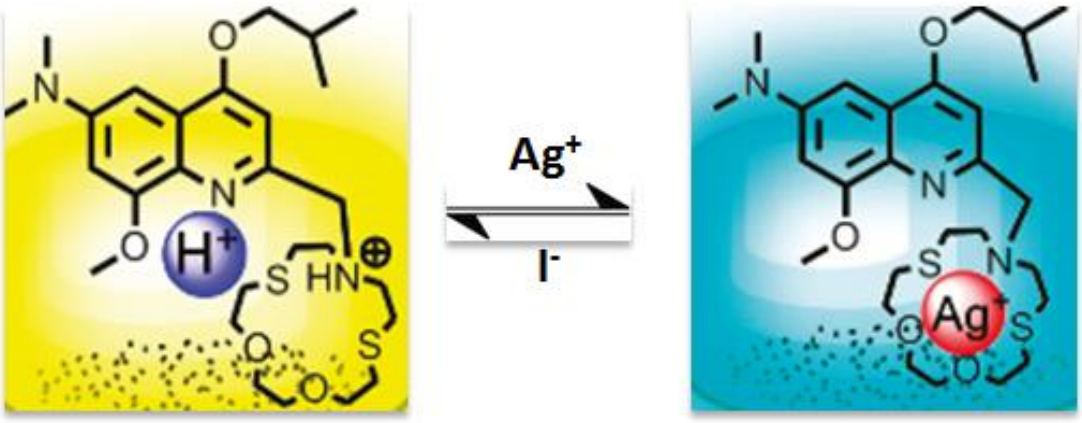

Figure 1.6. Sequential sensing of Ag^+ and I^- by probe **7**.

Recently our group had synthesized a new indole functionalized rhodamine derivative **8**[1.26] which specifically binds to Cu^{2+} in the presence of other competing ions with observable changes in its spectral behaviour. The receptor could be employed as a resonance energy transfer (RET) based sensor for detection of Cu^{2+} based on the process involving the donor indole and the acceptor Cu^{2+} bound xanthene fragment. Studies reveal that **8**–Cu complex is selectively and fully reversible in presence of sulphide anion (Fig. 1.7).

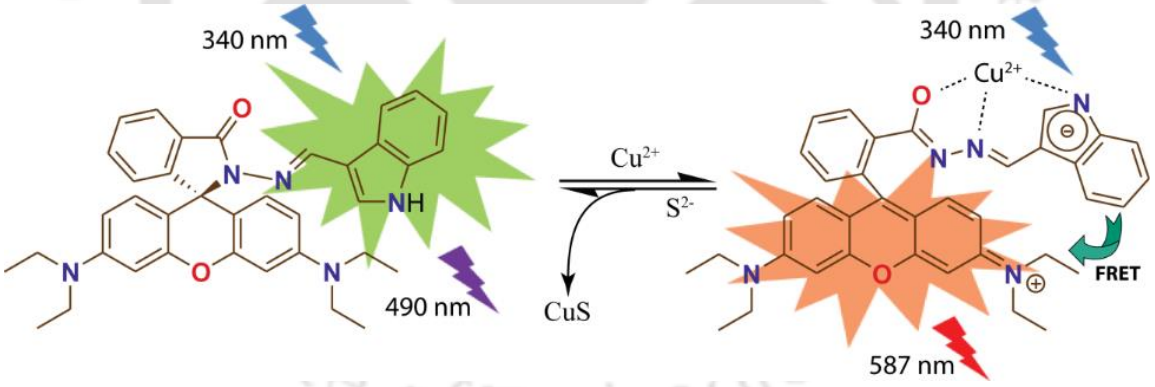

Figure 1.7. Sequential sensing of Cu^{2+} and S^{2-} by probe **8**.

Recently another new fluorescent chemosensor **9**[1.27] have been reported by our group which exhibited relay recognition of Zn^{2+} and pyrophosphate anion in a mixed buffer solution at physiological condition. The probe exhibited excellent Zn^{2+} induced turn-on response in emission spectroscopy and it can detect Zn^{2+} as low as 71ppb. Furthermore, addition of the pyrophosphate ion led to quenching of the fluorescence signal of the **9**–Zn^{2+} ensemble. The sensitive fluorescence behaviour of the **9** rendered a useful probe for in vitro assays of the intracellular Zn^{2+} and PPi ions in a model human cell line (Fig. 1.8).

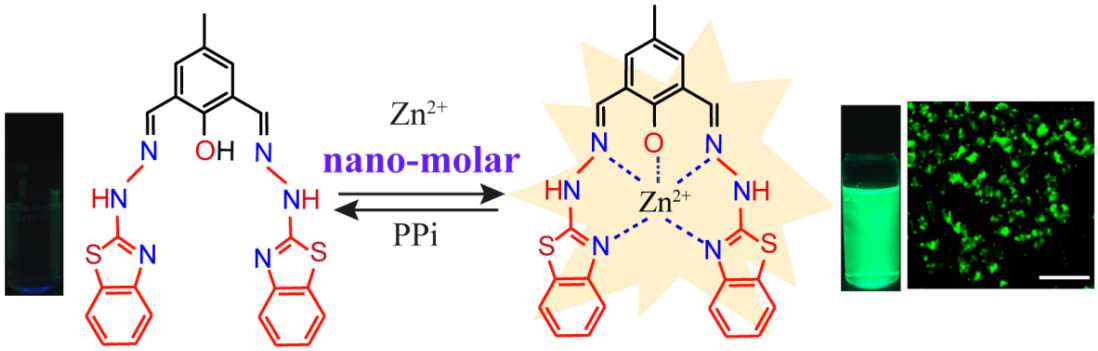

Figure 1.8. Sequential sensing of Zn^{2+} and PPi by probe **9**.

A highly selective inorganic pyrophosphate (PPi) sensor (**10**) have been designed, synthesized and reported by our group lately[1.28]. The novel phenylbenzimidazole functionalized imine containing chemosensor could sense PPi through "turn-on" colorimetric and fluorimetric responses in a very competitive environment. The overall sensing mechanism is based on the aggregation-induced emission (AIE) phenomenon. Moreover, a real time in-field device application was demonstrated by sensing PPi in paper strips coated with **10**. Interestingly, detection of intracellular PPi ions in model human cells could also be possible by fluorescence microscopic studies (Fig. 1.9).

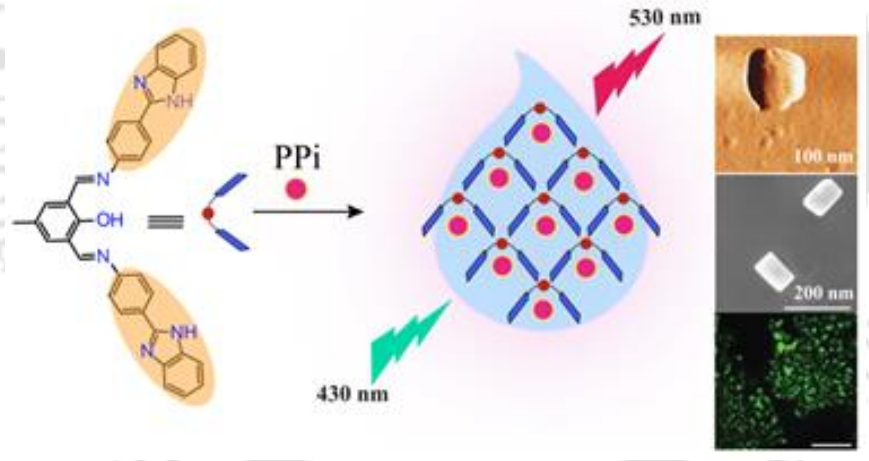

Figure 1.9. AIE induced sensing of Zn^{2+} by probe **10**.

Tang *et al.* have developed an excellent zinc sensor using the tricarbocyanine unit and that was the first NIR zinc sensor (**11**).[1.29] The sensing mechanism of **11** is based on PET and gave a 20-fold turn-on response for detecting zinc. The probe has a large Stokes shift and is highly sensitive and selective to zinc. Moreover, **11** is cell-permeable and can respond to zinc quickly, which demonstrated that **11** is an excellent NIR fluorescence probe for zinc imaging (Fig. 1.10).

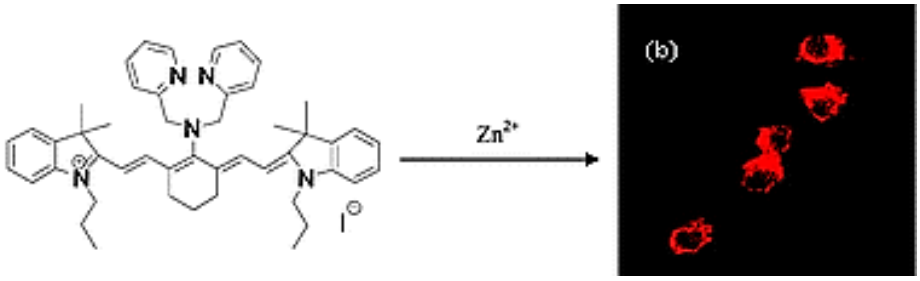

Figure 1.10. AIE induced sensing of Zn^{2+} by probe **11**.

The first NIR fluorescent sensor for sulphide anions was developed, synthesized and reported by Cao *et al.* based on the displacement approach[1.30]. The sensing ensemble is composed of a cyanine dye, a piperazine linker, an 8-aminoquinoline ligand, and copper. The ensemble has several advantages such as large NIR fluorescence turn-on signal in aqueous ethanol, high sensitivity, and high selectivity (Fig. 1.11).

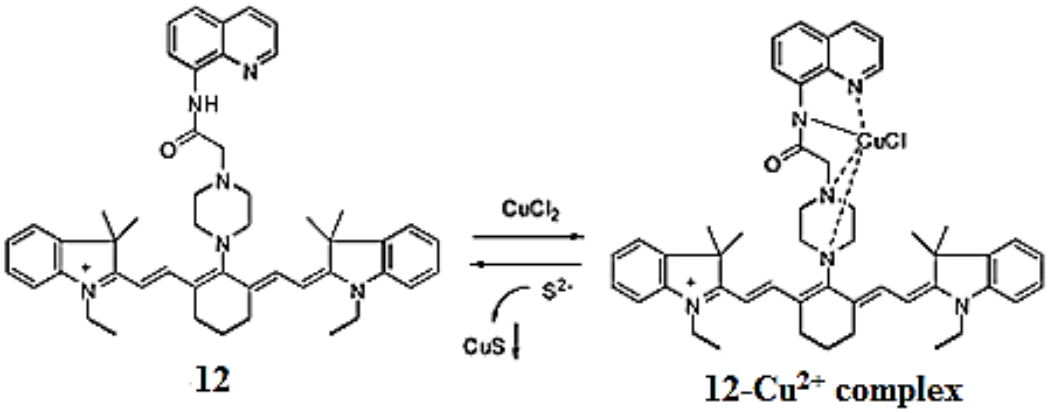

Figure 1.11. AIE induced sensing of Zn^{2+} by probe **12**.

1.4. Real-life Applications of Chemosensors: from design to deployment

Owing to the numerous advantages and potentiality of the Chemosensors, they have been employed in various fields. Luminol is used by the crime scene investigators to detect very trace amount of blood in the crime scenes. It emits blue fluorescence when it comes in contact with blood and it has very low detection limit. So even if the criminal has tried to clean off the blood from the crime scene, luminol still can detect that much of blood sample. Chemosensors have been also employed in medical sciences as well. The electrolyte levels in the blood sample of a car accident victim are determined rapidly and reliably on the accident spot by the paramedics with a family of fluorescent PET sensors (**13**[1.31] and **14**[1.32]). So, when the victim is transferred to the hospital, a blood bag balanced with electrolytes matching the patients' blood has already been

prepared and it's ready for use. Probe **13** is used to determine the level of Na^+, while probe **14** is used to determine the K^+ level. The sensor molecules are covalently immobilised on an amino cellulose fibre substrate. Before engagement with the sensor molecules, the blood is filtered through the cellulose fibre mat, so that only the comparatively colourless serum makes the passage. As soon as the serum encounters with the sensor molecules, the Na^+ in the serum binds with the appropriate fraction of the sensor molecules. Now, as the Na^+-bound fraction is strongly fluorescent and it emits a green-yellow fluorescence, upon exciting all the sensor molecules by an inexpensive blue light-emitting diode, the Na^+-bound molecules emit green-yellow fluorescence while the free molecules remain practically silent. The intensity of the green-yellow light flash is measured by an inexpensive photodiode and easily converted into a blood Na^+ level.

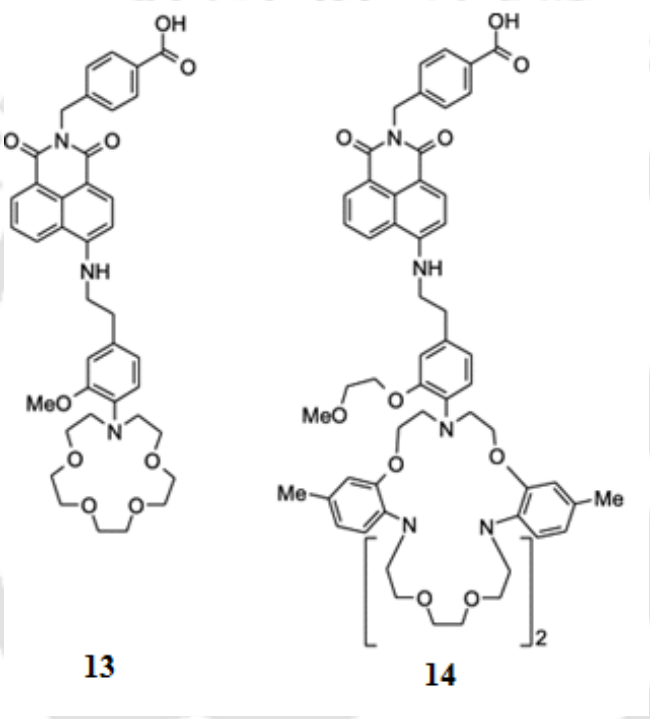

Figure 1.12. Structures of probe **13** and **14**.

1.5. Concluding Remarks and objective of thesis

The literature review evidently reveals the popularity and importance of the Chemosensors for their significant advantages and applications. The scientific community has developed thousands of Chemosensors in the last few decades. However, most of them have some limitations, like requirement of organic solvent as working media, low sensitivity and selectivity, emission at shorter wavelengths, made of expensive materials or obtained after multistep reactions. Due to the above mentioned limitations many of them are not suitable for practical employment. So, though a number of chemosensors are reported, there is still need of sensors which will have better solubility especially in physiological conditions, high selectivity, inexpensive, made *via* simple steps, emission at longer wavelength and cell permeable.

The literature also shows that most of the chemosensors developed during the last few decades are based on the following mechanisms: ICT, PET, CHEF and FRET. Depending on the above mechanisms switch on-off, switch off-on and ratiometric chemosensors have been designed and synthesized. Switch off-on probes are better than the switch on-off or ratiometric probes due to their capability of effortless detection of low-concentration difference relative to a "dark" background, which is rather suited for qualitative analysis due to the high sensitivity. On the other hand, ratiometric probes are better for quantitative analysis. Although ratiometric calculations need much more time for ratio calculation/measurement, but this process can eliminate the influence of several variants (e.g., probe concentration, instrumental efficiency, and environmental conditions) by built-in correction of two emission bands, which is why this process is perfect for precise quantitative analysis.

Development of fluorescent probes with absorption and emission in the near infrared (NIR) region (650–900 nm) are highly desirable due to the reduced propensity of photo-damage to biological samples, increased sample penetration and minimum background auto-fluorescence, which would significantly assist bio-imaging studies and in-vivo imaging.[6.32-6.40] Therefore, design of chromogenic and fluorogenic probes for biologically important cations and anions with longer emission wavelength is our first target.

So, from all the above discussions it is obvious that development of new probes with the following properties will be much appreciated. First of all, they should be very simple in design, inexpensive and easy to synthesize. Secondly, they should have the potential to work in physiological conditions which will empower practical applications of the probes in biochemical studies (especially for cell imaging studies). And last of all, probes with spectral responses at longer wavelengths are highly anticipated for better biochemical applications.

So, finally the focus of the thesis-work is 1) to design and synthesize simple, stable fluorogenic receptor molecules or chemosensor molecules with the potential to work in physiological conditions for optical detection n of ionic analytes, 2) application of the developed chemosensors in environmental or biological samples and 3) evolution of new receptor molecules which will have spectral responses in the longer wavelength region.

References

1.1. G. P. C. Drummen, *Molecules*, 2012, **17**, 14067.

1.2. J. F. Callan, A. P. de Silva, D. C. Magri, *Tetrahedron*, 2005, **61**, 8551.

1.3. A.P. de Silva, H. Q. N. Gunaratne, T. Gunnlaugsson, A. J. M. Huxley, C.P. McCoy, J. T. Rademacher, T. E. Rice, *Chem. Rev.*, 1997, **97**, 1515.

1.4. A.W. Czarnik (Ed.), Fluorescent Chemosensors for Ion and Molecule Recognition, A. C. S, Washington, 1992.

1.5. R. A. Bissel, A. P. de Silva, H. Q. N. Gunaratne, P. L. M. Lynch, G. E. M. Maguire, K. R. A. S. Sandanayake, *Chem. Soc. Rev.*, 1992, 187.

1.6. (a) E. Bakker, P. Bu¨hlmann, E. Pretsch, *Chem. Rev.*, 1997, **97,** 3083. (b) P. Bu¨hlmann, E. Pretsch, E. Bakker, *Chem. Rev.*, 1998, **98**, 1593.

1.7. I. Bertini, H. B. Gray, E. I. Stiefel, J. S. Valentine, Biological Inorganic Chemistry, 1st ed.; Eds.; University Science Books: Sausalito, CA, 2007.

1.8. E. Bianchi, K. Bowman-James, E. G.-Espan˜a, Eds. Supramolecular Chemistry of Anions; Wiley-VCH: New York, 1997.

1.9. H. N. Kim, M. H. Lee, H. J. Kim, J. S. Kim and J. Yoon, *Chem. Soc. Rev.*, 2008, **37**, 1465.

1.10. C. Lodeiro, F. Pina, *Coord. Chem. Rev.*, 2009, **253**, 1353.

1.11. G. Accorsi, A. Listorti, K. Yoosaf, N. Armaroli, *Chem. Soc. Rev*., 2009, **38**, 1690.

1.12. R. M.-Manez, F. Sancenon, *Chem. Rev*., 2003, **103**, 4419.

1.13. T. Gunnlaugsson, H. D. Paduka, M. Glynn, P. E. Kruger, G. M. Hussey, F. M. Pfeffer, C. M. Dos Santos, J. Tierney, *J. Fluoresc.*, 2005, **15**, 287.

1.14. E. J. O'Neil, B. D. Smith, *Coord. Chem. Rev.*, 2006, **250**, 3068.

1.15. V. Amendola, L. Fabbrizzi, *Chem. Commun.*, 2009, 513.

1.16. L. Prodi, *New J. Chem.*, 2005, **29**, 20.

1.17. (a) S. L. Wiskur, H. Ait-Haddou, J. J. Lavigne, E. V. Anslyn, *Acc. Chem. Res.*, 2001, **34**, 963. (b) B. T. Nguyen, E. V. Anslyn, *Coord. Chem. Rev*., 2006, **250**, 3118. (c) S. L. Tobey, E. V. Anslyn, *Org. Lett.*, 2003, **5**, 2029. (d) T. Zhang and E. V. Anslyn, *Tetrahedron*, 2004, **60,** 11117. (e) S. L. Tobey, B. D. Jones, E. V. Anslyn, *J. Am. Chem. Soc.*, 2003, **125**, 4026.

1.18. L. Zhu, Z. Zhong, E. V. Anslyn, *J. Am. Chem. Soc*., 2005, **127**, 4260.

1.19. A. Matsui, K. Umezawa, Y. Shindo, T. Fujii, D. Citterio, K. Oka, K. Suzuki, *Chem. Commun.*, 2011, **47**, 10407.

1.20. S. Gaillard, A. Yakovlev, C. Luccardini, M. Oheim, A. Feltz, J.-M. Mallet, *Org. Lett.*, 2007, **9**, 2629.

1.21. (a) E. Tamanini, A. Katewa, L. M. Sedger, M. H. Todd, M. Watkinson, *Inorg. Chem.*, 2009, **48**, 319. (b) K. Jobe, C. H. Brennan, M. Motevalli, S. M. Goldup, M. Watkinson, *Chem. Commun.*, 2011, **47**, 6036.

1.22. D. H. Lee, S. Y. Kim, J. Hong, *Angew. Chem. Int. Ed.*, 2004, **43**, 4777.

1.23. J. F. Zhang, S. Kim, J. H.Han, S.J. Lee, T. Pradhan, Q. Y. Cao, S. J. Lee, C. Kang, J. S. Kim, *Org. Lett.*, 2011, **13**, 5294.

1.24. S.Y. Chung, S.W. Nam, J. Lim, S. Park, J. Yoon, *Chem. Commun.*, 2009, 2866.

1.25. H. Wang, L. Xue, H. Jiang, *Org. Lett.*, 2011, **13**, 3844.

1.26. C. Kar, M. D. Adhikari, A. Ramesh, and G. Das, *Inorg. Chem.*, 2013, **52**, 743.

1.27. A. Gogoi, S. Mukherjee, A. Ramesh and G. Das, *RSC Adv.*, 2015,**5**, 63634.

1.28. A. Gogoi, S. Mukherjee, A. Ramesh and G. Das, *Anal. Chem.*, 2015, **87**, 6974.

1.29. B. Tang, H. Huang, K. Xu, L. Tong, G. Yang, X. Liua, L. An, *Chem. Commun.*, 2006, 3609.

1.30. X. Cao, W. Lin, L. He, *Org. Lett.*, 2011, **13**, 4716.

1.31. H. He, M. Mortellaro, M. J. P. Leiner, S. T. Young, R. J. Fraatz, J. Tusa, *Anal. Chem.*, 2003, **75**, 549.

Chapter 2

Experimental Methods

Chapter 2

2.1.1. General Information and Materials

All the materials used for synthesis were purchased from commercial suppliers and used without further purification. 2,6-Diformyl-4-methylphenol was prepared by modification of the literature method.[2.1] Absorption spectra were recorded on a Perkin-Elmer Lamda-25 UV−vis spectrophotometer using 10 mm path length quartz cuvettes in the range of 250−700 nm wavelength. Fluorescence measurements were conducted on a Horiba Fluoromax-4 spectrofluorometer using 10 mm path length quartz cuvettes with a slit width of 5 nm at 298 K. All the mass spectra were obtained using Agilent Technologies 6520 Accurate mass spectrometer. NMR spectra were recorded on a Varian FT-400 MHz instrument. The chemical shifts were recorded in parts per million (ppm) on the scale. The following abbreviations are used to describe spin multiplicities in ^{1}H NMR spectra: s = singlet; d = doublet; t = triplet; m = multiplet. Elemental analyses were performed with a Perkin-Elmer 2400 elemental analyzer.

2.1.2. UV−visible and Fluorescence Spectroscopic Studies of L_1

Stock solutions of various ions (1×10^{-3} mol L^{-1}) were prepared in deionized water. Perchlorate, chloride or nitrate salts of metal ions were used to prepare metal stock solutions. Tetra butyl, tetraethyl or sodium salts of the corresponding anions were used for anion sensing experiments. In the experiment with Ca^{2+}, chloride salt was used. A stock solution of **L_1** (1×10^{-3} mol L^{-1}) was prepared in DMSO. The solution of **L_1** was then diluted to 1×10^{-6} mol L^{-1} with MeOH: aqueous HEPES buffer (1 mM, pH 7.4; 3:2 v/v). All the spectroscopic experiments have been performed in a mixed solvent MeOH: aqueous HEPES buffer (1 mM, pH 7.4; 3:2 v/v). In titration experiments, a solution of **L_1** (1×10^{-6} M) was filled in a quartz optical cell of 1.0 cm optical path length, and the ion stock solutions were added gradually by using a micropipette to achieve a concentration of 1×10^{-5} mol L^{-1}. In selectivity experiments, the test samples were prepared by interacting appropriate amounts of the anions/cations stock into 2 mL of **L_1** solution (2×10^{-5}mol L^{-1}). For all the samples, the spectra were recorded following 1 min of the addition of the ions. For fluorescence measurements, excitation was set at 400 nm and emission was recorded from 420 nm to 650 nm.The selective binding of **L_1** with Zn^{2+} among all other metal ions was also studied by fluorescence emission spectroscopy of the solution of **L_1** (10.0×10^{-6}

M) in the absence and presence of an excess (10 eq) of each of the metal ions in mixed solvent. Reversible behavior of **L_1** upon the sequential addition of Zn^{2+} and PPi was carried out in the same mixed solvent. Based on this experimental result molecular logic gate has been designed.

2.1.3. Evaluation of the Apparent Binding Constant for the Formation of $L_1 \cdot 2Zn^{2+}$

A stock solution of $Zn(ClO_4)_2$, having a concentration of 0.5×10^{-3} M, in an aqueous HEPES buffer (pH 7.4) solution was used. Receptor **L_1** with an effective concentration of 10.0×10^{-6} $molL^{-1}$ in mixed solvent was used for the emission titration studies. The effective Zn^{2+} concentration was varied between 0 and 10×10^{-5} M for this titration. The solution pH was adjusted to 7.4 using an aqueous HEPES buffer solution having an effective concentration of 1.0 mM.

The apparent binding constant for the formation of the respective complexes were evaluated using the Benesi−Hildebrand (B−H) plot (equation 1).[2.2]

$$1/(I-I_0)=1/\{K(I_{max}-I_0)C\}+1/(I_{max}-I_0) \quad (2.1)$$

I_0 is the emission intensity of **L_1** at λ = 480 nm, I is the observed emission intensity at that particular wavelength in the presence of a certain concentration of the metal ion (C), I_{max} is the maximum emission intensity value that was obtained at λ = 480 nm during titration with varying metal ion concentration, K is the apparent binding constant (M^{-1}) and was determined from the slope of the linear plot, and C is the concentration of the Zn^{2+} ion added during titration studies.

2.1.4. Detection Limit for Zn^{2+} ion and PPi

The detection limit was calculated on the basis of the fluorescence titration. The fluorescence emission spectrum of **L_1** was measured 10 times, and the standard deviation of blank measurement was achieved. To gain the slope, the ratio of the emission intensity at 480 nm was plotted as a concentration of Zn^{2+}. The detection limit was calculated using the following equation

$$\text{Detection limit} = 3\sigma/k \quad (2.2)$$

where σ is the standard deviation of blank measurement, and k is the slope between the ratio of emission intensity versus $[Zn^{2+}]$. Detection limit for PPi was also calculated as per the above mentioned process.

2.1.5. Detection of PPi in PCR Experiment

Escherichia coli (*E.coli*) MTCC 433 was grown for 6h aerobically at 37°C in nutrient broth (NB) medium. Template DNA was isolated from the cells using the urea–SDS–

NaOH method as described previously.[2.3] PCR was performed with triplicate samples, each consisting of 2.0 µL of the extracted template DNA along with universal primers for bacterial 16S rRNA gene (Forward primer: 5'- AGAGTTTGATCCTGGCTCAG3' and reverse primer: 5'- GGTTACCTTGTTACGACTT3'). In a total reaction volume of 25.0 µL, the PCR mix contained PCR buffer (diluted from a 10X stock), 200 µM of each deoxynucleoside triphosphate (dNTP), 1U of *Taq* DNA polymerase (Bioline, India) and 50 pmol each of forward and reverse primers. The template DNA was initially subjected to denaturation for 2 min at 94°C followed by amplification cycles in a programmable thermal cycler (CG Palmcycler). Separate set of samples in triplicate were subjected to varying duration of PCR ranging from 5 to 35 cycles. Each cycle included denaturation for 1.0 min at 94°C, primer annealing for 1.0 min at 55°C and extension for 1.0 min at 72°C. A final extension for 10 min at 72°C followed the last cycle for every sample. Following PCR, the reaction mixture was allowed to come down to room temperature. To ascertain the level of PPi generated in the PCR experiments, a 10 µL aliquot of PCR mixture from every sample (5 to 35 cycles) was then added separately to 400 µL of 10 mM HEPES buffer (pH 7.4) containing 5 µM of $\mathbf{L_1}$.2Zn complex and the fluorescence emission intensity was measured at 540 nm. The mean fluorescence intensity from triplicate samples and the standard deviation was calculated and statistical analysis was performed by a one-way analysis of variance (AOVA) using Sigma Plot version 11.0. To visualize the PCR products, the generated amplicons corresponding to various samples (5 to 35 cycles) were also subjected to agarose gel (0.8%) electrophoresis.[2.4]

2.1.6. Detection of PPi in PCR Experiment and Estimation of Bacterial Cell Numbers

Cells of *Escherichia coli* MTCC 433 were grown as mentioned previously. Subsequently, the culture was serially diluted to achieve a cell concentration ranging from 1.0 CFU $ml^{-1}$to 10^6 CFU mL^{-1}. Template DNA was isolated from this series using the method reported earlier [2.3] and PCR was performed with bacterial universal primers as mentioned previously. The level of PPi generated in the PCR experiments from various cell numbers and intermittent cycles (5 to 35 cycles) was measured by interacting the PCR products with $\mathbf{L_1}$.2Zn complex and measuring the fluorescence change at 540 nm as mentioned before.

Template DNA was isolated from an overnight grown culture of *E. coli* MTCC 433 and PCR was performed with universal primers for bacterial 16S rRNA gene. Following PCR, the level of PPi generated in intermittent cycles (5 to 35 cycles) was ascertained by interacting the PCR mix with $\mathbf{L_1}$.2Zn complex and measuring the fluorescence emission intensity at 540 nm. Rapid estimation of bacterial cells numbers was pursued by measuring PPi generated in PCR experiments from various cell numbers (1.0 CFU mL^{-1} to 10^6 CFU mL^{-1}). The detailed experimental protocol for

PPi sensing in PCR and estimation of bacterial cell numbers is mentioned in the Supporting Information.

2.2.1. UV−visible and Fluorescence Spectroscopic Studies of L_2

Stock solutions of various ions (1×10^{-3} molL^{-1}) were prepared in deionized water. Perchlorate, chloride or nitrate salts of metal ions were used to prepare metal stock solutions. A stock solution of **L_2** (1×10^{-3} molL^{-1}) was prepared in DMSO. The solution of **L_2** was then diluted to 1×10^{-6} molL^{-1} with aqueous HEPES buffer (1 mM, pH 7.4). All the spectroscopic experiments were performed in aqueous HEPES buffer medium (1 mM, pH 7.4) containing 0.33% of DMSO. In titration experiments, a solution of **L_2** (1×10^{-6} molL^{-1}) was filled in a quartz optical cell of 1.0 cm optical path length, and the ion stock solutions were added gradually to achieve a concentration of 1×10^{-5} molL^{-1}. In selectivity experiments, the test samples were prepared by interacting appropriate amounts of the cations stock into 2 mL of **L_2** solution (2×10^{-5} molL^{-1}). For all the samples, the spectra were recorded following 1 min of the addition of the ions. For fluorescence measurements, excitation wavelength was set at 470 nm and emission was recorded from 480 nm to 700 nm. The selective binding of **L_2** with Zn^{2+} among all other metal ions was also studied by fluorescence emission spectroscopy of the solution of **L_2** (10.0×10^{-6} molL^{-1}) in the absence and presence of an excess (10 eq.) of each of the metal ions in mixed solvent.

2.2.2. Evaluation of the Apparent Binding Constant for the Formation of $L_2{\cdot}2Zn^{2+}$

A stock solution of $Zn(ClO_4)_2$, having a concentration of 0.5×10^{-3} molL^{-1}, in an aqueous HEPES buffer (pH 7.4) solution was used. Receptor **L_2** with an effective concentration of 10.0×10^{-6} molL^{-1} in the aforementioned HEPES buffer medium was used for the emission titration studies. The effective Zn^{2+} concentration was varied between 0 and 10×10^{-5} molL^{-1} for this titration. The solution pH was adjusted to 7.4 using an aqueous HEPES buffer solution having an effective concentration of 1.0 mM.

The apparent binding constant for the formation of the respective complexes were evaluated using the Benesi−Hildebrand (B−H) plot (equation 2.1). I_0 is the emission intensity of **L_2** at λ = 550 nm, I is the observed emission intensity at that particular wavelength in the presence of a certain concentration of the metal ion (C), I_{max} is the maximum emission intensity value that was obtained at λ = 550 nm during titration with varying metal ion concentration, K is the apparent binding constant (M^{-1}) and was determined from the slope of the linear plot, and C is the concentration of the Zn^{2+} ion added during titration studies.

2.2.3. Detection Limit for Zn^{2+} ion

The detection limit was calculated on the basis of the fluorescence titration. The fluorescence emission spectrum of **L_2** was measured 10 times, and the standard deviation of blank

measurement was achieved. To gain the slope, the ratio of the emission intensity at 550 nm was plotted as a concentration of Zn^{2+}. The detection limit was calculated using equation 2.2 where σ is the standard deviation of blank measurement, and k is the slope between the ratios of emission intensity versus [Zn^{2+}].

2.2.4. Cytotoxicity assay for L_2 and L_2-Zn complex

A standard MTT assay was performed to determine the cytotoxic effect of **L_2** and **L_2**–Zn complex on HeLa cells. MTT (3-(4,5-dimethylthiazol-2-yl)-2,5-diphenyltetrazolium bromide) solution was procured from Sigma-Aldrich, USA. Initially HeLa cells were grown in 25 cm^2 tissue culture flask in Dulbecco's modified Eagle medium (DMEM) supplemented with 10% (v/v) fetal bovine serum (FBS), penicillin (100g/mL) and streptomycin (100µg/mL) at 37◦C in a CO_2 incubator. Prior to MTT assay, cells were seeded onto 96-well tissue culture plates (approximately 10^4 cells per well) and incubated with various concentrations of compound **L_2** and **L_2**–Zn complex (5.0µM, 12.5µM, 15µM, 25µM and 50µM) made in DMEM for a period of 24h. HeLa cells treated with DMSO or $Zn(ClO_4)_2$ alone were also included in parallel sets. Following 24 h incubation, the growth media was carefully aspirated and fresh DMEM containing MTT solution was added to the cells and incubated for 3–4 h at 37◦C. Subsequently, the MTT solution was removed and the insoluble colored formazan product was solubilized in DMSO and its absorbance was measured in a microtitre plate reader (Infinite M200, TECAN, Switzerland) at 550 nm. MTT assay for every sample was performed in six sets. Data analysis and calculation of standard deviation was performed with Microsoft Excel 2010 (Microsoft Corporation, USA).

2.2.5. Detection of Zn^{2+} in HeLa Cells by fluorescence microscope analysis

HeLa cells (human cervical carcinoma cells) were initially cultured in a 25 cm^2 tissue culture flask containing DMEM medium supplemented with 10% FBS, penicillin (100 µg/mL) and streptomycin (100 µg/mL) in a CO_2 incubator. Prior to cell imaging studies, HeLa cells were seeded into a 6 well plate and grown in DMEM medium at 37◦C till 80% confluency in a CO_2 incubator. Subsequently, the cells were washed thrice with sterile phosphate buffered saline (PBS), incubated with 25 µM **L_2** in DMEM at 37◦C for 1 hr in a CO_2 incubator and their images were acquired using a fluorescence microscope (Eclipse Ti–U, Nikon, USA) with a filter that allowed green light emission. The cells were further washed with sterile PBS in order to remove excess **L_2**, and then incubated for 1 hr with 50 µM $Zn(ClO_4)_2$ made in sterile PBS. The images of the cells were again acquired with a fluorescence microscope as mentioned earlier.

2.3.1. UV−Vis and fluorescence spectral studies with L_3

Stock solutions of various ions (1×10^{-3} mol L^{-1}) were prepared in deionized water. Perchlorate, chloride or nitrate salts of metal ions were used to prepare metal stock solutions. In case of anions

tetra-butyl or tetra-ethyl ammonium salts were dissolved in deionized water to prepare the stock solutions. A stock solution of **L_3** (1×10^{-3} mol L^{-1}) was prepared in DMSO. The solution of **L_3** was then diluted to 1×10^{-5} mol L^{-1} as required in different cases. All the spectroscopic experiments of the cations were performed in aqueous HEPES buffer medium (1 mM, pH 7.4) containing 0.33% of DMSO. In titration experiments, a solution of **L_3** (1×10^{-5} mol L^{-1}) was filled in a quartz optical cell of 1.0 cm optical path length, and the ion stock solutions were added gradually to achieve a concentration of 1×10^{-5} mol L^{-1}. Spectroscopic studies of **L_3** in presence of different anions were performed in acetonitrile medium containing 0.33% DMSO. In selectivity experiments, the test samples were prepared by interacting appropriate amounts of the cations stock into 2 mL of **L_3** solution (2×10^{-5} mol L^{-1}). For all the samples, the spectra were recorded following 1 min of the addition of the ions. For fluorescence measurements, excitation wavelength was set at 450 nm and emission was recorded from 460 nm to 720 nm.

2.3.2. Evaluation of the binding constant

Stock solutions of Al^{3+} and Zn^{2+}, having a concentration of 0.5×10^{-3} $molL^{-1}$, in aqueous HEPES buffer (pH 7.4) solution were used. Receptor **L_3** with an effective concentration of 10.0×10^{-5} $molL^{-1}$ in the aforementioned HEPES buffer medium was used for the emission titration studies. The effective Zn^{2+} concentration was varied between 0 and 30×10^{-5} M for this titration. The solution pH was adjusted to 7.4 using an aqueous HEPES buffer solution having an effective concentration of 1.0 mM. The basic equation (2.3) for determination of the ligand–metal complexation is:

$$D + nM = C \qquad (2.3)$$

where D is the ligand molecule; M is the metal ion, and C is the complex. The binding constant K of the metal complex was determined by Eq. (2.4), assuming the concentration of free metal is about equal to its total concentration ($[M] \approx [M]_t$),

$$I - I_0 \,/\, I - Im = [C]/[D] = K\,[M]^n \qquad (2.4)$$

where I_0, I, and I_m are the corrected fluorescence emission intensity (at λ = 500 nm for Al^{3+} and λ = 550 nm for Zn^{2+}) of the complex at initial, interval t, and the final state at which the complex was fully formed upon addition of metal ion, respectively. The binding constant K was determined from the plot of the linear regression of $\log[(I - I_0)/(I_m - I)]$ vs. log[M] in Eq.(2.5), derived from Eq. (2.4), to obtain the intercept as log K and the slope as n:

$$\log[(I - I_0)/(I_m - I)] = \log K + n \log[M] \qquad (2.5)$$

The apparent binding constant for the formation of the **L_3**-F complex was evaluated using the Benesi−Hildebrand (B−H) plot (equation 2.1). I_0 is the emission intensity of **L_3** at λ = 575 nm, I is the observed emission intensity at that particular wavelength in the presence of a certain

concentration of ion (C), I_{max} is the maximum emission intensity value that was obtained at that λ-value during titration with varying ion concentration, K is the apparent binding constant (M^{-1}) and was determined from the slope of the linear plot, and C is the concentration of ion added during titration studies.

2.3.3. Detection Limit of L_3 for different ions

The detection limit was calculated on the basis of the fluorescence titration. The fluorescence emission spectrum of **L_3** was measured 10 times, and the standard deviation of blank measurement was achieved. To gain the slopes, the ratios of the emission intensities at respective λ's were plotted against the concentration of different ions. The detection limits were calculated using the equation 2.2.

2.3.4. X-ray crystallography

Block shaped crystal of suitable size was selected from the mother liquor and immersed in silicone oil, and it was mounted on the tip of a glass fiber and cemented using epoxy resin. The intensity data were collected using a Bruker SMART APEX-II CCD diffractometer, equipped with a fine focus 1.75 kW sealed tube Mo-Kα radiation (λ = 0.71073 Å) at 298(3) K, with increasing ω (width of 0.3° per frame) at a scan speed of 5 s per frame. The SMART software was used for data acquisition. Data integration and reduction were undertaken with SAINT and XPREP[2.5] software. Multi-scan empirical absorption corrections were applied to the data using the program SADABS.[2.6] Structures were solved by direct methods using SHELXS-97[2.7] and refined with full-matrix least-squares on F2 using SHELXL-97. All non-hydrogen atoms were refined anisotropically and hydrogen atoms attached to all carbon atoms were geometrically fixed and the positional and temperature factors were refined isotropically. Structural illustrations have been drawn with MERCURY-1.3 for Windows.[2.8]

2.3.5. Cytotoxicity assay

The cytotoxic effect of **L_3**, **L_3**–Al complex and **L_3**–Zn complex on HeLa cells (human cervical carcinoma cells) was ascertained by MTT assay. MTT (3-(4,5-Dimethylthiazol-2-yl)-2,5-Diphenyltetrazolium Bromide) solution was procured from Sigma-Aldrich, USA. HeLa cells were initially grown in 25 cm^2 tissue culture flask in Dulbecco's modified Eagle medium (DMEM) supplemented with 10% (v/v) fetal bovine serum (FBS), penicillin (100g/mL) and streptomycin (100µg/mL) at 37◦C in a CO_2 incubator. Subsequently, the cells were seeded onto 96-well tissue culture plates (approximately 10^4 cells per well) and incubated with various concentrations of compound **L_3**, **L_3**–Al complex and **L_3**–Zn complex (10 µM, 20 µM, 30 µM, 40 µM, 50 µM and

100 μM) made in DMEM for a period of 24h. HeLa cells treated with DMSO or the metal salts were also included in parallel sets as control. Following 24 h incubation, the growth media was carefully aspirated and fresh DMEM containing MTT solution was added to the cells and incubated for 4 h at 37°C. Subsequently, the MTT solution was carefully removed and the insoluble colored formazan product was solubilized in DMSO and its absorbance was measured in a microtitre plate reader (Infinite M200, TECAN, Switzerland) at 550 nm. MTT assay for every sample was performed in six sets. Data analysis and calculation of standard deviation was performed with Microsoft Excel 2010 (Microsoft Corporation, USA).

2.3.6. Cell imaging studies

Initially HeLa cells were propagated in a 25 cm^2 tissue culture flask containing DMEM medium supplemented with 10% FBS, penicillin (100μg/mL) and streptomycin (100μg/mL) in a CO_2 incubator. Prior to imaging studies, the cells were seeded into a 6 well plate and grown in DMEM medium at 37°C till 80% confluency in a CO_2 incubator. Subsequently, the cells were washed thrice with sterile phosphate buffered saline (PBS) and incubated with 25 μM **L_3** in DMEM at 37◦C for 1 h in a CO_2 incubator. The cells were again washed thrice with sterile PBS to remove excess ligand and bright field and dark field images were recorded in separate sets using an epifluorescence microscope (Nikon eclipse Ti) having a filter that allowed blue light excitation and UV excitation. The cells were subsequently incubated in sterile PBS in separate sets with either 50 μM of aluminium nitrate or 50 μM of zinc nitrate salt for 1 h. Following in incubation, the cells were washed thoroughly with sterile PBS. Bright field and dark field images of the cells were again recorded in an epifluorescence microscope using blue light excitation (green emission) for Al(III) and UV excitation (yellow emission) for Zn(II).

2.4.1. UV−visible and Fluorescence Spectroscopic Studies of L_4

Stock solutions of various metal ions (1×10^{-3} $molL^{-1}$) were prepared in deionized water. Perchlorate, chloride or nitrate salts of metal ions were used to prepare metal stock solutions. A stock solution of **L_4** (1×10^{-3} $molL^{-1}$) was prepared in DMSO. The solution of **L_4** was then diluted to 1×10^{-6} $molL^{-1}$ with aqueous HEPES buffer (5 mM, pH 7.4). All the spectroscopic experiments were performed in mixed solvent medium methanol: HEPES buffer (2:3) medium (5 mM, pH 7.2) containing 0.33% of DMSO. In titration experiments, a solution of **L_4** (1×10^{-6} $molL^{-1}$) was filled in a quartz optical cell of 1.0 cm optical path length, and the ion stock solutions were added gradually to achieve a concentration of 1×10^{-5} $molL^{-1}$. In selectivity experiments, the test samples were prepared by interacting appropriate amounts of the cations stock into 2 mL of **L_4** solution (2×10^{-5} $molL^{-1}$). For all the samples, the spectra were recorded following 1 min of the addition of

the ions. For fluorescence measurements, excitation wavelength was set at 640 nm and emission was recorded from 650 nm to 900 nm. The selective binding of **L_4** with Al^{3+} among all other metal ions was also studied by fluorescence emission spectroscopy of the solution of **L_4** (10.0×10^{-6} $molL^{-1}$) in the absence and presence of an excess (10 eq.) of each of the metal ions in mixed solvent.

2.4.2. Evaluation of the Apparent Binding Constant for the Formation of $L_4 \cdot Al^{3+}$

A stock solution of $Al(NO_3)_3$, having a concentration of 0.5×10^{-3} $molL^{-1}$, in an aqueous HEPES buffer (pH 7.4) solution was used. Receptor **L_4** with an effective concentration of 10.0×10^{-6} $molL^{-1}$ in the aforementioned HEPES buffer medium was used for the emission titration studies. The effective Al^{3+} concentration was varied between 0 and 10×10^{-5} $molL^{-1}$ for this titration. The solution pH was adjusted to 7.4 using an aqueous HEPES buffer solution having an effective concentration of 5.0 mM.

The apparent binding constant for the formation of the respective complexes were evaluated using the Benesi−Hildebrand (B−H) plot (equation 2.1). I_0 was taken as the emission intensity of **L_4** at λ = 730 nm, I is the observed emission intensity at that particular wavelength in the presence of a certain concentration of the metal ion (C), I_{max} is the maximum emission intensity value that was obtained at λ = 730 nm during titration with varying metal ion concentration, K is the apparent binding constant (M^{-1}) and was determined from the slope of the linear plot, and C is the concentration of the Al^{3+} ion added during titration studies.

2.4.3. Detection Limit for Al^{3+} ion

The detection limit was calculated on the basis of the fluorescence titration. The fluorescence emission spectrum of **L_4** was measured 10 times, and the standard deviation of blank measurement was achieved. To gain the slope, the ratio of the emission intensity at 730 nm was plotted as a concentration of Al^{3+}. The detection limit was calculated using equation 2.2, where σ is the standard deviation of blank measurement, and k is the slope between the ratio of emission intensity versus [Al^{3+}].

2.4.4. Cytotoxicity assay for L_4 and L_4-Al^{3+} complex

A standard MTT assay was performed to determine the cytotoxic effect of **L_4** and **L_4**–Al^{3+} complex on HeLa cells. MTT (3-(4,5-Dimethylthiazol-2-yl)-2,5-Diphenyltetrazolium Bromide) solution was procured from Sigma-Aldrich, USA. Initially HeLa cells were grown in 25 cm^2 tissue culture flask in Dulbecco's modified Eagle medium (DMEM) supplemented with 10% (v/v) fetal bovine serum (FBS), penicillin (100g/mL) and streptomycin (100µg/mL) at 37◦C in a CO_2

incubator. Prior to MTT assay, cells were seeded onto 96-well tissue culture plates (approximately 10^4 cells per well) and incubated with various concentrations of compound **L_4** and **L_4**–Al^{3+} complex (5.0 µM, 12.5 µM, 15 µM, 25 µM and 50 µM) made in DMEM for a period of 24h. HeLa cells treated with DMSO or $Al(NO_3)_3$ alone were also included in parallel sets. Following 24 h incubation, the growth media was carefully aspirated and fresh DMEM containing MTT solution was added to the cells and incubated for 3–4 h at 37◦C. Subsequently, the MTT solution was removed and the insoluble colored formazan product was solubilized in DMSO and its absorbance was measured in a microtitre plate reader (Infinite M200, TECAN, Switzerland) at 550 nm. MTT assay for every sample was performed in six sets. Data analysis and calculation of standard deviation was performed with Microsoft Excel 2010 (Microsoft Corporation, USA).

2.4.5. Detection of Al^{3+} in HeLa cells by fluorescence microscope analysis

HeLa cells (human cervical carcinoma cells) were initially cultured in a 25 cm^2 tissue culture flask containing DMEM medium supplemented with 10% FBS, penicillin (100 µg/mL) and streptomycin (100 µg/mL) in a CO_2 incubator. Prior to cell imaging studies, HeLa cells were seeded into a 6 well plate and grown in DMEM medium at 37°C till 80% confluency in a CO_2 incubator. The cells were then washed thrice with sterile phosphate buffered saline (PBS) and DAPI stain (6.0 µM in PBS) was added to the cells and incubated for 5 min. The cells were again washed with sterile PBS to remove excess DAPI stain. Subsequently the cells were incubated with 25 µM **L_4** in DMEM at 37°C for 1 hr in a CO_2 incubator. The cells were then washed with sterile PBS in order to remove excess **L_4** and their images were acquired using a fluorescence microscope (Eclipse Ti–U, Nikon, USA) with a filter that allowed UV excitation for DAPI and green light excitation for ligand. The cells were further incubated for 1 hr with 50 µM $Al(NO_3)_3$ made in sterile PBS. The images of the cells were again acquired with a fluorescence microscope as mentioned earlier.

2.4.6. Interaction with calf thymus DNA (CT-DNA) and tracking DNase I activity

CT-DNA was procured from Sisco Research Laboratories (SRL, Mumbai) and a 1.0 mg/mL stock solution was made in nuclease-free MilliQ water. Deoxyribonuclease I (DNase I) ex Bovine pancreas was procured from Sisco Research Laboratories Pvt. Ltd., India. A stock solution of DNase I (10,000 Units/mL) was prepared in 10 mM HEPES-KOH (pH 7.9) supplemented with 30 mM $CaCl_2$, 30 mM $MgCl_2$ and 50% (v/v) glycerol. The DNase I treatment experiments were carried out in multiple sets in a reaction buffer consisting of 50 mM Tris-HCl (pH 7.5) solution supplemented with 10 mM $MgCl_2$. In these experiments, 500 ng of CT-DNA was interacted with 2.0 units of DNase I at 37°C for various time periods (0 min, 5 min, 10 min, 15 min, 20 min, 25

min and 30 min) in a total reaction volume of 40 µL. Following the specified incubation time, the reaction mixtures were added in separate sets to 1.0 mL solution of $\mathbf{L_4}$-Al^{3+} complex (2.5 µM) made in 5.0 mM HEPES buffer: MeOH (3:2) and the contents were mixed thoroughly by inverting the tubes. Subsequently, the fluorescence emission intensity of the samples was measured at an excitation wavelength of 640 nm and collecting the emission spectra in scanning mode from 660 nm to 800 nm.

2.5. Synthesis and characterization of the compounds

2.5.1. Synthesis of L_1

2,6-Diformyl-4-methylphenol was prepared by modification of the literature method.[2.1] Detail of the sources of the chemical, characterization data and analytical instrument used is listed earlier. The ligand $\mathbf{L_1}$ was synthesized following Scheme 3.1 as a deep red colored compound. $\mathbf{L_{1C}}$ was synthesized and characterized according to the reported procedure.[2.9]

^{1}H NMR [400 MHz, DMSO-d_6, J (Hz), δ (ppm)]: 9.12-9.10 (2H, d, J = 8), 8.68 (2H, s), 8.44-8.42 (2H, d, J = 8.4), 7.90-7.88(2H, d, J = 7.6), 7.73-7.71 (2H, d, J = 3.6), 7.53 (2H, s), 7.50-7.47 (2H, t, J = 8.8), 7.32 (2H, s), 2.26 (3H, s). ^{13}C NMR [100 MHz, DMSO-d_6, SiMe4, δ (ppm)]: 164.0, 155.1, 154.2, 147.1, 136.1, 130.9, 130.5, 128.9, 128.6, 127.0, 126.0, 124.1, 120.0, 110.8, 20.1. ESI-MS (positive mode, *m/z*) Calculated [$\mathbf{L_1}$+H_2O+H] = 435.4971, Found 435.4931.

2.5.2. Synthesis of L_2

The synthetic routes of the two compounds $\mathbf{L_2}$ and $\mathbf{L_{2C}}$ are depicted in scheme 4.1.

2.5.3. Synthesis of picolinichydrazide

Picolinic acid was dissolved in ethanol and in ice cold condition thionyl chloride was added drop wise over a period of 30 min with constant stirring. After 1 hour stirring, the hazy mixture was refluxed overnight. After evaporation of the solvent, water was added and the pH was adjusted to 8.0 by the addition of sodium bicarbonate. Subsequently the mixture was extracted with ethyl acetate (3x50 ml). The organic layer was dried over sodium sulphate and evaporation of the solvent gave the ethyl ester of picolinic acid as a colourless liquid. This ester was used without further purification. This ester was then treated with excess hydrazine monohydrate in ethanol. The mixture was heated to reflux for overnight. After evaporation of the solvent and the excess hydrazine under reduced pressure, a white solid was obtained, which was dried in vacuum and was used in the next step without further purification.

2.5.4. Synthesis of L_2

2,6-Diformyl-4-methylphenol (1 mmol) was dissolved in ethanol. Picolonic hydrazide (2 mmol) was added to the above solution and the mixture was refluxed for 4 hours to give a yellow crystalline product. Yield 72%. ^{1}H NMR [400 MHz, DMSO-d_6, δ (ppm)]: 11.47 (2H, s), 11.26 (1H, s), 7.84 (2H, s), 7.67 (2H, d, J = 4.4 Hz), 7.08 (2H, d, J = 7.6 Hz), 7.01 (2H, t, J= 7.8 Hz), 6.62 (2H, t, J = 5.8 Hz), 6.48 (2H, s), 1.25 (3H, s). ^{13}C NMR [100 MHz, DMSO-d_6, δ (ppm)]: 160.8, 155.0, 149.3, 148.8, 147.8, 138.2, 130.8, 128.4, 127.3, 122.9, 120.1, 20.0. ESI-MS (positive mode, *m/z*) Calculated for $C_{21}H_{19}N_6O_3$ [**L_2** +H] = 403.1519, Found 403.1546.

2.5.5. Synthesis of L_{2C}

Isophthaldehyde (1 mmol) was dissolved in ethanol, picolonic hydrazide (2 mmol) was added to the above solution and the mixture was refluxed for 4 hours to give a white crystalline product. Yield 75%. ^{1}H NMR [400 MHz, $CDCl_3$, δ (ppm)]: 11.09 (2H, s), 8.60 (2H, d, J=8 Hz), 8.32 (4H, d, J = 8.4 Hz), 8.17 (1H, s), 7.94-7.89 (4H, m, J = 3.6 Hz), 7.52-7.47 (3H, s). ^{13}C NMR [100 MHz, $CDCl_3$, $SiMe_4$, δ (ppm)]: 160.4, 149.2, 148.3, 148.1, 137.8, 134.4, 129.6, 129.3, 127.7, 127.0, 123.1. ESI-MS (positive mode, *m/z*) Calculated for $C_{20}H_{17}N_6O_2$ [**L_{2C}** +H] = 373.1413, Found 373.1426.

2.5.6. Synthesis of L_3

The synthetic route of **L_3** is illustrated in scheme 5.1. Quinaldicic acid was dissolved in ethanol and in ice cold condition thionyl chloride was added drop wise over a period of 30 min with constant stirring. After 1 hour stirring, the hazy mixture was refluxed overnight. After evaporation of the solvent, water was added and the pH was adjusted to 8.0 by the addition of sodium bicarbonate. Subsequently the mixture was extracted with ethyl acetate (3x50 ml). The organic layer was dried over sodium sulphate and evaporation of the solvent gave the ethyl ester of quinaldic acid as a colourless liquid. This ester was used without further purification. This ester was then treated with excess hydrazine monohydrate in ethanol. The mixture was heated to reflux for overnight. After evaporation of the solvent and the excess hydrazine under reduced pressure, a white solid was obtained, which was dried in vacuum and was used in the next step without further purification.

2,6-Diformyl-4-methylphenol (1mmol) was dissolved in ethanol. Quinaldicic hydrazide (2mmol) was added to the above solution and the mixture was refluxed for 4 hours to give a yellow product. ^{1}H NMR [400 MHz, $CDCl_3$, δ (ppm)]: 11.60 (1H, s), 11.23 (2H, s), 8.67 (2H, s), 8.37(2H, d), 8.32(2H, d), 8.17 (2H, d), 7.89 (2H, d), 7.82 (2H, q), 7.65 (3H, t), 1.69(3H,s). ^{13}C NMR [100 MHz, CDCl3, δ (ppm)]: 160.2, 155.8, 148.9, 146.6, 147.8, 138.0, 130.6, 129.9, 129.8,

129.1, 128.5, 128.0, 119.3, 20.4. ESI-MS (positive mode, *m/z*) Calculated [$\mathbf{L_3}$ +H]$^+$= 503.1832, Found 503.1867.

2.5.7. Synthesis of L_4

The receptor $\mathbf{L_4}$ was synthesized according to the step illustrated in Scheme 6.1.[2.10] The rationale guiding the design of the fluorescence-based sensor essentially involved the selection of a carbocyanine unit as an NIR-emissive fluorophore and tethering of an imidazole sidearm for metal chelation.

2.5.8. Synthesis of N-ethyl-2, 3, 3-trimethyl-3H-indolium iodide (1)

To a solution of 2,3,3-trimethyl-3H-indole (16 mmol) in acetonitrile, ethyl iodide (30 mmol) was added in a 50 mL round-bottomed flask. The mixture was heated under an N_2 atmosphere at 75 °C for 24 h. After being cooled to room temperature, the solid was filtered off and dried under vacuum to afford compound **1** (yield: 93 %), which was then used for next step reaction without further purification.

2.5.9. Synthesis of 2

At 0 °C, phosphorus oxychloride (0.12 mol) was added dropwise from a pressure-equalizing addition funnel to anhydrous DMF (0.17 mol). After 30 min, cyclohexanone (0.053 mol) was added and the mixture was refluxed for 1 h. Next, with constant cooling at 20 °C, an aniline/EtOH [1:1 (v/v), 18 mL] mixture was added drop wise. Reaction was continued for an additional 30 min after aniline addition, and then the deep purple mixture was poured into ice cold H_2O/ concentrated HCl (10:1, 150 mL). Crystals were allowed to form for 2 h in an ice bath, then filtered, washed with cold H_2O and Et_2O, and then dried *in vacuo*: yield 87%.

2.5.10. Synthesis of Cy.7.Cl (3)

N-ethyl-2, 3, 3-trimethyl-3H-indolium iodide (**1**) (2 mmol) and salt **2 (**1 mmol) were dissolved in 30 ml of absolute ethanol in an oven dried round bottom flask. Anhydrous sodium acetate (6 mmol) was added to the above mixture and the mixture was refluxed under N_2 atmosphere for 4 hours. After cooling overnight at -10 ^oC, the green crystals are filtered out, washed with water, with a little amount of cold ethanol and plenty of diethylether. Yield 81%. ^{1}H NMR ($CDCl_3$) δ (ppm) 1.47 (t, J=7.3 Hz, 6H), 1.73 (s, 12H), 2.02 (quint., J=6.6 Hz, 2H), 2.76 (t, J=6.6 Hz, 4H), 4.27(q, J=7.3 Hz, 4H), 6.22 (d, J=14.0 Hz, 2H), 7.16e7.46 (m, 8H), 8.36 (d, J=14.0 Hz, 2H). *m/z* 511.3.

2.1.4. Synthesis of L_4

Cy.7.Cl (1 mmol) was dissolved in 7 ml of dry DMF in an oven dried round bottom flask and to this 1-(3-Aminopropyl) imidazole (3 mmol) was added. The above mixture was stirred at 85 ^{o}C for 6 hours. The final solution was cooled to the room temperature and after that the solution was poured into 200 ml of ice cooled water with constant stirring. The resultant precipitate was collected through filtration. The crude product was separated by column chromatography. ^{1}H NMR ($CDCl_3$) δ (ppm): 0.79 (t, J= 7.2 Hz), 1.20 (t, J=7.2 Hz), 1.26 (t, J=6.6), 1.70 (s), 1.87 (T, J=6 Hz), 2.71 (quint., J=6 Hz), 3.47 (q, J=7.2 Hz), 5.54 (d, J=12.6 Hz), 6.52 (d, J= 7.8 Hz), 6.59 (d, J= 7.8Hz), 6.68 (d, J= 7.8 Hz), 6.73 (t, J= 7.2 Hz), 6.82 (t, J=7.2 Hz), 7.14 (m), 7.47 (d, J= 7.2 Hz), 8.45 (d, J= 13.2 Hz). ^{13}C-NMR ($CDCl_3$) δ (ppm): 11.2, 14.4, 22.6, 28.0, 28.7, 29.7, 30.3, 36.9, 38.7, 44.9, 45.9, 66.0, 92.3, 105.7, 11.8, 116.2, 118.0, 119.4, 121.8, 123.0, 125.2, 125.8, 127.7, 127.7, 127.8, 132.4, 137.3, 139.5, 144.6, 146.8, 152.0, 156.9, 165.0. *m/z* 600.44.

References

2.1. D. A. Denton, H. J. Suschitzky, *Chem. Soc.*, **1963**, 4741.

2.2. H. A. Benesi, J. H. Hildebrand, *J. Am. Chem. Soc.*, 1949, **71**, 2703.

2.3. A. K. Singh, A. Ramesh, *Food Microbiology.*, 2009, **26**, 504.

2.4. J. Sambrook, D.W. Russell, *Molecular Cloning: A Laboratory Manual*, 3rd ed.; Cold Spring Harbor: New York, 2001.

2.5. *Saint, Smart and XPREP*, Siemens Analytical X-ray Instruments Inc., Madison, Wisconsin, USA, 1995.

2.6. G. M. Sheldrick, *SADABS: software for Empirical Absorption* Correction, University of Gottingen, Institute fur Anorganische Chemieder Universitat, Tammanstrasse 4, D- 3400 Gottingen, Germany, 1999–2003.

2.7. (a) G. M. Sheldrick, *SHELXS-97*, University of Gottingen, Germany, 1997; (b) G. M. Sheldrick, *SHELXL-97, Program for Crystal Structure Refinement*, University of Gottingen, Germany, 1997.

2.8. *Mercury 1.3 Supplied with Cambridge Structural Database, CCDC*, Cambridge, U.K., 2003–2004.

2.9. J. Lewkowski, R. Skowronski, *Heteroatom Chemistry.*, 2001**, 12**, 27.

2.10. J. H. Flanagan Jr., S. H. Khan, S. Menchen, S. A. Soper, R. P. Hammer, *Bioconjugate Chem.*, 1997, **8**, 751.

Appendix

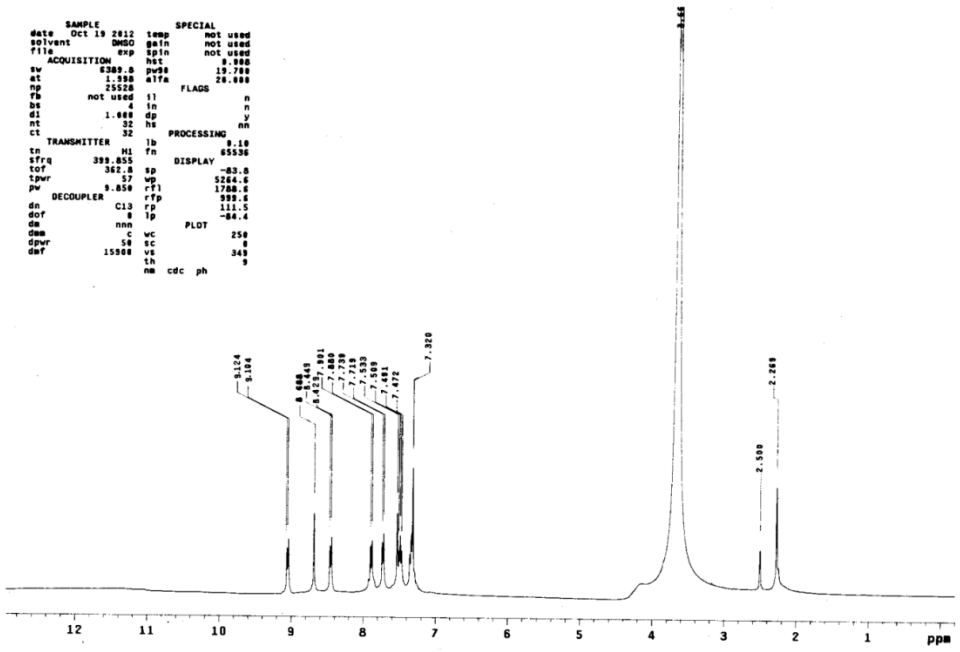

Figure A2.1. ^{1}H NMR spectrum of $\mathbf{L_1}$ in DMSO-d_6.

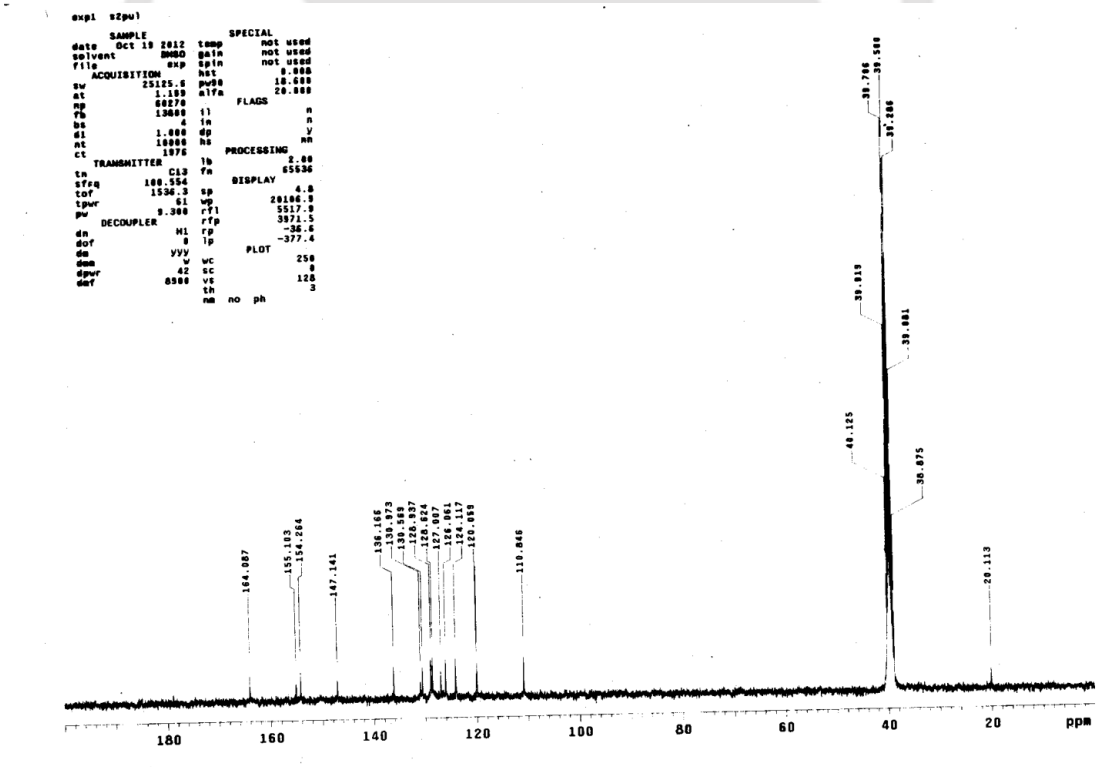

Figure A2.2. ^{13}C NMR spectrum of $\mathbf{L_1}$ in DMSO-d_6.

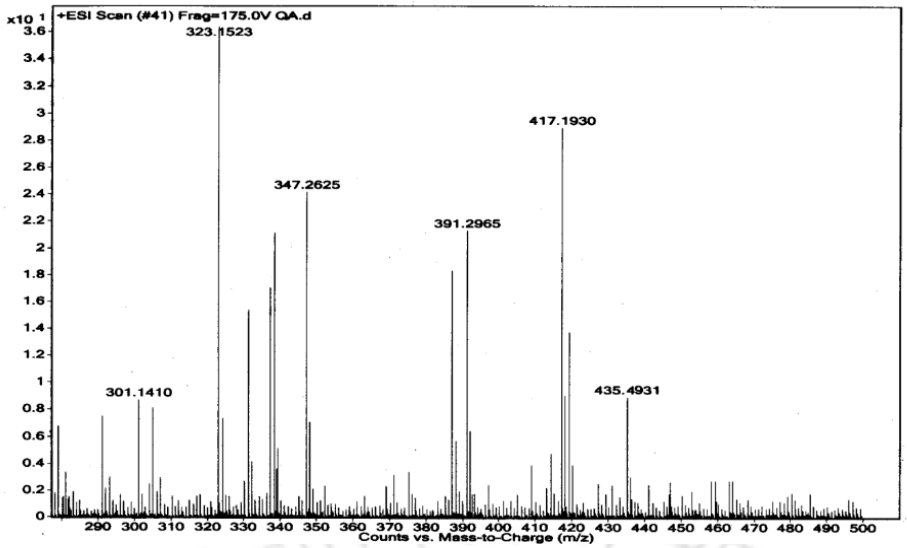

Figure A2.3. Mass spectrum of $\mathbf{L_1}$, Calculated [$\mathbf{L_1}$+H_2O+H] $^+$= 435.4971, Found 435.4931(Mass spectrum obtained in positive mode)**.**

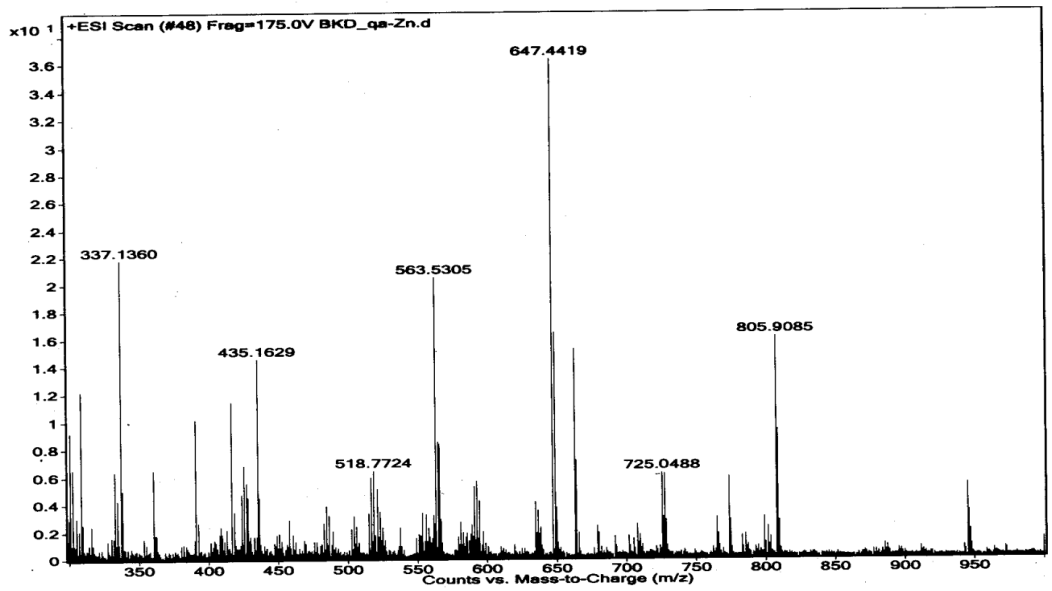

Figure A2.4. Mass spectrum of $\mathbf{L_1}$-Zn complex, Calculated [$\mathbf{L_1}$+2Zn+3Br+H_2O+2H] = 805.9891, Found 805.9085(Mass spectrum obtained in positive mode)**.**

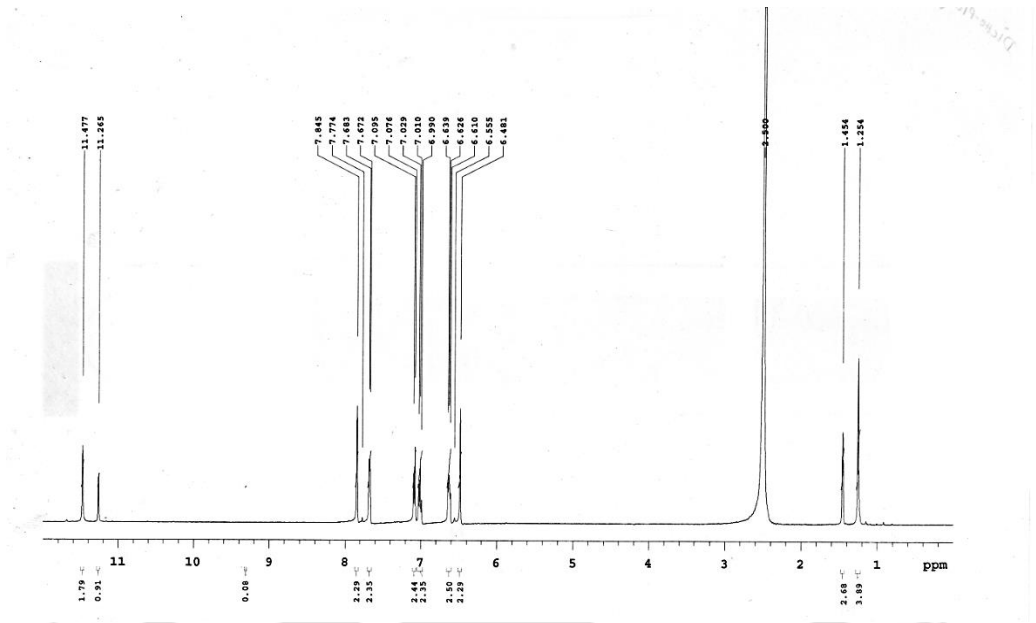

Fig. A2.5: ^{1}H- NMR spectra of $\mathbf{L_2}$ in DMSO-d_6.

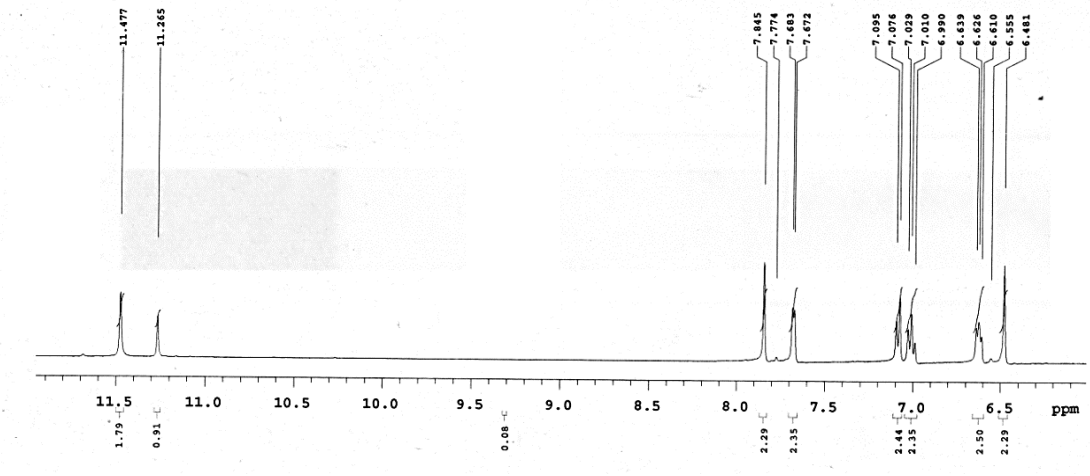

Fig. A2.6: Expanded ^{1}H- NMR spectra of $\mathbf{L_2}$ in DMSO-d_6.

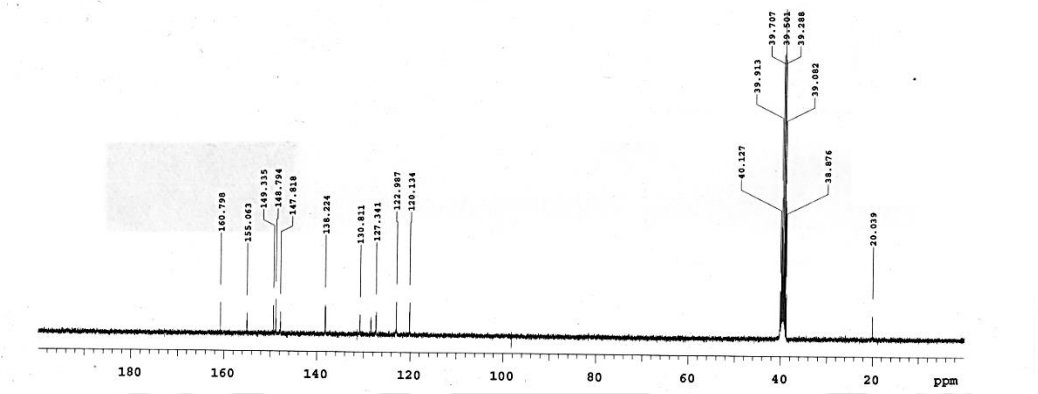

Fig. A2.7: ^{13}C- NMR spectra of $\mathbf{L_2}$ in DMSO-d_6.

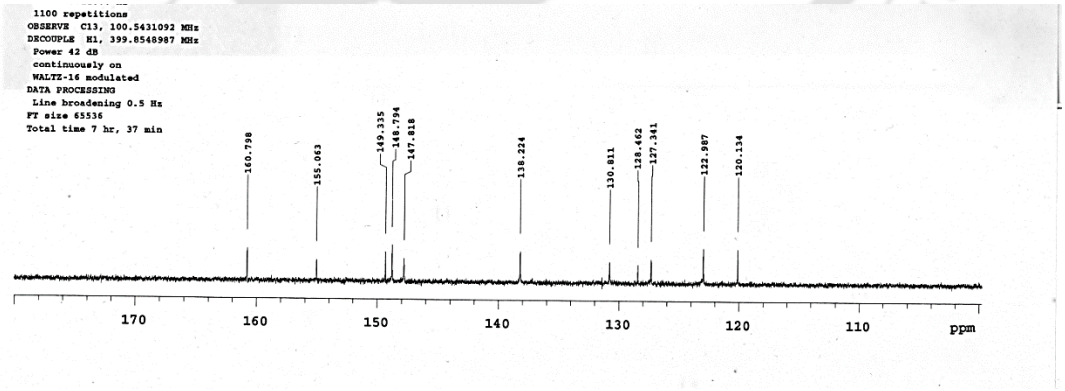

Fig. A2.8: Expanded ^{13}C- NMR spectra of $\mathbf{L_2}$ in DMSO-d_6.

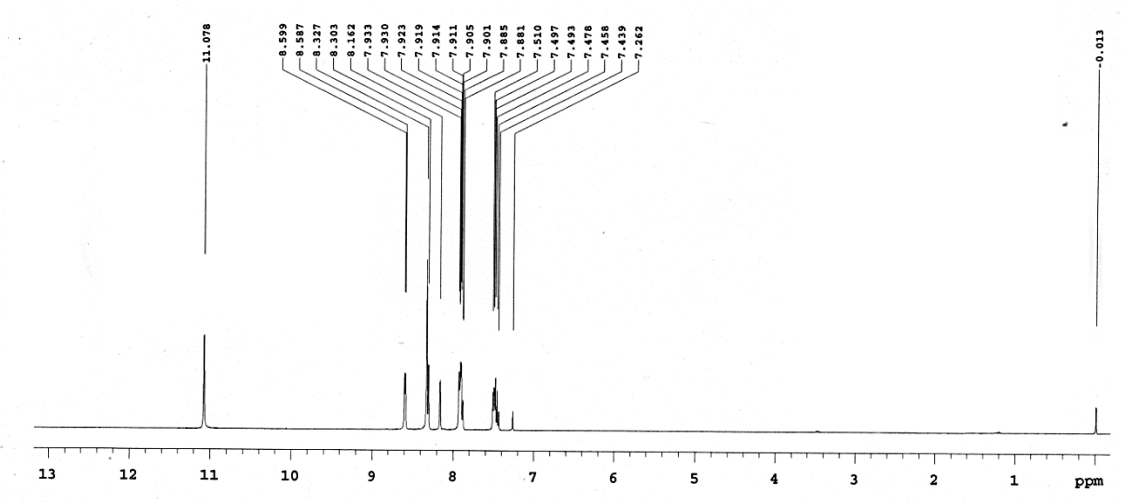

Fig. A2.9: ^{1}H- NMR spectra of $\mathbf{L_{2C}}$ in $CDCl_3$.

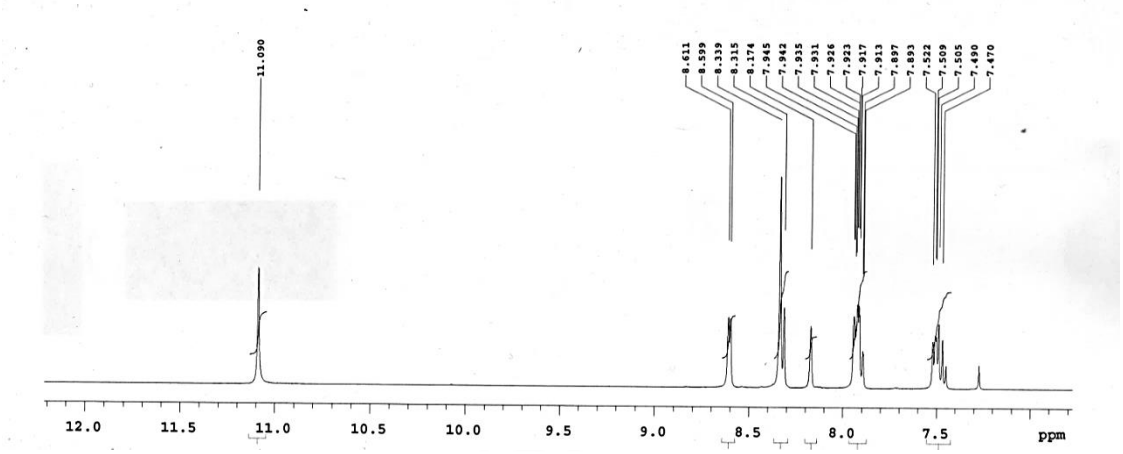

Fig. A2.10: Expanded ^{1}H- NMR spectra of $\mathbf{L_{2C}}$ in $CDCl_3$.

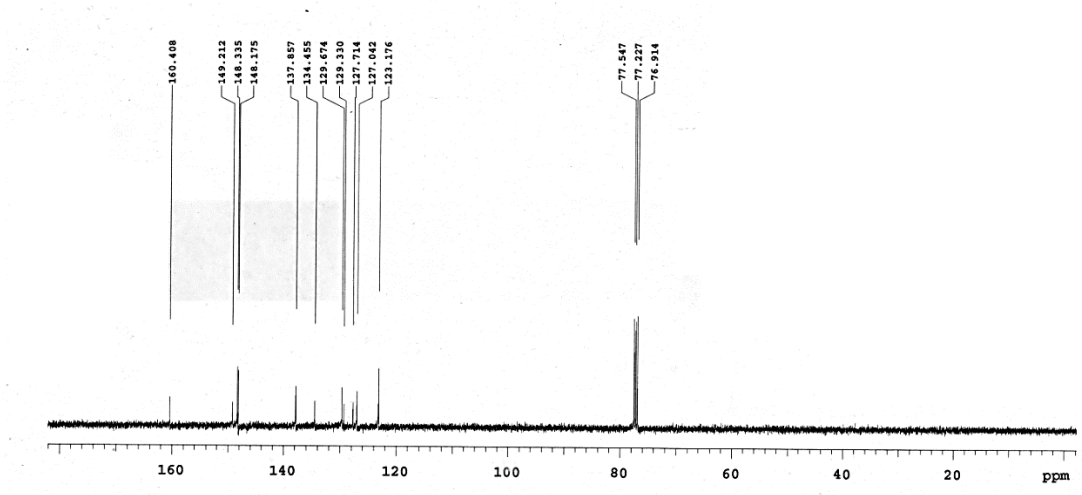

Fig. A2.11: ^{13}C- NMR spectra of $\mathbf{L_{2C}}$ in $CDCl_3$.

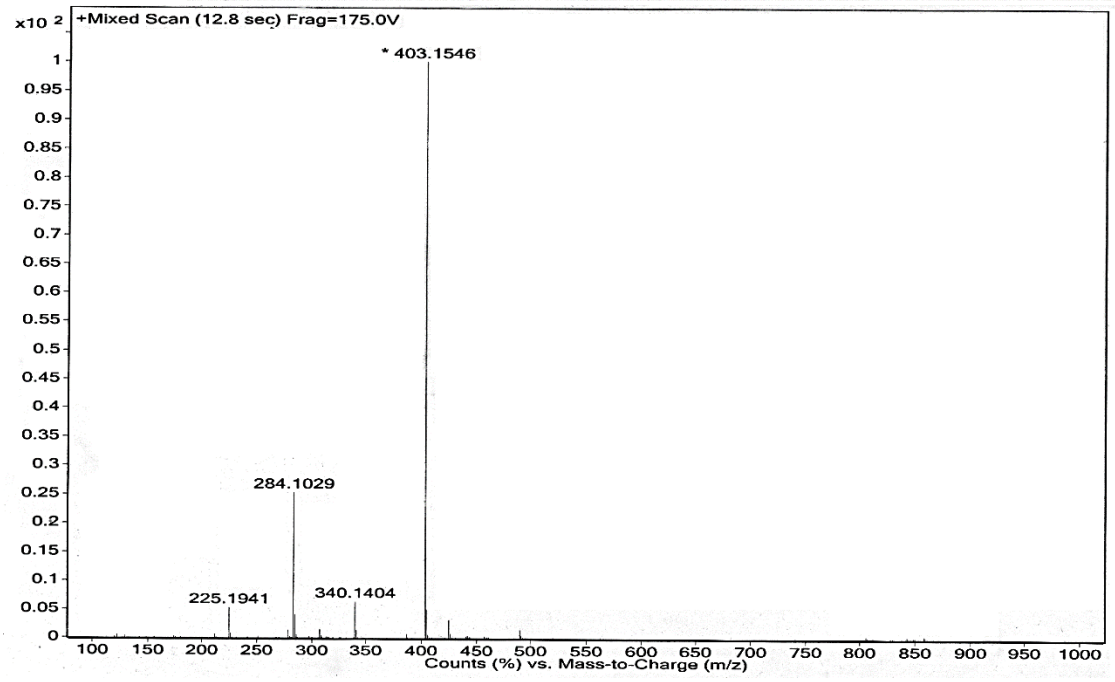

Fig. A2.12: Mass spectrum of $\mathbf{L_2}$ (positive mode), Expected *m/z* for $C_{21}H_{19}N_6O_3$ $(\mathbf{L_2}+H)^+$ = 403.1519, Found 403.1546.

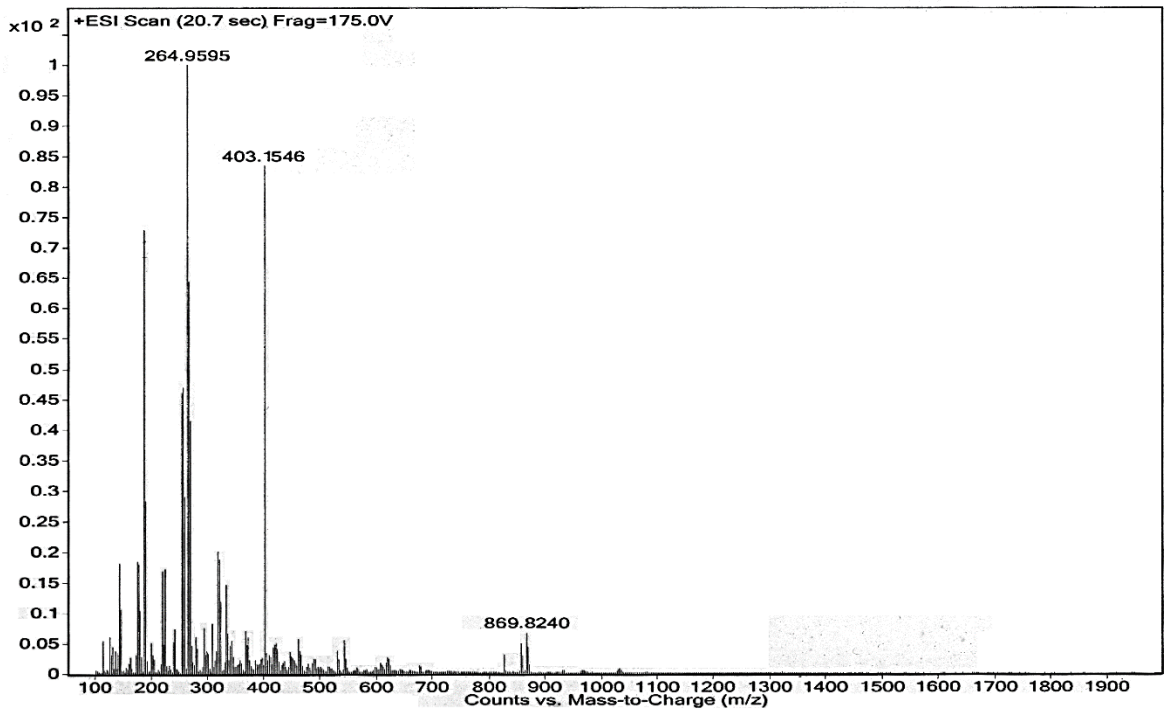

Fig. A2.13: Mass spectrum of zinc complex of $\mathbf{L_2}$ (positive mode). Expected *m/z* for $C_{23}H_{21}Cl_3N_7O_{15}Zn_2$ ($\mathbf{L_2}$+2Zn+3ClO_4+CH_3CN) = 869.8713, found 869.8240.

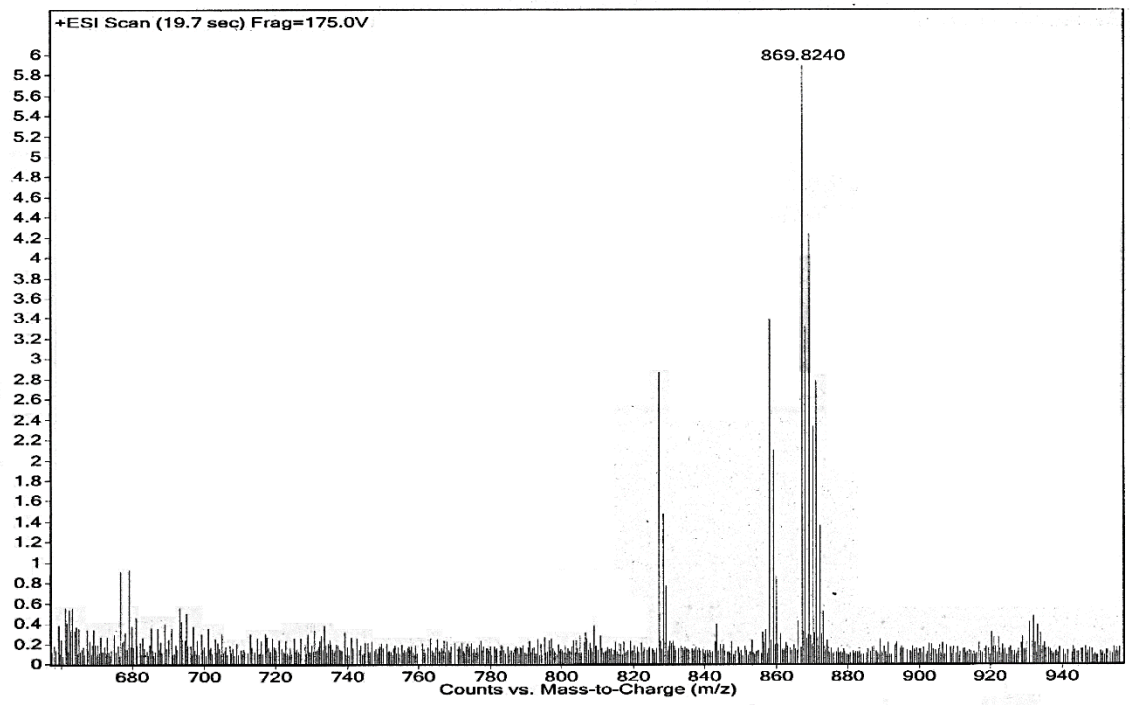

Figure A2.14. Expanded mass spectrum of zinc complex of $\mathbf{L_2}$ (positive mode).

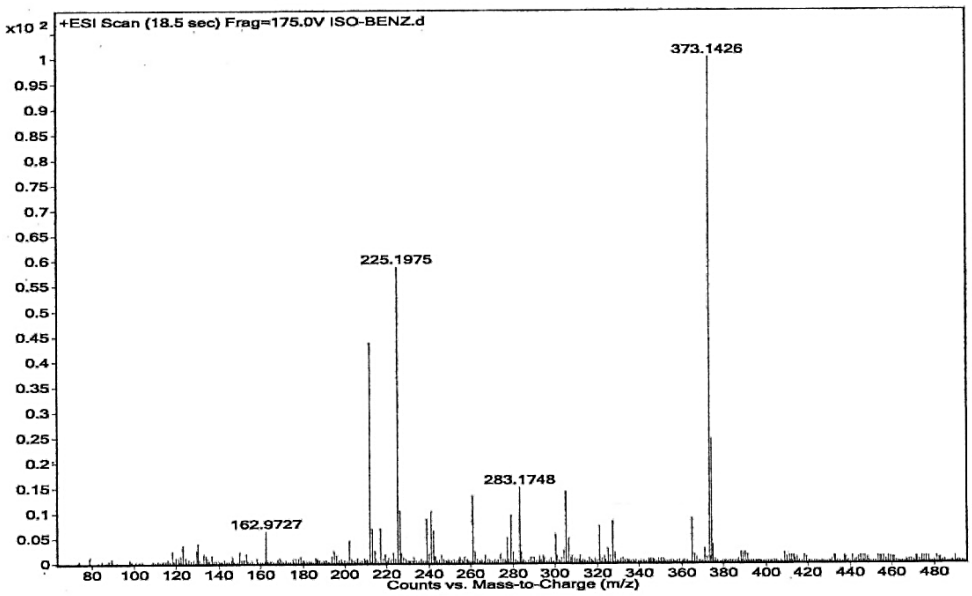

Fig. A2.15: Mass spectrum of $\mathbf{L_{2C}}$ (positive mode), Expected *m/z* for $C_{20}H_{17}N_6O_2$ $(\mathbf{L_{2C}}+H)^+$ = 373.1413, Found 373.1426.

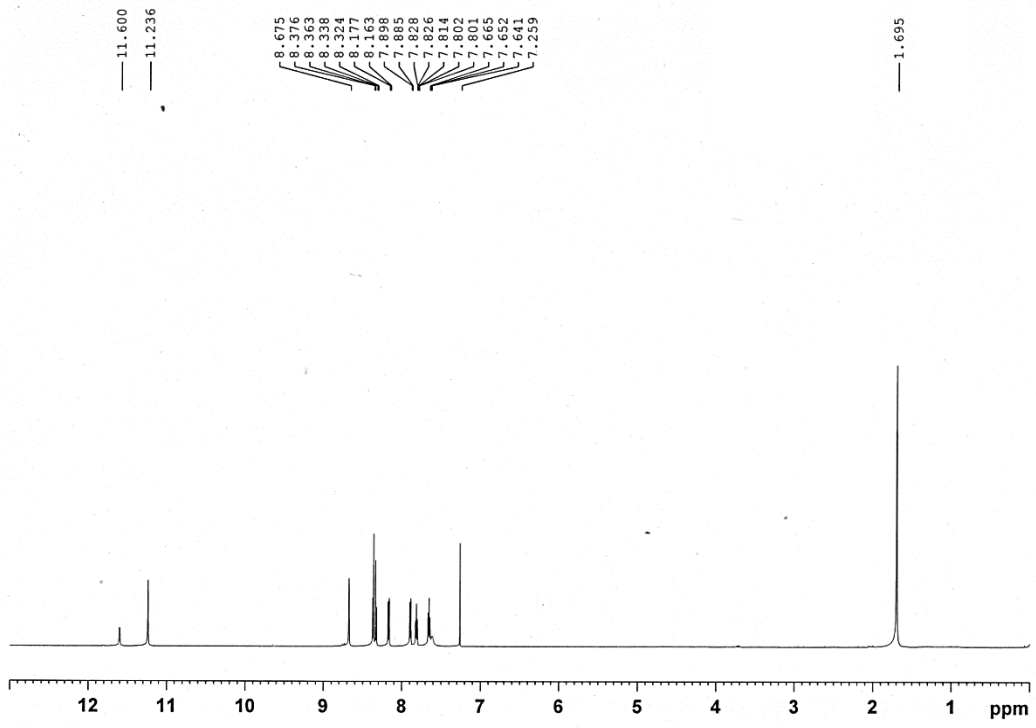

Fig A2.16: ^{1}H-NMR spectra of $\mathbf{L_3}$ in $CDCl_3$.

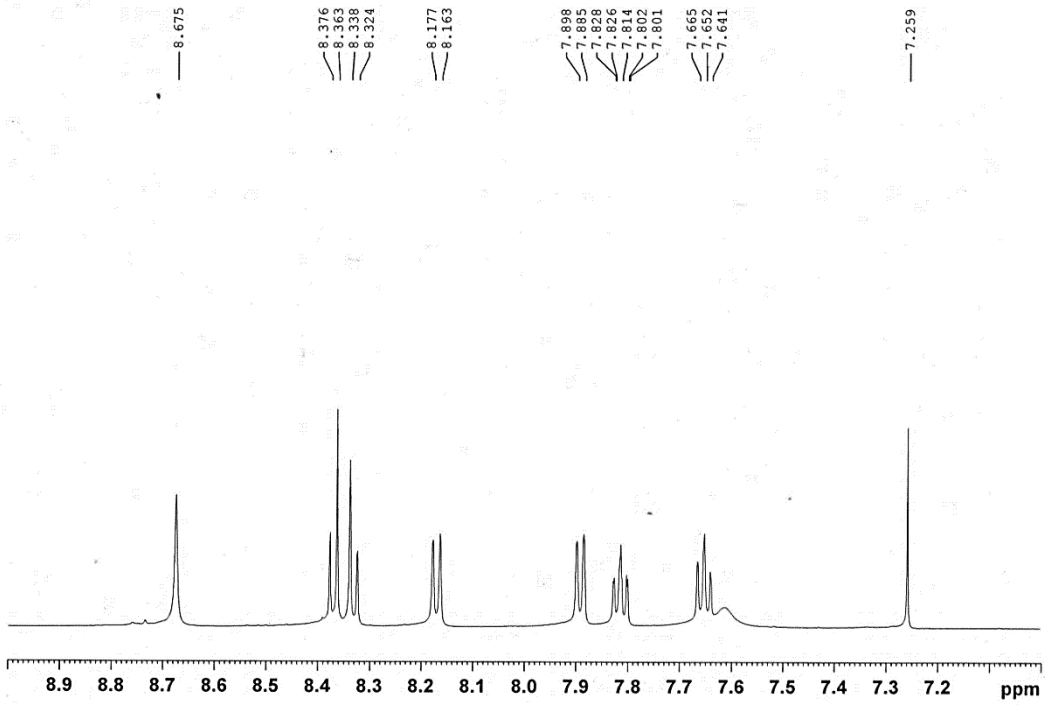

Fig A2.17: Expanded ^{1}H-NMR spectra of **L_3** in $CDCl_3$.

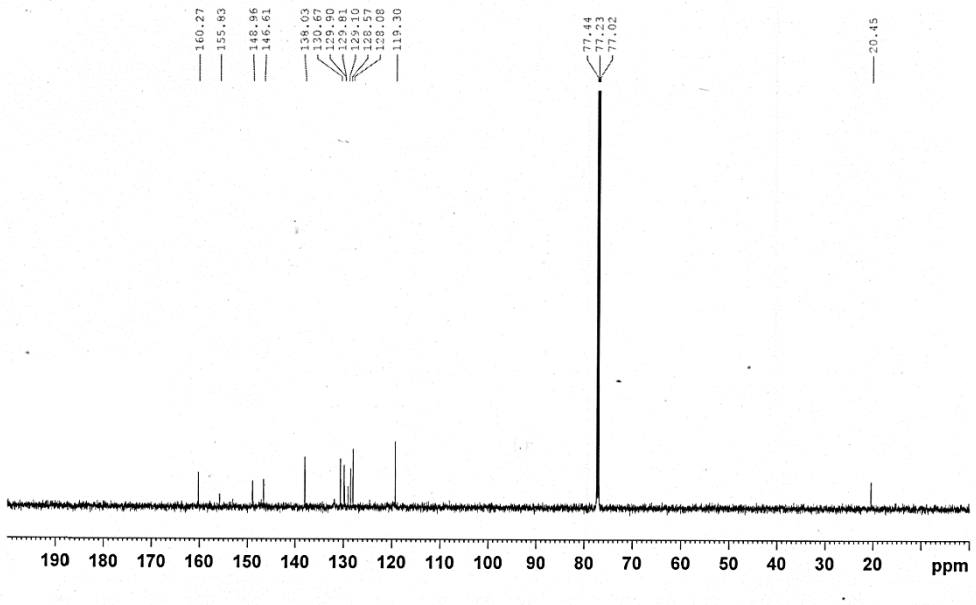

Fig A2.18: ^{13}C-NMR spectra of **L_3** in $CDCl_3$.

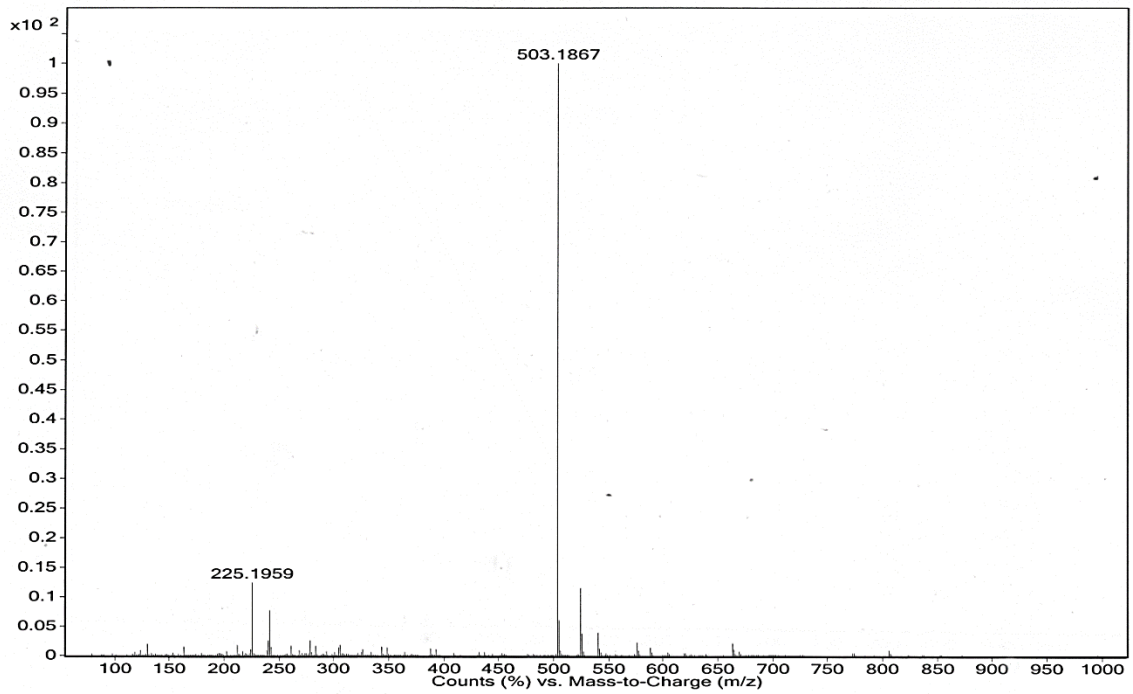

Fig A2.19: Mass spectrum of $\mathbf{L_3}$, Calculated $[\mathbf{L_3}+H]^+$= 503.1832, Found 503.1867 (Mass spectrum obtained in positive mode).

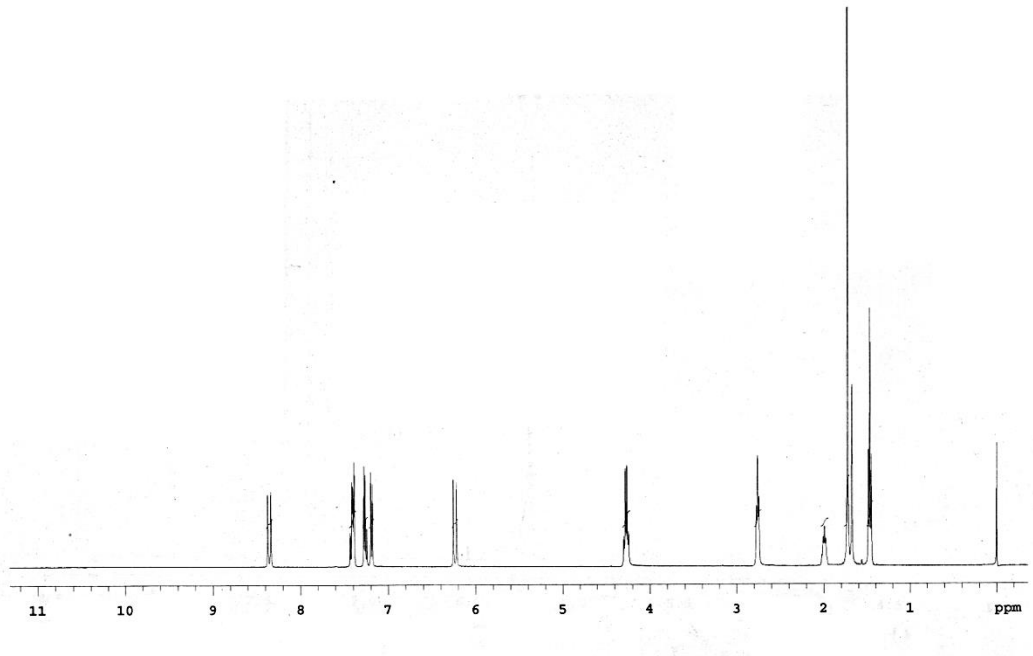

Figure. A2.20: ^{1}H-NMR of **3** in $CDCl_3$.

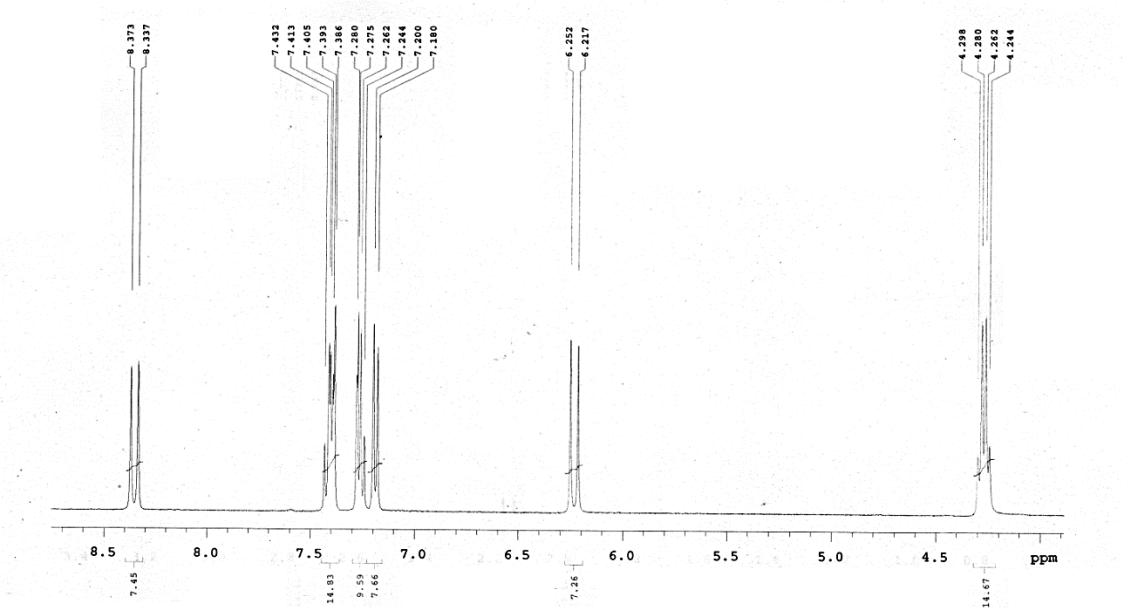

Figure. A2.21: Expanded ^{1}H-NMR of **3** in $CDCl_3$.

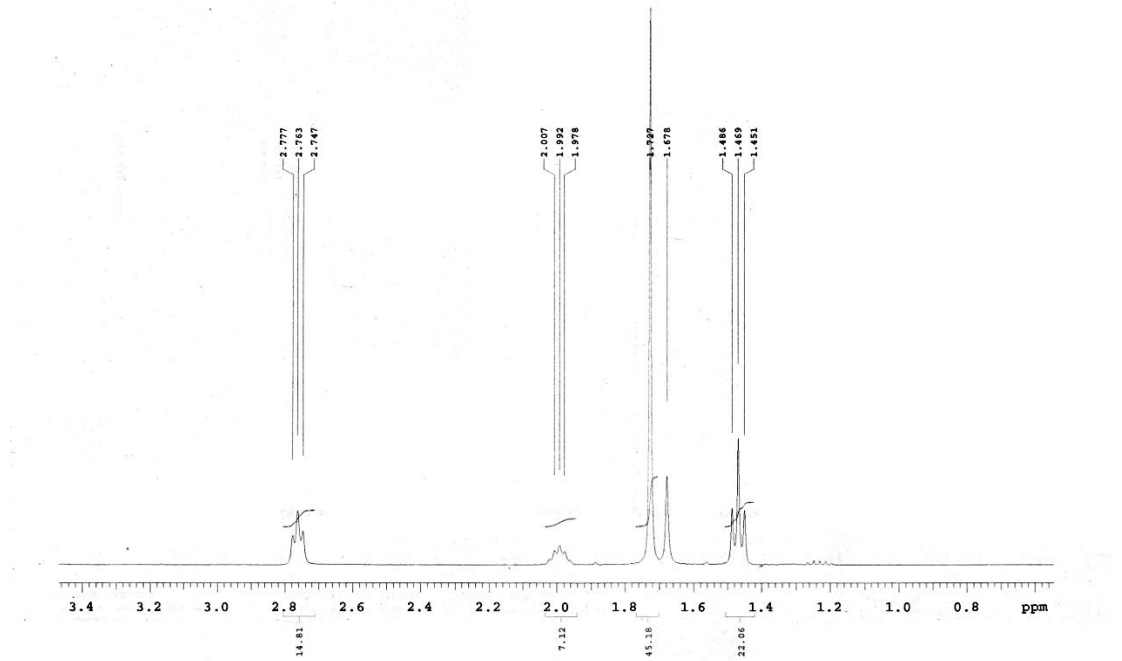

Figure. A2.22: Expanded ^{1}H-NMR of **3** in $CDCl_3$.

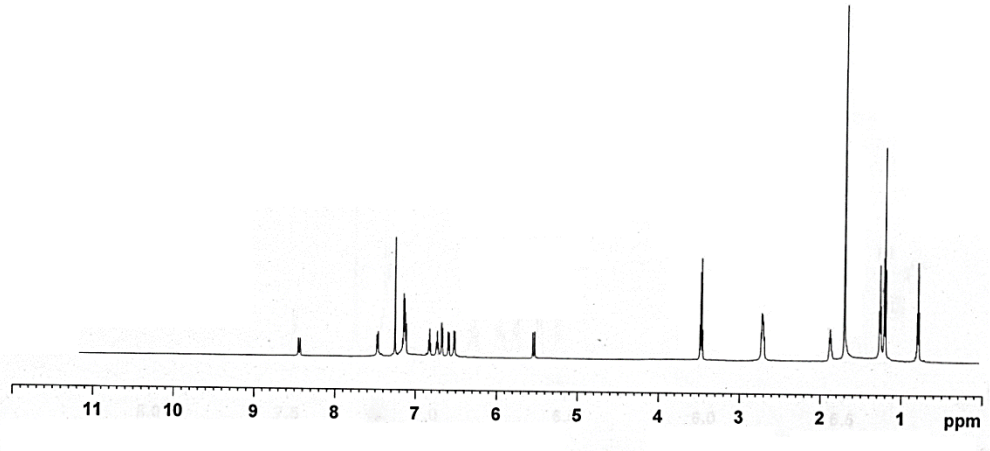

Figure. A2.23: ^{1}H-NMR of **L_4** in $CDCl_3$.

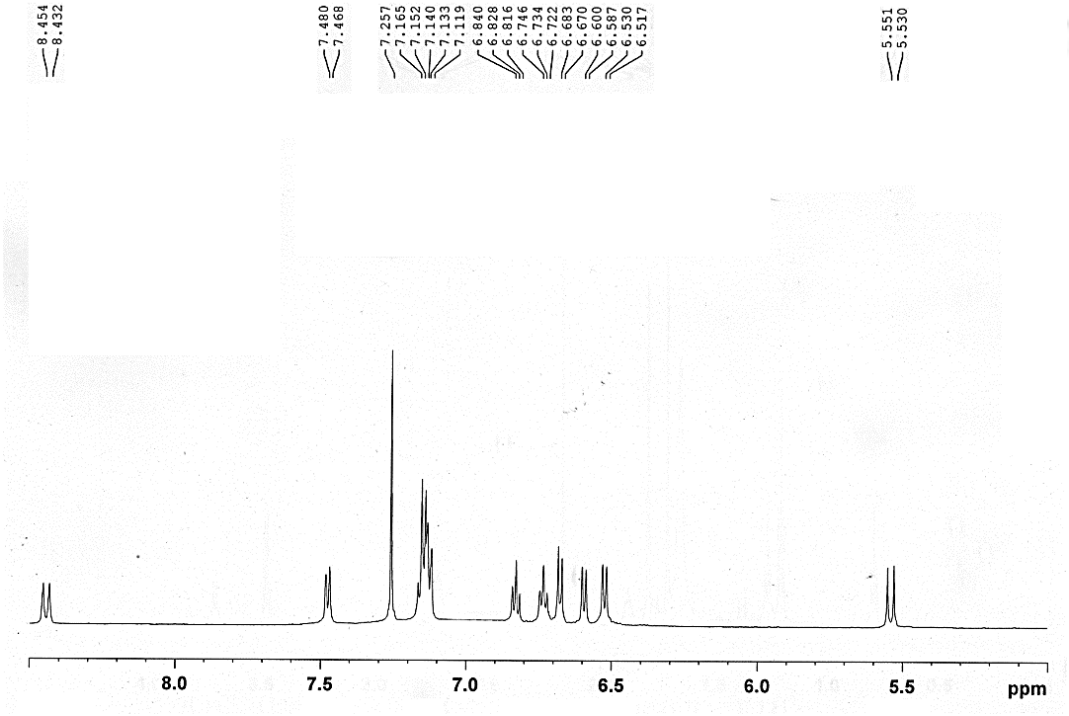

Figure. A2.24: Expanded ^{1}H-NMR of **L_4** in $CDCl_3$.

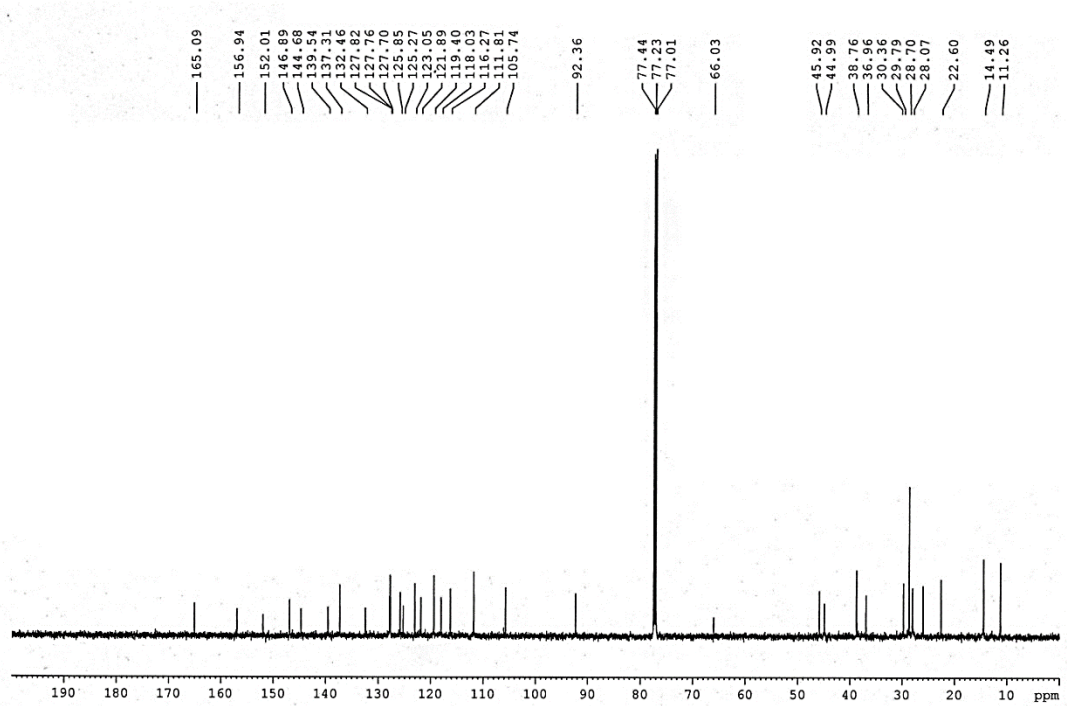

Figure. A2.25: ^{13}C-NMR of **L_4** in $CDCl_3$.

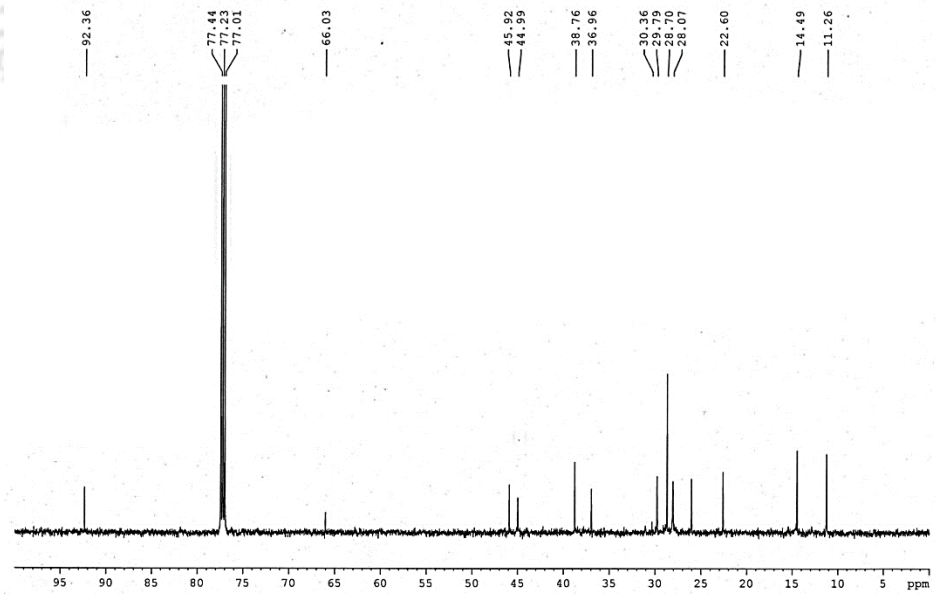

Figure. A2.26: Expanded ^{13}C-NMR of **L_4** in $CDCl_3$.

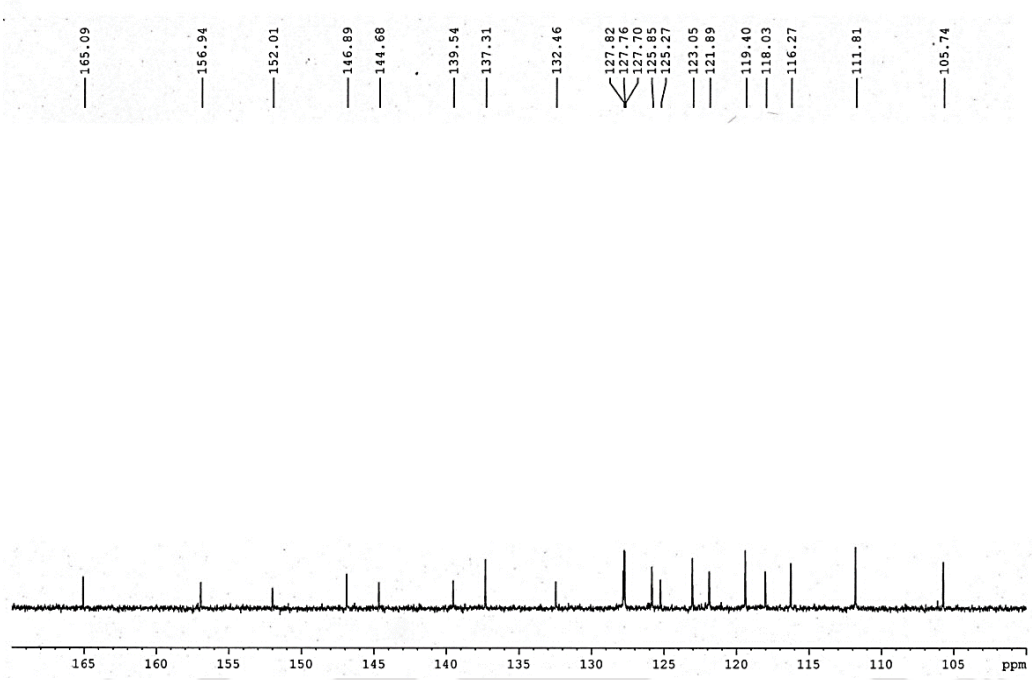

Figure. A2.27: Expanded ^{13}C-NMR of **L_4** in $CDCl_3$.

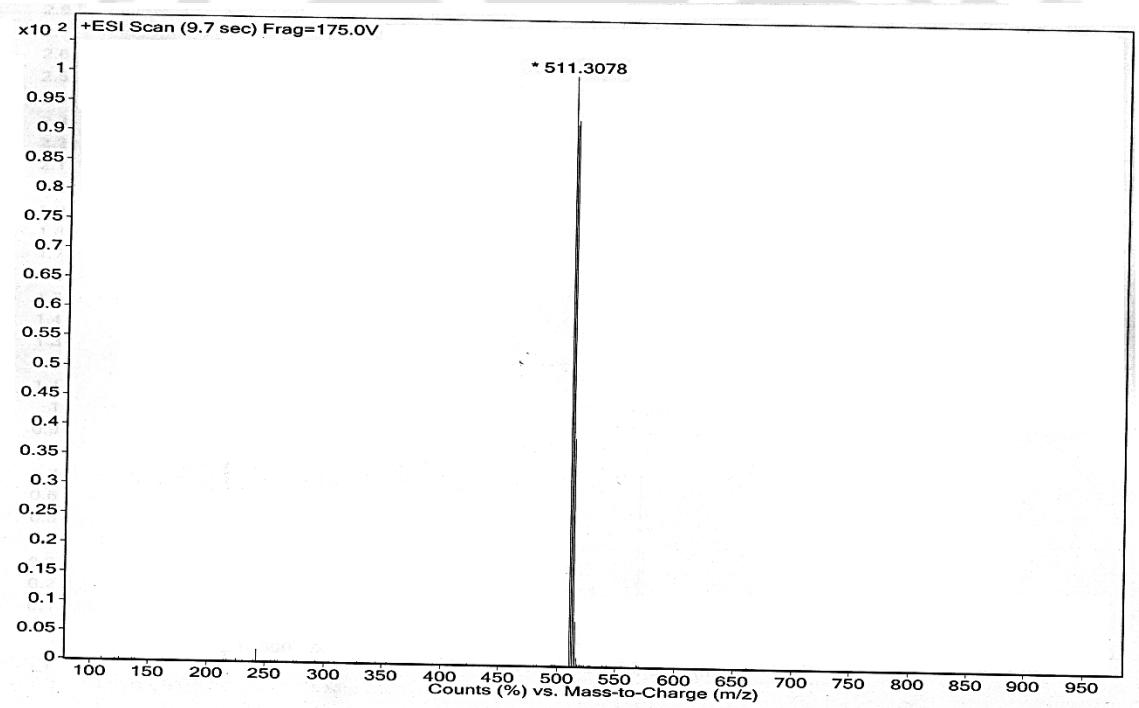

Figure. A2.28: ESI-MS spectra of **3**.

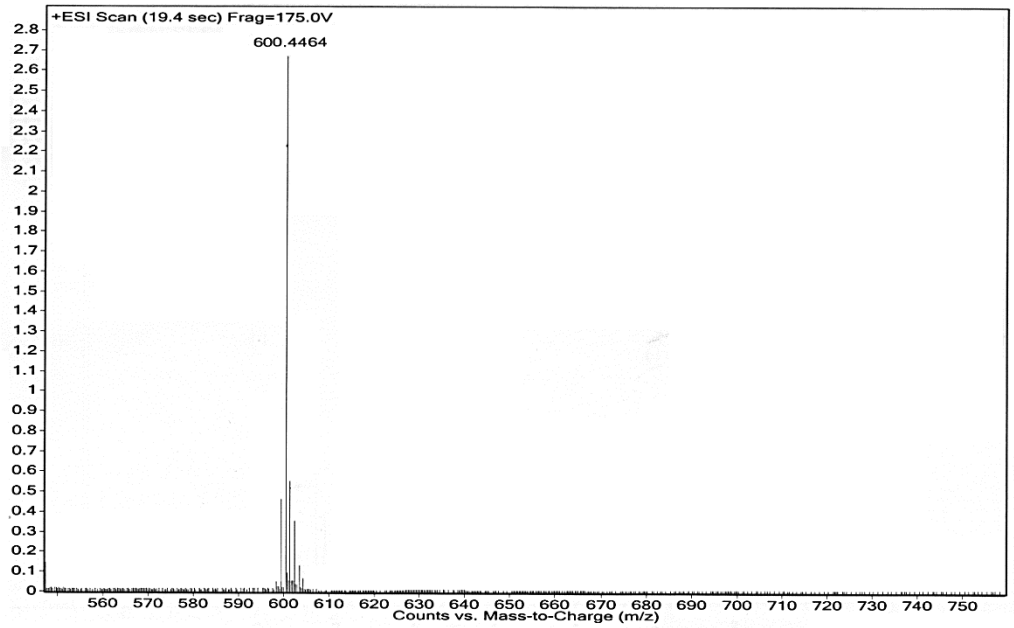

Figure. A2.29: ESI-MS spectra of **L_4**.

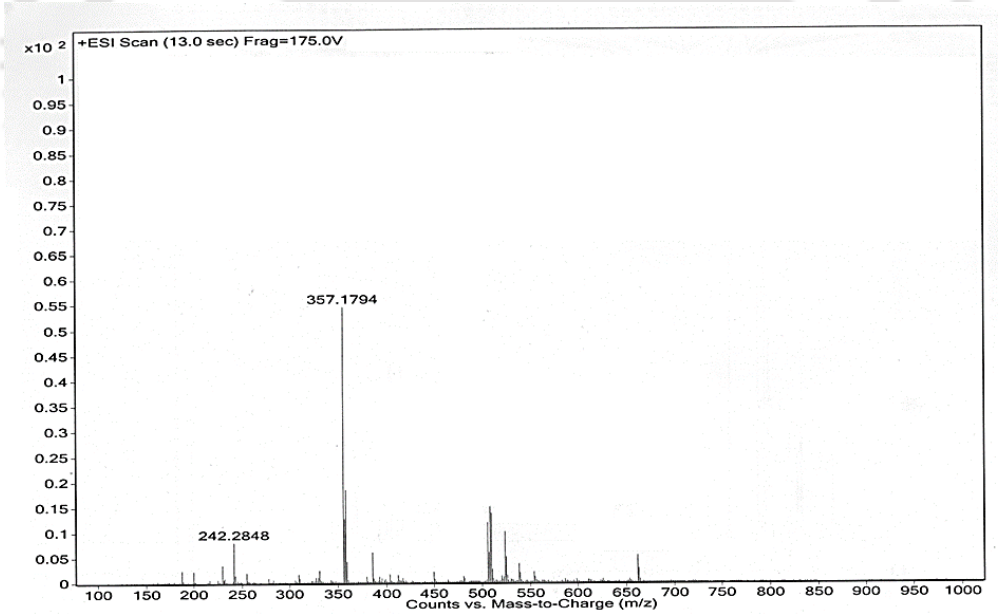

Figure. A2.30: ESI-MS spectra of **L_4-Al** complex.

Chapter 3

Zn^{2+} and Pyrophosphate Sensing: Selective Detection in Physiological Conditions and Application in DNA-Based Estimation of Bacterial Cell Numbers

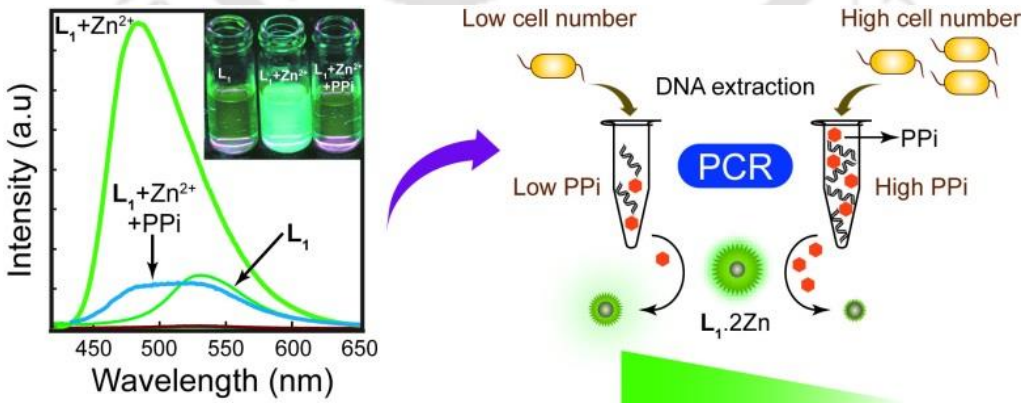

Chapter 3

3.1. Background and Focus of the Chapter

Zinc, is an essential element involved in a plethora of biological processes, such as cellular metabolism, neurotransmission, and apoptosis and is also implicated in the patho-physiological consequences manifested in many diseases.[3.1] Zinc has been known to act as a structural component of proteins or in the catalytic site of enzymes.[3.2] Zn^{2+} is an essential micronutrient whose deficiency can lead to impaired cognition, immune dysfunction, diarrhea, and death, particularly in children under the age of 5 years.[3.3] The human genome has been shown to encode two dozen Zn^{2+} specific transporters and many metal-buffering proteins, which are expressed in a tissue specific manner.[3.4] Zinc is also important for environmental safety as it is a harmful pollutant. [3.5] Recognizing the physiological significance of zinc and its biomedical relevance there is a growing interest in developing selective and sensitive zinc sensors. But, unlike other biologically important transition metal ions (*viz.* Fe^{2+}, Mn^{2+}, Cu^{2+}), Zn^{2+} ion is spectroscopically and magnetically neutral. Consequently, common analytical techniques, such as Mossbauer, NMR, and EPR are unable to detect a typical zinc ion in complex biological systems. Hence development of innovative methods for selective and sensitive detection of zinc ions in complex biological milieu is in great demand.[3.6, 3.7]

Development of selective and efficient signaling units for detection of various chemically and biologically important anions by colorimetric and fluorescent methods has been of considerable interest to chemists and biologists.[3.8] Notably, sensing of trace amounts of pyrophosphate (PPi) has come into limelight, given the fundamental role of PPi in many biological processes and in DNA sequencing applications.[3.9] In recent times, phosphate sensing using metal ion complexes has been adopted as a common strategy owing to the specific metal ion–anion interactions.[3.10] In this regard, the strong affinity of Zn^{2+} towards phosphates has been particularly exploited to develop fluorescence-based PPi sensors.[3.11] However, developing a sensor for PPi compatible with physiological condition and with high selectivity over other biologically important anions and structurally similar phosphates such as ATP, ADP, other nucleotide analogues and DNA is still a formidable challenge to the analytical chemist.

In this chapter we have described the synthesis, characterization and selective recognition behavior of a simple Schiff's base ($\mathbf{L_1}$) of a diformyl core with 8-amino quinoline. The ligand exhibits selectivity towards Zn^{2+} in mixed solvent medium. Sensing properties of the zinc complex, $\mathbf{L_1}$.2Zn has been exploited to recognize PPi selectively among the other biologically important phosphates in solution. We envisaged that the hydroxyl group and the N-atom of the

quinoline ring in $\mathbf{L_1}$ is responsible for the sensing behavior, which was further validated by employing a control compound $\mathbf{L_{1C}}$ (Scheme 3.1). The *in situ* formed zinc-complex can selectively detect PPi among all other anions even in the presence of an excess amount of other anions. In the context of biological application, the ability of $\mathbf{L_1}$.2Zn complex to sense minute levels of PPi has been explored to track DNA amplification in a prototype PCR setup. Finally, the potential of the developed PPi sensor to afford rapid bacterial cell estimation through DNA amplification reaction is also demonstrated in the present work.

All the materials used for synthesis were purchased from commercial suppliers and used without further purification. 2,6-Diformyl-4-methylphenol was prepared by modification of the literature method. [3.12] Detail of the sources of the chemical, characterization data and analytical instrument used is listed in the supporting information. The ligand $\mathbf{L_1}$ was synthesized following Scheme 3.1 as a deep red colored compound. $\mathbf{L_{1C}}$ was synthesized and characterized according to the reported procedure. [3.13]

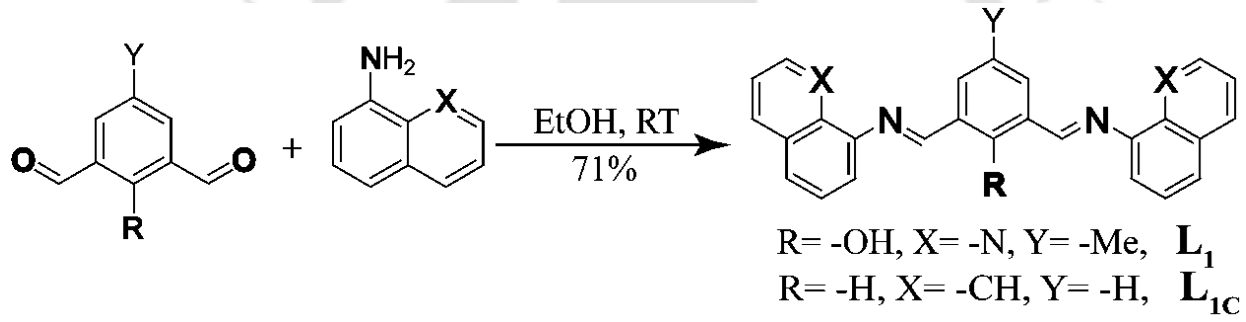

Scheme 3.1. Synthesis of the receptor $\mathbf{L_{1\text{-}1C}}$.

3.2. Absorption Spectroscopic Studies of $\mathbf{L_1}$ in Presence of Metal ions

$\mathbf{L_1}$ displayed two characteristic absorption peaks at ~350 nm and ~ 460 nm, which may be attributed to the π–π* transitions and long conjugation present in the polyaromatic system. Upon interaction with 5.0 equivalent of various metal ions (Na^+, K^+, Mg^{2+}, Ca^{2+}, Co^{2+}, Ni^{2+}, Cu^{2+}, Cd^{2+}, Ag^+, Pb^{2+}, Hg^{2+}, Al^{3+}, Cr^{3+}, Fe^{3+}, Zn^{2+}) only Zn^{2+} caused a change in the absorption spectra of $\mathbf{L_1}$ (Fig. 3.1a), indicating the specificity for Zn^{2+} ion. Upon addition of Zn^{2+} ion, the absorbance at ~350 nm decreases with an emergence of a new shoulder at ~430 nm, while absorbance at ~460 nm increases with two isosbestic points at 329 nm and 370 nm. Incremental addition of Zn^{2+} ion resulted in gradual increase in the absorption at ~ 430 nm and 450 nm while the absorption at 350 nm decreases gradually (Fig. 3.1b). The color of the solution changes from light yellow to deep yellow during the titration experiment (inset Fig. 3.1b).

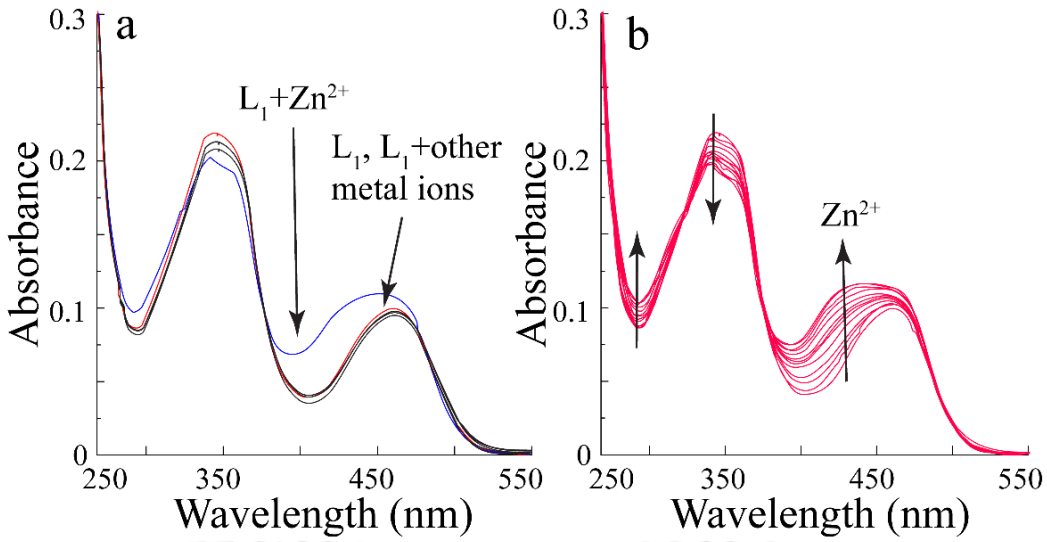

Figure 3.1. UV-Vis absorption of $\mathbf{L_1}$ upon addition of (a) 5.0 equivalent of various metal ions, (b) incremental addition of Zn^{2+}.

3.3. Emission Spectroscopic Studies of L_1 in Presence of Metal ions

Upon excitation at 350 nm, $\mathbf{L_1}$ exhibited a weak emission at ~540 nm. Addition of Zn^{2+} enhanced the emission intensity of $\mathbf{L_1}$ remarkably (Fig. 3.2a), while interaction with other metal ions resulted in considerable quenching of its emission band. Interestingly, this dramatic fluorescence change with only Zn^{2+} was visualized under UV lamp (inset Fig. 3.2b). This result also supports the specific interaction of $\mathbf{L_1}$ with Zn^{2+} as observed in UV-Vis studies. An incremental addition of

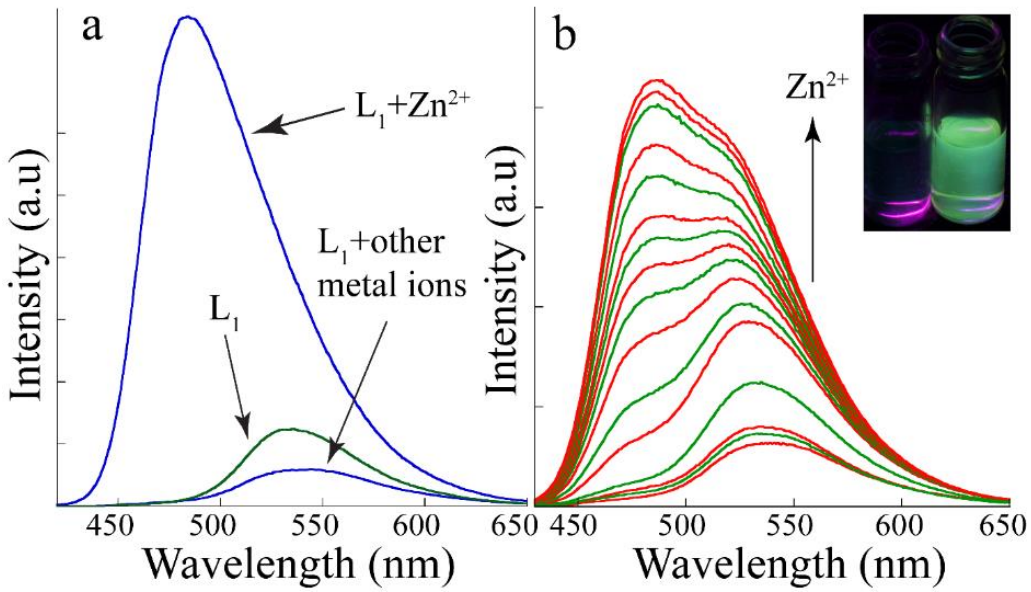

Figure 3.2. Changes in the fluorescence emission of $\mathbf{L_1}$ upon addition of (a) various metal ion solution; (b) Zn^{2+} ion.Inset: Changes in the fluorescence intensity (I_{480}) vs. [Zn^{2+}], inset (b) Visual changes in fluorescence of $\mathbf{L_1}$ in presence of Zn^{2+}.

Zn^{2+} (upto 2 eq.) led to the emergence of a new peak at ~480 nm with concomitant increase in the emission intensity at ~ 540 nm accompanied by a small blue-shift of the order of about 20 nm (Fig. 3.2b). Job's plot of the data revealed a 1:2 complex formation between $\mathbf{L_1}$ and Zn^{2+} (Fig. A3.1a.), which was also supported by ESI-MS experiment. The association constant [3.14] and detection limit of $\mathbf{L_1}$ for Zn^{2+} was observed to be 3.97×10^5 M^{-1} (Fig. A3.1b.) and approximately 56 ppb, respectively.

For a realistic appraisal of $\mathbf{L_1}$ as a specific Zn^{2+} sensor and for its potential application in the bio-analytical regime, the selectivity of the ligand for Zn^{2+} over other competing metal ions in the biological milieu is critical. Hence, the response of $\mathbf{L_1}$ towards Zn^{2+} over other metal ions was investigated in the presence of each of those metal ions (5eq.) mimicking the physiological condition. It was indeed encouraging to observe that the Zn^{2+} induced fluorescence of $\mathbf{L_1}$ was preserved in each of the cases clearly suggesting the high selectivity of $\mathbf{L_1}$ towards Zn^{2+} even in presence of these metal ions (Fig. A3.2a.).

Binding mode of $\mathbf{L_1}$ was investigated using ESI-MS experiment, the peak at *m/z* 805.9085 indicated the mass of [$\mathbf{L_1}$+2Zn+3Br+H_2O+2H] *i.e.* the 1:2 binding mode was re-established. Another peak at *m/z* 725.0488 indicated the mass of [$\mathbf{L_1}$+2Zn+2Br+H_2O+3H] (Fig. A3.5.). The proposed binding mode of the Zn^{2+} ion is illustrated in Scheme 3.2. In the absence of any metal ions intra ligand charge transfer (ICT) was prohibited within $\mathbf{L_1}$ which perhaps results in very low fluorescence. It is also possible that the weak fluorescence of $\mathbf{L_1}$ is a consequence of free rotation around the azomethine (C═N) carbon which brings flexibility within the ligand. As shown in Scheme 2, in presence of Zn^{2+}, $\mathbf{L_1}$ forms a rigid phenoxo-bridged binuclear zinc complex which switched-on the ICT process and restricts the free rotation around the azomethine carbon which results in enhancement of fluorescence intensity. A similar mode of metal ion binding was also recorded for analogous ligands. [3.15]

3.4. Spectroscopic Studies of $\mathbf{L_1}$.2Zn Complex in Presence of Various Anions

Given the selective recognition of zinc by $\mathbf{L_1}$ in physiological conditions even in a competitive environment, it was conceived that the generated binuclear $\mathbf{L_1}$.2Zn complex could be an effective binding ensemble for anions. This hypothesis was verified by UV-vis spectroscopy of $\mathbf{L_1}$.2Zn complex in the presence of different anions. Only a noticeable change in the absorption spectra of $\mathbf{L_1}$.2Zn was observed with PPi while the other anions did not affect the absorption spectra of $\mathbf{L_1}$.2Zn (Fig. 3.3a). Upon addition of PPi, the resulting spectra almost resembled the spectra of free $\mathbf{L_1}$ which suggested decomplexation of $\mathbf{L_1}$.2Zn and regeneration of $\mathbf{L_1}$. Titration of $\mathbf{L_1}$.2Zn complex with different concentration of PPi resulted in lowering of the intensity of the absorbance

bands at 430 nm and 450 nm, while the absorption peak at 350 nm increased marginally (Fig. 3.3b).

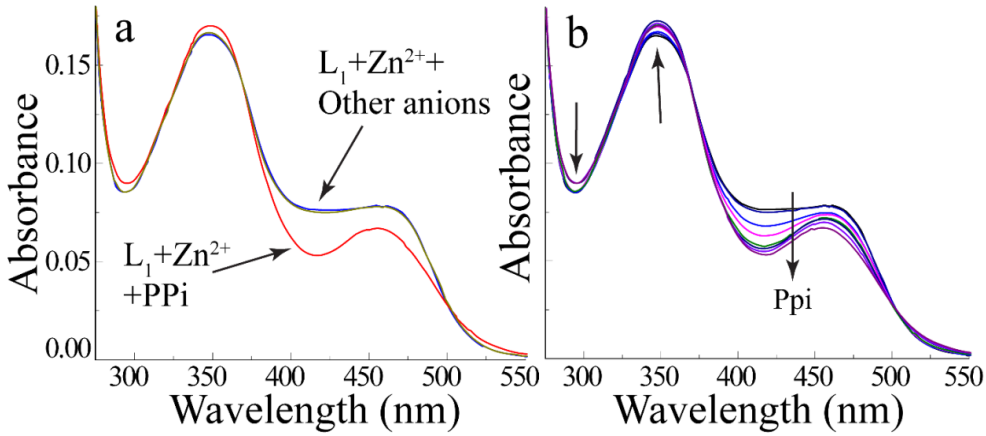

Figure 3.3. Changes in the UV-visible absorption spectra of **L_1.2Zn** (10 μM) upon addition of (a) various anion solution (10 eq), (b) increasing amount of PPi.

Complexation of **L_1** with Zn^{2+} resulted in the formation of a binuclear phenoxo-bridged metal complex[3.16] (Scheme 3.2) which contained an anion binding site in each of the metal center. The secondary sensing behavior of the *in situ* generated highly fluorescent **L_1**.2Zn complex toward different anionic species (e.g., F^-, Cl^-, Br^-, I^-, NO_3^-, HSO_3^-, SO_4^{2-}, ClO_4^-, ClO_3^-, CN^-, S^{2-}, $H_2PO_4^-$, PO_4^{3-}, AMP, ADP, ATP, $H_2P_2O_7^{2-}$) was investigated and it displayed highly selective fluorescence quenching in presence of inorganic pyrophosphate (PPi) only (Fig. 3.4a) and complete quenching was observed at >1.0 equivalent PPi (Fig. 3.4b). It is to be noted that the other phosphate-based anions revealed no noticeable change in fluorescence of **L_1**.2Zn complex even at higher concentrations. Careful analysis of the Job's plot revealed a 1:1 binding stoichiometry between **L_1**.2Zn and PPi (Fig. A3.3a.). The apparent association constant (K) was determined to be 1.76×10^4 M^{-1} for **L_1**.2Zn and PPi (Fig. A3.3b.). Based on these emission spectra, the detection limit of **L_1**.2Zn complex for PPi was determined to be 2 ppb. The changes in the color of the solutions of **L_1**.2Zn complex in presence of different anions was studied under UV light (365 nm). It was observed that in presence of PPi, the **L_1**.2Zn complex solution became non-fluorescent, akin to a solution of **L_1** alone, while the bright green fluorescence of the complex solution remained unaffected in presence of all the other anions (inset Fig. 3.4b). This is attributed to the binding of PPi to the **L_1**.2Zn complex followed by sequestration of Zn^{2+} in the form of Zn•PPi complex, thus releasing the free **L_1**.

Even in the presence of competing anions, the **L_1**.2Zn complex could sense PPi selectively as evident from the striking quenching of its fluorescence, which was a contrast to the complete lack

of fluorescence quenching observed with the other anions (Fig. A3.2b.). This clearly suggests that the **L$_1$**.2Zn complex is a specific chemo-sensing ensemble for PPi.

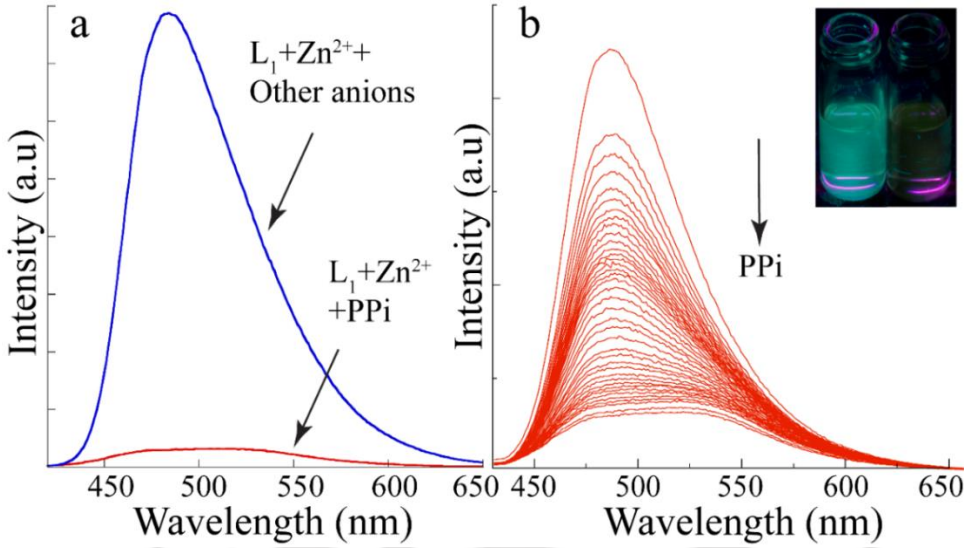

Figure 3.4. Changes in the fluorescence emission spectra of **L$_1$.2Zn** (10μM) in the mixed solvent upon addition of (a) different anions and (b) increasing concentration of PPi. Inset: (b) Visual change in the fluorescence of **L$_1$.2Zn** in presence of various anions.

The change in the emission spectrum of **L$_1$**.2Zn upon the addition of PPi can be understood by considering the strong binding affinity of PPi towards Zn^{2+}. As shown in scheme 2, one PPi unit can effectively bind with two Zn^{2+} ions in the complex, and consequently form a more stable ZnPPi adduct, releasing the free ligand **L$_1$** in solution. Thus sequestration of Zn^{2+} ions by PPi which results in switching-off the ICT process, which leads to quenching of the fluorescence. It therefore can be construed that the turn-off fluorescence in **L$_1$**.2Zn complex required an anion which could simultaneously bind two Zn^{2+} sites in the binuclear complex. This prerequisite is perhaps met by only PPi, which resulted in the formation of **L$_1$.**2ZnPPi adduct and accounted for the selective sensing of PPi.

The 1:1 binding mode between **L$_1$**.2Zn and PPi was further confirmed by ESI-MS data (Fig. A3.6.). The peak at *m/z* 1009.7143 indicating the mass of the adduct of **L$_1$**.2Zn and PPi $C_{28}H_{27}Br_3N_4O_{10}P_2Zn_2$ (**L$_1$**.2Zn+3Br+P_2O_7+MeOH+H_2O+2H), $C_{29}H_{25}N_4O_9P_2Zn_2$ (**L$_1$**.2Zn+P_2O_7+EtOH+2H), another peak at *m/z* 765.9707 representing the mass of the complex $C_{29}H_{24}N_4O_9P_2Zn_2$ (**L$_1$**.2Zn+P_2O_7+EtOH+H) (Fig. A3.6.). A peak at *m/z* 685.0491 indicate the mass of (**L$_1$**.Zn+P_2O_7+EtOH+2H) which is due to the release of one of the two zinc atoms from the system confirming our proposed binding mode. Further, a peak at *m/z* 305.6643 (Fig. A3.6.) indicated the di-zinc complex with PPi ($HO_7P_2Zn_2$) supporting the complete release of both the

zinc ions from the complex. Hence it can be surmised that the selective PPi sensing is plausible due to the stronger binding affinity of the PPi anion with the di-nuclear complex and regeneration of the free **L_1** proceeds via the formation of **L_1**.Zn.P_2O_7 complex.

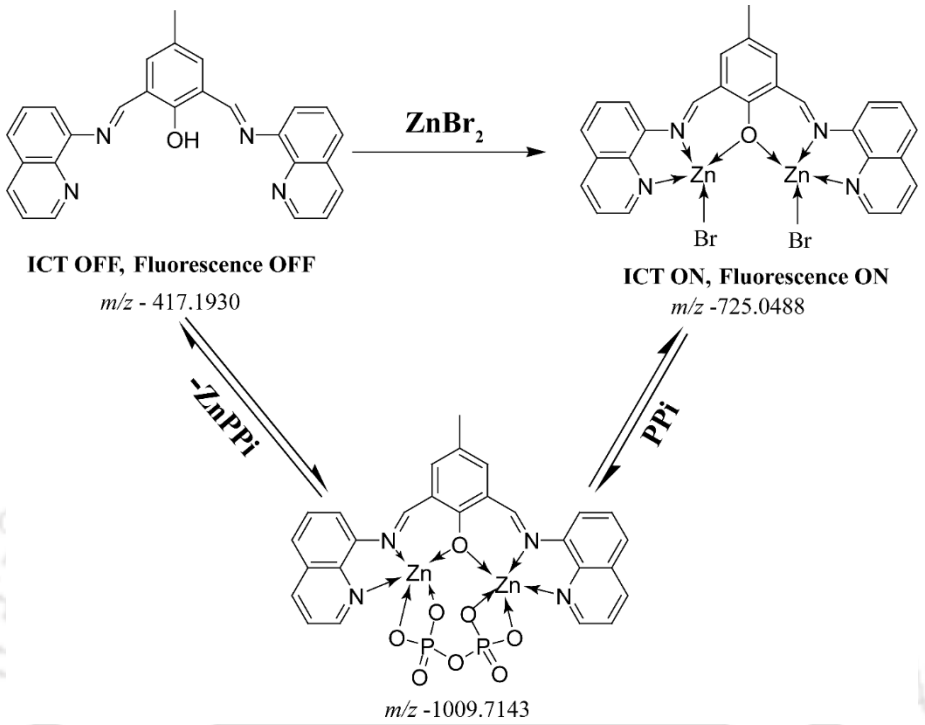

Scheme 3.2. Proposed fluorescence-based mechanism of Zn^{2+} and PPi sensing.

3.5. Reversible and Recyclable Sensing Behavior of L_1

The reversible sensing behavior of **L_1** was investigated by emission spectroscopy over five cycles by the addition of Zn^{2+} followed by PPi. Quenching of the fluorescence emission peak of **L_1**.2Zn at 480 nm ensues upon addition of PPi through the formation of Zn-PPi complex, which releases the free **L_1**. The free ligand is now able to bind Zn^{2+} and thereafter form the highly fluorescent **L_1**.2Zn complex. This switch-ON and switch-OFF behavior of **L_1** was monitored by the addition of Zn^{2+} followed by addition of PPi over five successive cycles. Notable reversal of the fluorescence intensity was observed in those five cycles (Figure 3.5a-b). These findings strongly suggested that **L_1** is a reversible and recyclable sensor for Zn^{2+} and its zinc complex (**L_1**.2Zn) is a secondary sensor for PPi.

3.6. Molecular Logic Gate Based on the Reversible Behavior of L_1 with Sequential Addition of Zn^{2+} and PPi

Construction of molecular-level electronic devices[3.17] is one of the niche areas of interest in analytical chemistry. Chemical systems which undergo reversible changes under the effect of

suitable input are exploited in the manufacture of miniaturized systems. The objective is to replace the macroscopic semiconductors and develop molecular switches that mimic Boolean

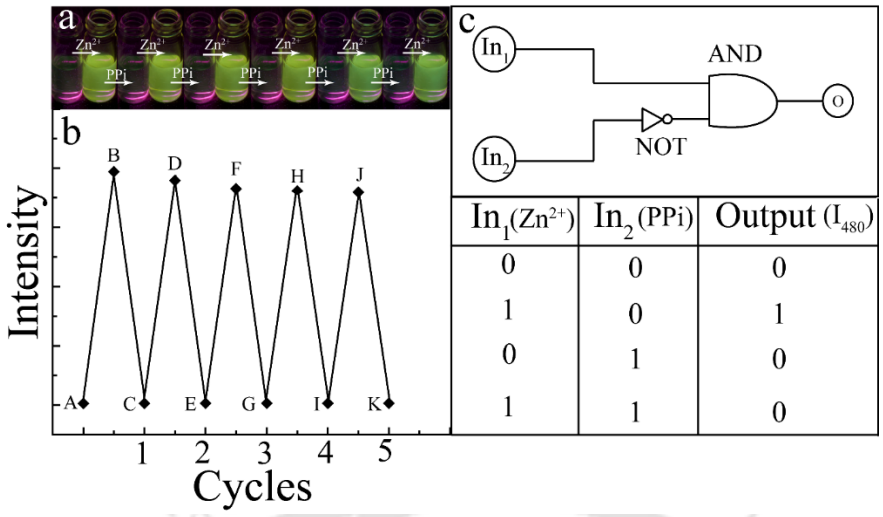

$In_1(Zn^{2+})$	In_2(PPi)	Output (I_{480})
0	0	0
1	0	1
0	1	0
1	1	0

Figure 3.5. (a) Visual fluorescent colour changes after each addition of Zn^{2+} and PPi sequentially; (a) A = **L_1**; B = [A + Zn^{2+}]; C = [B + PPi]; D = [C + Zn^{2+}]; E = [D + PPi]; F = [E + Zn^{2+}]; G = [F + PPi]; H = [G + Zn^{2+}]; I = [H + PPi]; J= [I + Zn^{2+}]; K = [J + PPi]. (b) Reversible and recyclable behaviour of **L_1** upon the sequential addition of Zn^{2+} followed by PPi in the fluorescence experiment observing the changes in intensity at λ = 480 nm. (c) Representation of a two-state molecular switch based on INHIBIT logic function.

logic[3.18] conventions to permit electronic computing at the molecular level through encoding and decoding of binary digits, *i.e.*, 0 and 1, in the form of input and output. In the present study, the reversible behavior of **L_1** towards zinc followed by PPi could be used in the formation of two inputs-one output INHIBIT logic gate (Fig. 3.5c). We used Zn^{2+} as input-1 and PPi as input-2 and the emission intensity at λ=480 nm as the only output. When both of them were absent (0,0) no output was obtained (0), when Zn^{2+} was present alone (1,0) then output was full (1), but in presence of only PPi (0,1) output was zero (0). In the presence of both inputs (1,1) output was again zero (0). Hence, using our receptor **L_1**, establishment of an INHIBIT logic gate was possible.

3.7. Detection of DNA Amplification by Sensing PPi

Development of fluorescent sensors for PPi has become a focal point of research in the realm of bio-analytical chemistry. The considerable interest in detection of inorganic pyrophosphate anion stems from the fact that PPi is known to play a fundamental role in many biological processes such as DNA polymerization, and several enzyme-driven reactions.[9b,c] Encouraged by the sensitive and selective detection of PPi at very low levels in solution, we envisaged that the **L_1**.2Zn complex could perhaps be employed to detect PPi generated during DNA strand synthesis in a prototype PCR setup. A measure of PPi produced in PCR cycles could in turn be extrapolated for quantitative estimation of DNA strands produced during the amplification cycles, given that

PPi formation is a direct consequence of DNA strand synthesis. To this end, PCR was performed with bacterial universal primers to amplify the 16S rRNA gene of *E.coli* MTCC 433 and PPi produced in specific cycle numbers was detected in solution with $\mathbf{L_1}$.2Zn complex. The PCR amplicons generated at various cycle numbers is indicated in Fig. 3.6a. It is evident from the figure that in agarose gel the amplicons corresponding to cycle numbers 5 and 10 could not be visualized, perhaps due to the limitations in the sensitivity of ethidium bromide in detecting low levels of DNA (Fig. 3.6a, lanes B-C). However, at higher cycle numbers (15-35 cycles), a specific amplicon representing the 16S rRNA gene of *E.coli* MTCC 433 was visible (Fig. 3.6a, lanes D-H). The size of the obtained amplicon was around 1.5 kbp, which coincided with the expected amplicon size using universal primers for bacterial 16S rRNA gene. [3.19] It is also quite apparent from the figure that the intensity of the amplicon bands corresponding to cycle numbers 15-35 increased progressively, reflecting higher levels of DNA strand synthesis with increase in cycle numbers. Aliquots of PCR reaction mix from various cycle numbers were also interacted separately with the $\mathbf{L_1}$.2Zn complex and the level of PPi produced in the samples was ascertained by measuring the fluorescence intensity of the complex. It can be observed from Fig. 3.6b that there was a systematic decrease in the fluorescence intensity of $\mathbf{L_1}$.2Zn complex upon interaction with the PCR mix obtained from increasing cycle numbers. This finding was also corroborated by % quenching of the fluorescence intensity of $\mathbf{L_1}$.2Zn complex, which revealed a linear correlation with increasing cycle numbers (inset of Fig. 3.6b). It is significant to mention here that the fluorescence intensity of $\mathbf{L_1}$.2Zn complex remained unaffected upon interaction with a no template control PCR mix obtained after 35 cycles (Fig. 3.6b, sample A). This strongly suggested that none of the PCR mix components, which included the nucleotide mix (dNTPs), *Taq* DNA polymerase enzyme, PCR buffer, $MgCl_2$ and oligo primers interfere with the fluorescence emission intensity of the complex and thus reiterate the exclusive specificity of the developed PPi sensor. From Fig. 3.6b, it is to be noted that the decrease in the fluorescence intensity of $\mathbf{L_1}$.2Zn complex was manifested even for samples corresponding to as early as 5 cycles whereas the decrease in the fluorescence intensity of $\mathbf{L_1}$.2Zn complex for samples obtained from 10-35 cycles was statistically significant when compared to the no template control sample. The results obtained through fluorescence-based estimation of PPi are significant as they clearly indicated that the $\mathbf{L_1}$.2Zn complex could detect very low levels of PPi generated during early cycles of DNA amplification and rendered superior sensitivity in detecting PCR amplicons as compared to conventional agarose gel electrophoresis.

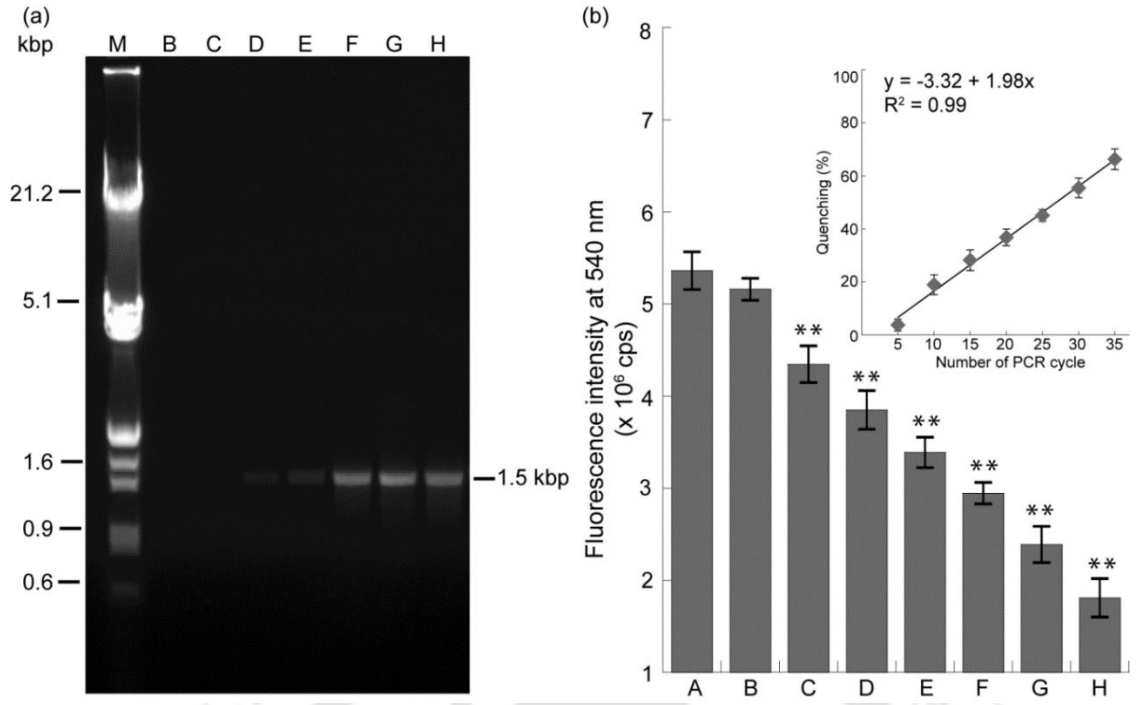

Figure 3.6. (a) Agarose gel electrophoresis of PCR amplicons obtained with universal primers specific for bacterial 16S rRNA gene. Lanes: (M) λ DNA *Eco*RI/*Hin*dIII double digest size marker; (B-H) PCR amplicons obtained from 5, 10, 15, 20, 25, 30 and 35 cycles, respectively. (b) Fluorescence intensity of $\mathbf{L_1}$.2Zn complex upon interaction with PCR reaction products. Sample A: No template DNA control PCR reaction product obtained after 35 cycles; Samples B-H: PCR reaction products obtained from 5, 10, 15, 20, 25, 30 and 35 cycles, respectively. Statistically significant values derived by ANOVA are indicated by asterisk marks. ** indicates p value < 0.001. Inset: % of fluorescence quenching of $\mathbf{L_1}$.2Zn complex following interaction with PCR reaction products corresponding to samples B-H.

3.8. Estimation of Bacterial Cell Numbers

The ability of the $\mathbf{L_1}$.2Zn complex to detect low levels of PPi in solution and track DNA amplification early was encouraging and it offered a possibility of implementing the PPi sensor as a bio-analytical tool. Given the exclusive PPi sensing capability of the $\mathbf{L_1}$.2Zn complex in a PCR mix, we conceived that estimation of bacterial cells numbers by nucleic acid-based amplification reaction could be an interesting sequel of the developed method of PPi estimation. Development of rapid, sensitive and reliable methods of estimating bacterial cell numbers is of paramount importance especially in the regime of clinical diagnosis, food safety, and environmental monitoring. Conventional microbiological tools for estimating bacterial cells can be quite arduous and prolonged and hence undesirable when rapid intervention is required as in the case of early clinical diagnosis. In recent times, nucleic acid-based molecular tools such as polymerase chain reaction (PCR) have come of age in the domain of pathogen detection. Development of various formats of PCR such as multiplex and real-time PCR in conjunction with advancement in

detection technologies has rendered high sensitivity and specificity to pathogen detection as reported extensively in previous studies. [3.20]

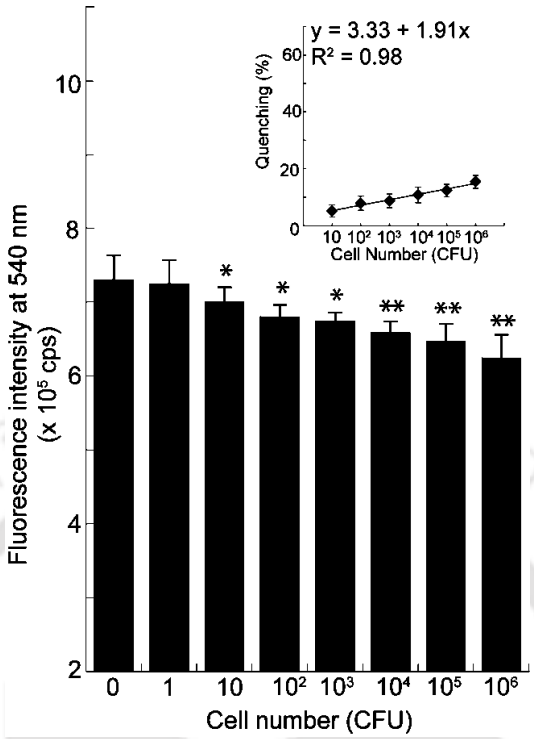

Figure 3.7. Fluorescence intensity of $\mathbf{L_1}$.2Zn complex upon interaction with PCR amplicons obtained after 10 cycles from varying cell numbers of *E.coli* MTCC 433. No template DNA control PCR reaction product corresponds to 0 cell number. Statistically significant values derived by ANOVA are indicated by asterisk marks. * indicates *p* value < 0.05 and ** indicates *p* value < 0.001. Inset: % of fluorescence quenching of $\mathbf{L_1}$.2Zn complex following interaction with PCR reaction products obtained after 10 cycles from varying cell numbers.

In the present study, the enhanced sensitivity afforded by the $\mathbf{L_1}$.2Zn complex in probing PPi formation early in PCR motivated us to exploit the sensor in ascertaining bacterial cell numbers in a prototype PCR setup. To this end, DNA extracted from varying cell numbers (1.0-10^6 CFU ml^{-1}) of *E.coli* MTCC 433 was subjected to PCR for specific cycle numbers with bacterial 16S rRNA universal primers. Subsequently the PCR products from intermittent cycles were interacted with the $\mathbf{L_1}$.2Zn complex to ascertain PPi generation, which in turn provided a measure of the cell numbers. It was observed that the change in fluorescence intensity of $\mathbf{L_1}$.2Zn complex upon interaction with the PCR products obtained after 5 cycles was negligible as compared with the no template control sample and this phenomenon was explicit across every cell number (Fig. 3.7 and Fig. A3.7, panel a). This suggested that the amount of PPi generated from varying cell numbers after 5 cycles was perhaps inadequate to elicit a notable change in the fluorescence intensity of complex. However, in case of PCR products obtained after 10 cycles from varying cell numbers, it was observed that there was a systematic reduction in the fluorescence intensity of $\mathbf{L_1}$.2Zn complex for PCR products obtained from increasing cell numbers and the change in the

fluorescence intensity of $\mathbf{L_1}$.2Zn complex was significant for samples corresponding to 10-10^6 CFU (Fig. 3.7). This result strongly suggested that PPi generation in PCR was a function of cell numbers and was also substantiated by a progressive increase in % quenching observed for varying cell numbers (Fig. 3.7, inset). It is reasonable to assume that the initial template DNA copy number is correlated to cell numbers and thus the PPi generation in PCR is markedly enhanced in case of high cell numbers. With increase in cycle numbers from 15-35, the general trend of a decrease in the fluorescence intensity of $\mathbf{L_1}$.2Zn complex upon interaction with PCR products obtained from increasing cell numbers became more prominent (Fig. A3.7, panel b-f). In the present study, the ability of the $\mathbf{L_1}$.2Zn complex to sense PPi generated as early as 10 cycles from 10 CFU of *E.coli* MTCC 433 highlighted the sensitivity of the PPi sensor. Given the pressing need to develop rapid and sensitive methods of estimating bacterial cell numbers especially in the context of clinical diagnosis, a limit of detection of 10 CFU in as early as 10 cycles of PCR achieved in the present study holds significant implications.

3.9. Conclusions

In the present study, a novel zinc selective colorimetric and fluorimetric-chemosensor ($\mathbf{L_1}$) has been developed, which sense zinc by switching-on the ICT process which was prohibited in the free ligand. Receptor $\mathbf{L_1}$ is highly selective towards Zn^{2+} among the other biologically important cations in physiological condition. Naked eye detection of zinc was possible under visible as well as UV light. As metal complexes offer chemo-sensing ensemble for anions, we have extended our work for anion recognition. Among all the other anions, the *in situ* generated chemo-ensemble ($\mathbf{L_1}$.2Zn) selectively and specifically recognized PPi in mixed aqueous medium at physiological pH due to sequestration of both Zn^{2+} simultaneously to form [Zn·PPi] adduct.

The ability of the developed PPi sensor to detect low levels of PPi in solution and track DNA amplification early highlights its merit as a bio-analytical tool. Given the excellent ability of $\mathbf{L_1}$.2Zn complex to quantitatively detect PPi with high specificity, it is conceivable that the developed sensor can be applied for diverse applications, which essentially encompass PPi estimations such as nucleic acid-based amplification reactions for detection and estimation of cells numbers, gene expression studies and pyrosequencing. One such application is demonstrated in the present work wherein the principle of probing PPi could be extended to sense the anion in a prototype PCR, which in turn facilitated rapid estimation of bacterial cell numbers. This enhances the analytical merit of the developed PPi sensor especially in the context of PCR-based rapid diagnostics. For instance, the essential principle of estimation of cell numbers through sensing of PPi generated in early PCR cycles can also be extended for rapid estimation of particular pathogenic bacteria through deployment of gene specific primers directed against specific

pathogens. Estimation of viable cell numbers is of critical importance and is a pertinent issue in pathogen detection. In this context, it may be construed that the PPi sensing platform developed in the present study can also be employed in a reverse transcription assay to facilitate estimation of viable cell numbers. Given the high specificity of the PPi sensor and its robustness, inclusion of the sensor in a real-time PCR format could be a worthwhile endeavor towards the development of an expeditious pathogen detection system. The reliability of the PPi sensing method in estimating cell numbers asserts its promise in the domain of pathogen detection with an additional potential use in PCR-based detection of antibiotic resistance genes in pathogens and in microbiological quality control operations.

References

3.1. (a) E. L. Que, D. W. Domaille, C. J. Chang, *Chem. Rev.*, 2008, **108**, 1517; (b) C. J. Frederickson, J. Y. Koh, A. I. Bush, *Nat. Rev. Neurosci.*, 2005, **6**, 449. (c) A. G. Scrimgeoura, C. H. Stahl, J. P. McClung, L. J. Marchitelli, A. J. Young, *J. Nutri. Biol.*, 2007, **18**, 813. (d) J. M. Berg, Y. Shi, *Science*., 1996, **271**, 1081.

3.2. (a) B. L. Vallee, K. H. Falchuk, *Physiol., Rev.* 1993, **73**, 79. (b) J. M. Berg, Y. G. Shi, *Science*., 1996, **271**, 1081.

3.3. M. *J*. Hambidge, *Nutr.* 2000, **130**, 1344S.

3.4. L. A. Lichten, R. Cousins, *Annu. Rev. Nutr*., 2009, **29**, 153.

3.5. A. Voegelin, S. Poster, A. C. Scheinost, M. A. Marcus, R. Kretzsch-mar, *Environ. Sci. Technol.*, 2005, **39**, 6616.

3.6. (a) S. Maruyama, K. Kikuchi, T. Hirano, Y. Urano, T. Nagano, *J. Am. Chem. Soc.*, 2002, **124**, 10650. (b) K. Kiyose, H. Kojima, Y. Urano, T. Nagano, *J. Am. Chem. Soc*., 2006, **128**, 6548. (c) C. C. Woodroofe, S. J. Lippard, *J. Am. Chem. Soc.*, 2003, **125**, 11458. (d) M. Taki, J. L. Wolford, T. V. O'Halloran, *J. Am. Chem. Soc*., 2004, **126**, 712. (e) C. J. Chang, J. Jaworski, E. M. Nolan, M. Sheng, S. J. Lippard, *Proc. Natl. Acad. Sci. USA*., 2004, **101**, 1129. (f) M. M. Henary, Y. Wu, C. J. Fahrni, *Chem.–Eur. J.*, 2004, **10**, 3015.

3.7. (a) N. C. Lim, C. Bruckner, *Chem. Commun.*, 2004, 1094. (b) A. Ajayaghosh, P. Carol, S. Sreejith, *J. Am. Chem. Soc.*, 2005, **127**, 14962. (c) K. Komatsu, Y. Urano, H. Kojima, T. Nagano, *J. Am. Chem. Soc.*, 2007, **129**, 13447. (d) X. Zhang, K. S. Lovejoy, A. Jasanoff, S. J. Lippard, *Proc.Natl. Acad. Sci. USA.*, 2007, **104**, 10780.

3.8. (a) V. Amendola, L. Fabbrizzi, F. Forti, M. Licchelli, C. Mangano, P. Pallavicini, A. Poggi, D. Sacchi, A. Taglieti, *Coord. Chem. Rev.*, 2006, **250**, 273. (b) K. Rurack, U. Resch-Genger, *Chem. Soc.Rev.*, 2002, **31**, 116. (c) B. Valeur, I. Leray, *Coord. Chem. Rev*., 2000, **205**, 3. (d) J. Yoon, S. K. Kim, N. J. Singh, K. S. Kim, *Chem. Soc. Rev.*, 2006, **35**, 355. (e) L. Mutihac, J.H. Lee, J. S. Kim, J. Vicens, *Chem. Soc. Rev.*, 2011, **40**, 2777.

3.9. (a) S. K. Kim, D. H. Lee, J. I. Hong, J. Yoon, *Acc. Chem. Res.*, 2009, **42**, 23. (b) M. Ronaghi, S. Haramohamed, B. Pettersson, M. Uhlen, P. Nyren, *Anal. Biochem.*, 1996, **242**, 84. (c) K. M. Steinberg, D. T. Okbu, M. E. Zwick, *Anal. Chem.*, 2008, **80**, 520.

3.10. (a) M. Ronaghi, S. Karamohamed, B. Pettersson, M. Uhlen, P. Nyren, *Anal. Biochem.*, 1996, **242**, 84. (b) G. V. Zyryanov, M. A. Palacios, P. Anzenbacher, *Angew. Chem. Int. Ed.*, 2007, **46**, 1. (d) L. Fabbrizzi, M. Licchelli, G. Rabaioli, A. Taglietti, *Coord. Chem. Rev.*, 2000, **205**, 85. (f) J. Y. Lee, M. Hirose, *J. Biol. Inorg. Chem.*, 1992, **267**, 14753.

3.11. (a) S. Mizukami, T. Nagano, Y. Urano, A. Odani, K. Kikuchi, *J. Am. Chem. Soc.*, 2002, **124**, 3920. (b) L. Fabbrizzi, N. Marcotte, F. Stomeo, A. Taglietti, *Angew. Chem., Int. Ed.*, 2002, **41**, 3811.(c) D. H. Lee, J. H. Im, S. U. Son, Y. K. Chung, J. I. Hong, *J. Am. Chem. Soc.*, 2003, **125**, 7752. (d) J. H. Lee, J. Park, M. S. Lah, J. Chin, J. I. Hong, *Org. Lett.*, 2007, **9**, 3729. (e) R. K. Pathak, K. Tabbasum, A. Rai, D. Panda, C. P. Rao, *Anal. Chem.*, 2012, **84**, 5117. (f) W-H. Chen, Y. Xing, Y. Pang, *Org. Lett.*, 2011, **13**, 1362.

3.12. D. A. Denton, H. Suschitzky, *J.Chem. Soc.*, 1963, 4741.

3.13. J. Lewkowski, R. Skowronski, *Heteroatom Chemistry.*, 2001, **12**, 27.

3.14. H. A. Benesi, J. H. Hildebrand, *J. Am. Chem. Soc.*, 1949, **71**, 2703.

3.15. (a) T. Mistri, M. Dolai, D. Chakraborty, A. R. Khuda-Bukhsh, K. K. Das, M. Ali, *Org. Biomol. Chem.*, 2012, **10**, 2380. (b) B. Srinivas, N. Arulsamy, P.S. Zacharias. *Polyhedron.*, 1991**,** **10**, 731. (c) Q. Chu, D. A. Medvetz, M. J. Panzner, Y. Pang, *Dalton Trans.*, 2010, **39**, 5254.

3.16. (a) M. Suzuki, H. Kanatomi, I. Murase, *Chem. Lett.*, 1981, **10**, 1745. (b) Munch, B. P. F. C. Bradley, P. D. Boyle, V. Papaefthymiou, L. Que, Jr. *J. Am. Chem. Soc.*, 1987, **109**, 7993. (c) S. S. Jin, N. D. Sung, R. C. Hynes, J. Chin, *Inorg. Chem.*, 1996, **35**, 7472. (d) M. S. Han, D. H. Kim, *Angew. Chem. Int. Ed.*, 2002, **114**, 3963. (e) P. Molenveld, J. F. J. Engbersen, D. N. Reinhoudt, *Chem. Soc. Rev.*, 2000, **29**, 75.

3.17. (a) V. Balzani, M. Venturi, A. Credi, *Molecular Devices and Machines*. Eds.; Wiley-VCH: Weinheim, 2003. (b) M. Kumar, N. Kumar, V. Bhalla, *Chem. Commun.*, 2013, **49**, 877. (c) K. Kim, Y. Ha, L. Kaufman, D. G. Churchill, *Inorg. Chem.*, 2012, **51**, 928. (d) X.J. Zhao, C. Z. Huang, *Analyst.*, 2010, **11**, 2853. (e) S. Khatua, S.H. Choi, J. Lee, K. Kim, Y. Do, D. G. Churchill, *Inorg. Chem.*, 2009, **48**, 2993.

3.18. M. Ben-Ari, *Mathematical Logic for Computer Science*. Ed.; Prentice-Hall: Hemel Hempstead, 1993.

3.19. W. G. Weisburg, S. M. Barns, D. A. Pelletier, D. J. Lane, *J. Bacteriol.*, 1991, **173**, 697.

3.20. (a) N. Mancini, S. Carletti, N. Ghidoli, P. Cichero, R. Burioni, M. Clementi, *Clin. Microbiol. Rev.*, 2010, **23**, 235. (b) C. D. Sibley, G. Peirano, D. L. Church, *Infect. Genet. Evol.*, 2012, **12**, 505. (c) K. Jeng, C. A. Gaydos, L. B. Blyn, S. Yang, H. Won, H. Matthews, D. Toleno, Y-H. Hsieh, K. C. Carroll, J. Hardick, B. Masek, A. Kecojevic, R. Sampath, S. Peterson, R. E. Rothman, *J. Clin. Microbiol.*, 2012, **50**, 3287.

Appendix

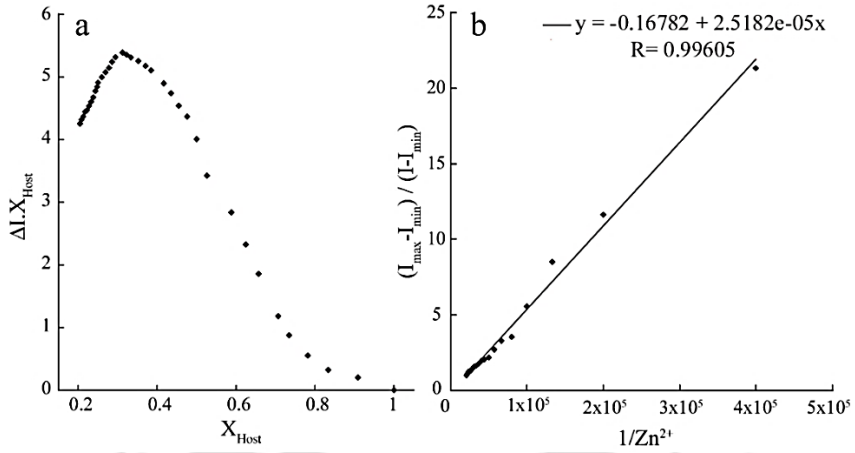

Figure A3.1. (a) Job's plot between $\mathbf{L_1}$ and Zn^{2+} ions. X_{Host} is the mole fraction of $\mathbf{L_1}$ and ΔI is the change $(I-I_0)$ in the intensity of the emission spectra in presence of guest. (b) Bensei-Hildebrand plot obtained from the emission experiment studies (emission intensity calculated from 480 nm).

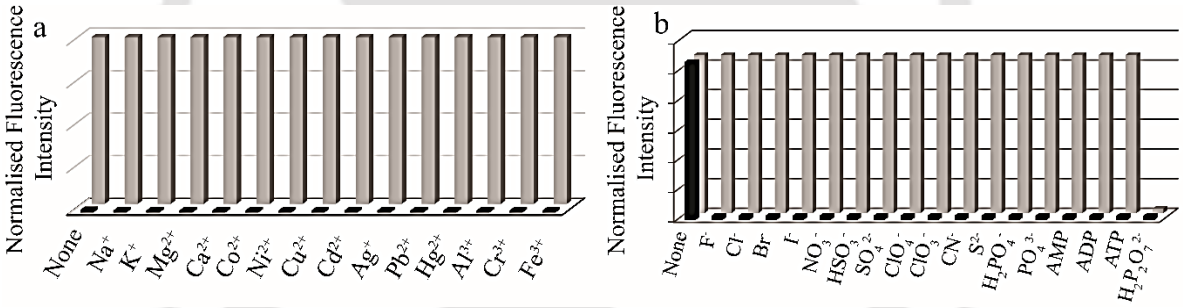

Figure A3.2. (a) Normalized fluorescence responses of $\mathbf{L_1}$ (10 μM) to various cations in mixed solvent. The blsck bars represent the emission intensities of $\mathbf{L_1}$ in the presence of cations of interest (5 eqv.). The gray bars represent the change of the emission that occurs upon the subsequent addition of Zn^{2+} to the above solution. (b) Normalized fluorescence responses of $\mathbf{L_1.2Zn}$ to various anions in mixed solvent. The red bars represent the emission intensities of $\mathbf{L_1}$in the presence of anions of interest (5 eq). The blue bars represent the change of the emission that occurs upon the subsequent addition of PPi to the above solution. The intensities were recorded at 480 nm.

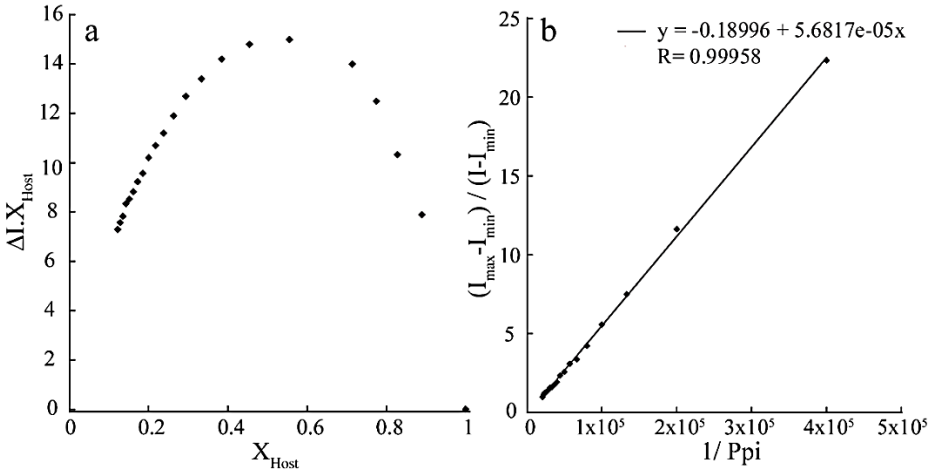

Figure A3.3. (a) Job's plot between $\mathbf{L_1}$.2Zn complex and PPi. Where X_{Host} = the mole fraction of $\mathbf{L_1}$.2Zn and ΔI is the change ($I-I_0$) in the intensity of the emission spectra in presence of guest. (b) Bensei-Hildebrand plot obtained from the emission experiment (emission intensity calculated from 480 nm) studies.

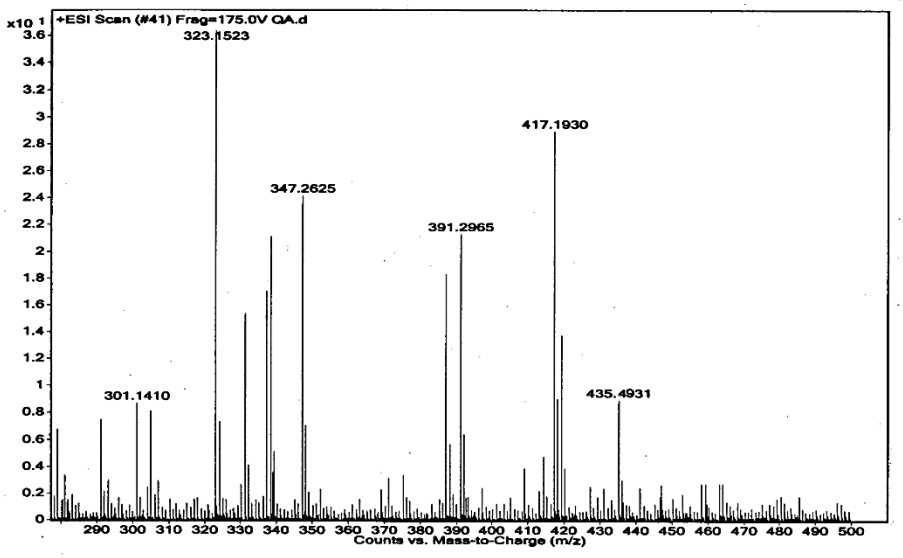

Figure A3.4. Mass spectrum of $\mathbf{L_1}$, Calculated $[\mathbf{L_1}+H_2O+H]^+$= 435.4971, Found 435.4931(Mass spectrum obtained in positive mode)**.**

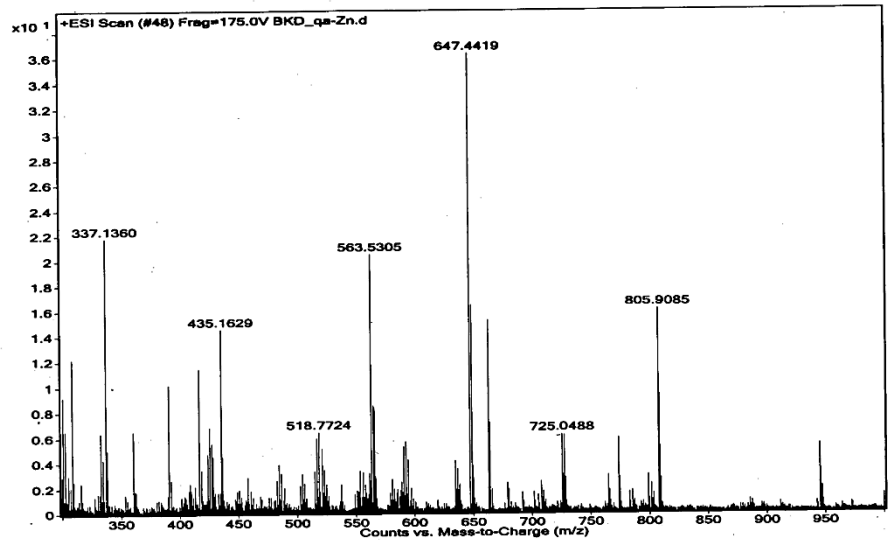

Figure A3.5. Mass spectrum of **L_1**-Zn complex, Calculated [**L_1**+2Zn+3Br+H_2O+2H] = 805.9891, Found 805.9085(Mass spectrum obtained in positive mode)**.**

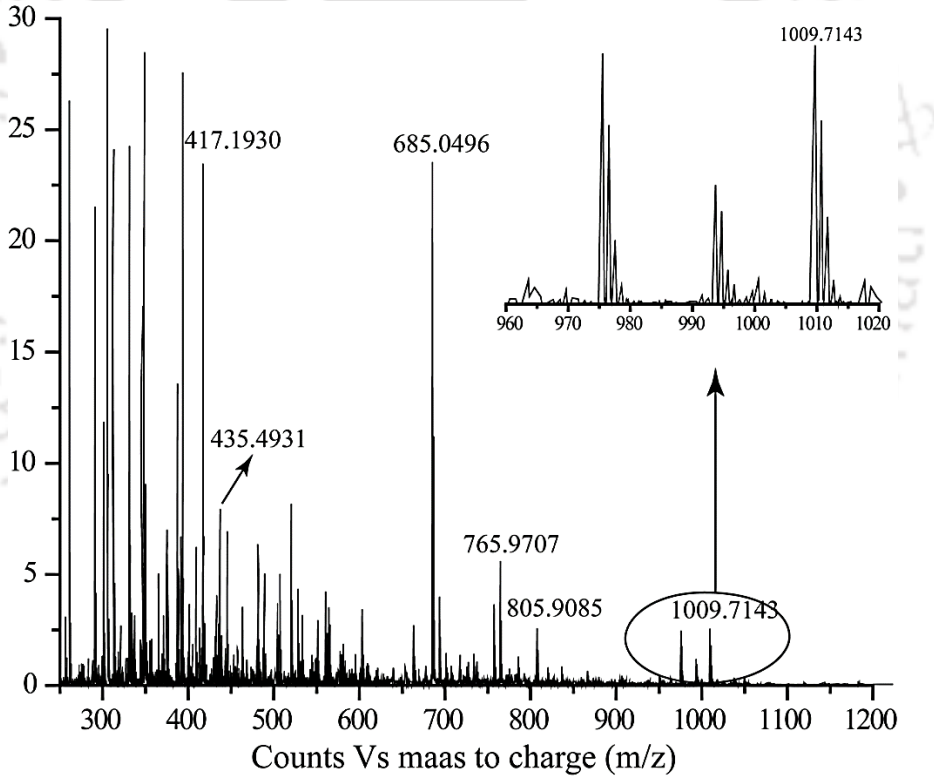

Figure A3.6. Mass spectrum of **L_1**-Zn complex (in positive ion mode), Calculated mass for [L_1.2Zn+3Br+P_2O_7+MeOH+H_2O+2H]$^+$ = 1009.7284, Found 1009.7143.

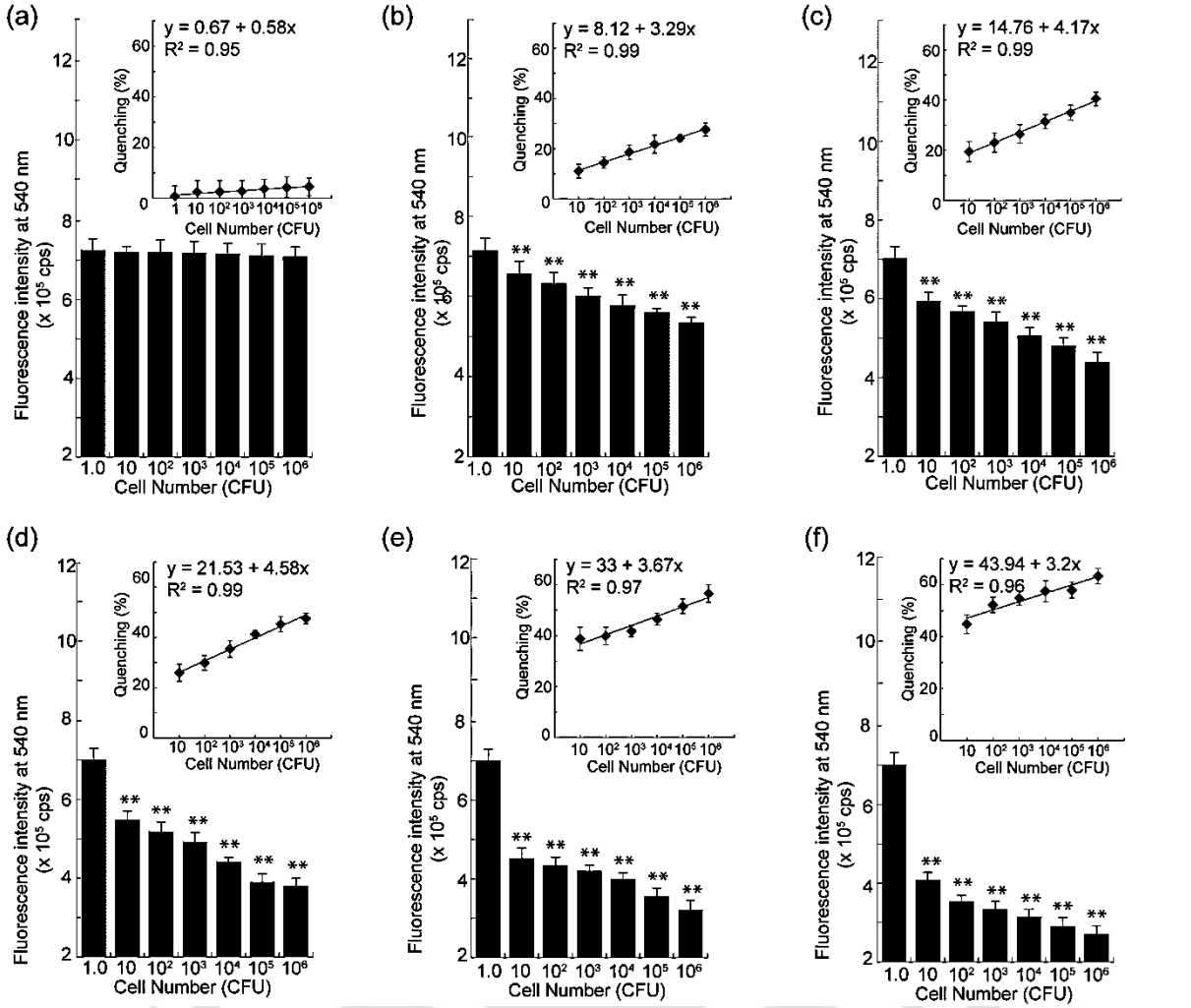

Figure A3.7. Fluorescence intensity of $\mathbf{L_1}$.2Zn complex following interaction with PCR amplicons obtained from varying cell numbers of *E.coli* MTCC 433. The PCR products were obtained from (a) 5 cycles, (b) 15 cycles, (c) 20 cycles, (d) 25 cycles, (e) 30 cycles and (f) 35 cycles, respectively. Statistically significant values derived by ANOVA are indicated by asterisk marks. ** indicates *p* value < 0.001. Inset indicates % quenching of the fluorescence intensity of $\mathbf{L_1}$.2Zn complex following interaction with PCR reaction products obtained from varying cell numbers.

Chapter 4

A novel chemosensor with visible light excitability for sensing Zn^{2+} in physiological medium and in HeLa cells

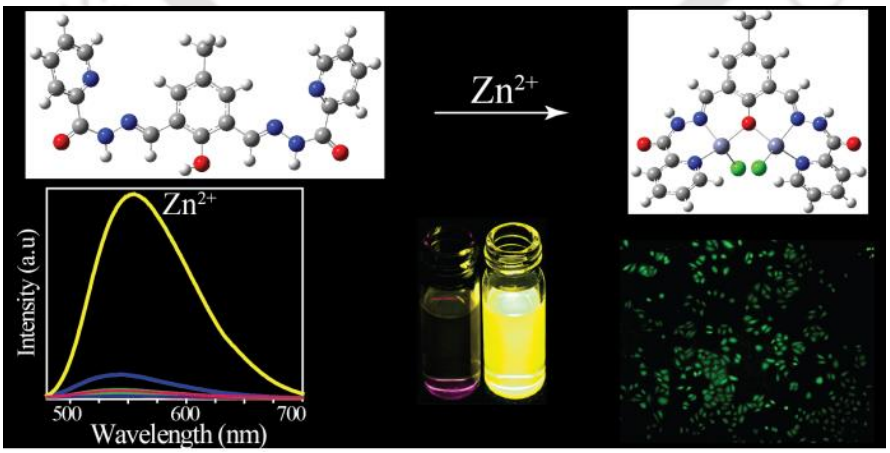

Chapter 4

4.1. Background and Focus of the Chapter

Detection and imaging of biologically relevant target molecules through fluorescence in living systems has emerged as an area of intense interest in the chemistry-biology interface owing to its significant biomedical implications.[4.1] As explained earlier in chapter 3, Zn(II) is known to play crucial roles in the activity of various enzymes and also a key component of some transcription factors, gene expression, apoptosis, neurotransmission and so forth.[4.2] Perturbations in zinc homeostasis is of high concern resulting in disorders such as impaired cognition, immune dysfunction, type 2 diabetes mellitus (T2DM), Alzheimer's disease, epilepsy, ischemic stroke, and age-related macular degeneration (AMD), infantile diarrhoea. [4.3] Being a harmful pollutant, zinc is also important for environmental safety. [4.4]

Imaging of intracellular Zn^{2+} with fluorescent chemosensors has been established as an efficient tool to provide chronological–spatial evidence on Zn^{2+} homeostasis in live cells.[4.5] In general, most fluorogenic chemosensors depend on the change of emission intensity (quenching, enhancement, or ratiometric) of the chromophore units which acts as signalling unit for the sensing ability.[4.6] Even though sensing of analytes in solution can be correlated with the systematic variations in emission intensity but the detection of analytes in cells is fraught with the challenge of specific sensing in a complex milieu. For example, during imaging cells using fluorescence microscopy, quenching may occur due to the photobleaching[4.7] and/or aggregation[4.8] to several degrees in different cellular environments. Furthermore, lives cell imaging with a probe within biological cells may result in heterogeneous labelling of the sensor, which can lead to varying emission intensities at different spatial positions.[4.9] The aforementioned anomaly present great challenge towards analysing signal change due to the recognition of the analytes with those arising from variations in probe concentration within cells. Therefore, it is significant to design new sensors which undergo profound spectroscopic changes like spectral shifts, upon binding with the analyte like Zn^{2+}. Fluorescent probes are designed on the basis of intraligand charge transfer (ICT), [4.10] photoinduced electron transfer (PET), [4.11] chelation-enhanced fluorescence (CHEF), [4.12] metal−ligand charge transfer (MLCT), [4.13] excimer/exciplex formation,[4.14] imine isomerization,[4.15] intermolecular hydrogen bonding, [4.16, 4.14e] excited-state intramolecular proton transfer,[4.17] displacement approach, [4.18] and fluorescence resonance energy transfer.[4.19] CHEF is an important process by which fluorescent probes detect analytes.[4.12] When the CHEF process is in switch-on condition, the conjugation increases drastically which leads to enhancement in the

emission and also a red shift is expected. So, the fluorophore senses a metal ion with enhancement in the emission intensity accompanied by a red shift.

So far, a number of fluorescent chemosensors for selective detection of Zn(II)- have been reported with some success in biological applications,[4.20] but most of the reported fluorescent as well as colorimetric sensors for Zn^{2+} work in either pure organic or mixture organic-aqueous solutions like our previous work.[4.21] This restricts their applications in a physiological environment. Hence there is a critical demand to develop fluorescent probe for Zn^{2+} that are based on easy synthesis, render visible light excitation, exhibit large red-shift in emission for Zn^{2+} sensing, and their sensing capability is immune from any pH interference in the physiological range.

In the previous chapter we took the Schiff base of a diformyl core with 8-amino quinoline. In this chapter we explored the synthesis, characterization and sensing behaviour of a simple Schiff base of the same diformyl core with pyridine hydrazide. We changed the amine group which was a derivative of 2-picolinic acid and the developed receptor exhibit selectivity towards Zn^{2+} with visible light excitability and the ability to sense the metal in completely physiological condition. The recognition of Zn^{2+} by our receptor $\mathbf{L_2}$ has been investigated by absorption spectroscopy, emission spectroscopy, DFT calculation, ESI-MS experiment and ^{1}H-NMR titration. Detection of intracellular zinc in live HeLa cells through fluorescence imaging is also demonstrated in the study.

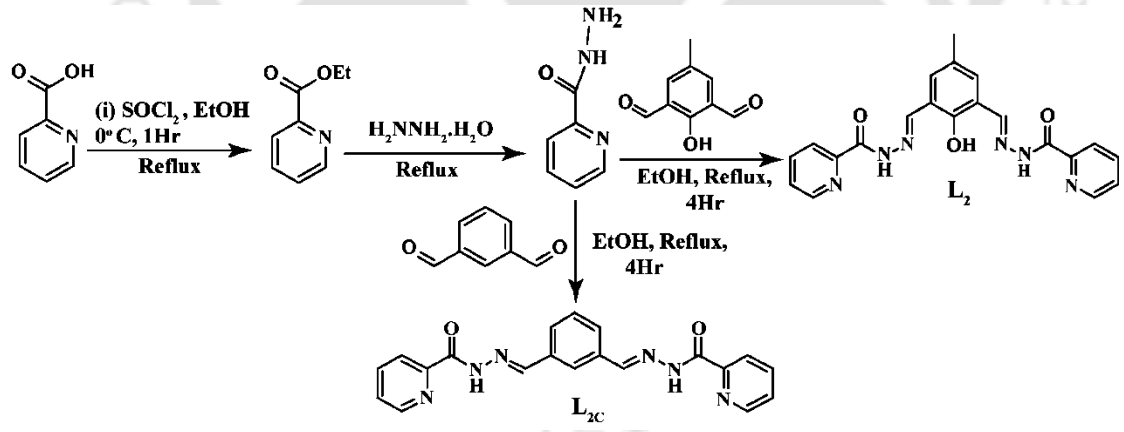

Scheme 4.1. Synthesis of $\mathbf{L_2}$ and $\mathbf{L_{2C}}$.

4.2. Absorption spectroscopic studies

All the spectroscopic studies were performed in HEPES buffer medium (1 mM, pH=7.4) containing 0.33% of DMSO. The ligand $\mathbf{L_2}$ exhibited two characteristic absorption peaks at 305 nm (ε= 4x10^4 M^{-1}cm^{-1}) and 367 nm (ε= 1.8x10^4 M^{-1}cm^{-1}). Comparing with $\mathbf{L_1}$, the conjugation decreases in $\mathbf{L_2}$ due to which the peak at the longest wavelength did not appear in the case of $\mathbf{L_2}$.

In case of $\mathbf{L_2}$ the conjugation breaks after the –C=O group, so the absorption peak is resided at much shorter wavelength (367 nm) compared to the absorption peak at 450 nm. Upon addition of 10 equivalent of different metal ions (Na^+, K^+, Mg^{2+}, Ca^{2+}, Co^{2+}, Ni^{2+}, Cu^{2+}, Cd^{2+}, Ag^+, Pb^{2+}, Hg^{2+}, Al^{3+}, Cr^{3+}, Fe^{3+}, Zn^{2+}) Zn^{2+} promoted a prominent change in the absorption spectra of $\mathbf{L_2}$ (Fig. 4.1a). Amongst other metals, only Cd^{2+} caused a nominal change in the absorption spectra of $\mathbf{L_2}$**.** However, this change was distinctly less in magnitude as compared to the change observed with Zn^{2+} (Fig. 4.1a). Upon the addition of Zn^{2+} ion (10 eq.), the absorption peak at 305 nm (ε= $1.8x10^4$ $M^{-1}cm^{-1}$) decreased and shifted to 326 nm and a new peak emerged at 450 nm (ε= $0.98x10^4$ $M^{-1}cm^{-1}$). On the other hand, with the addition of Cd^{2+} the absorption at 305 nm (ε= $3x10^4$ $M^{-1}cm^{-1}$) decreased, akin to that observed with Zn^{2+}, while a new peak appeared at 436 nm (ε= $0.24x10^4$ $M^{-1}cm^{-1}$). Incremental addition of Zn^{2+} to $\mathbf{L_2}$ resulted in three isosbestic points at 329

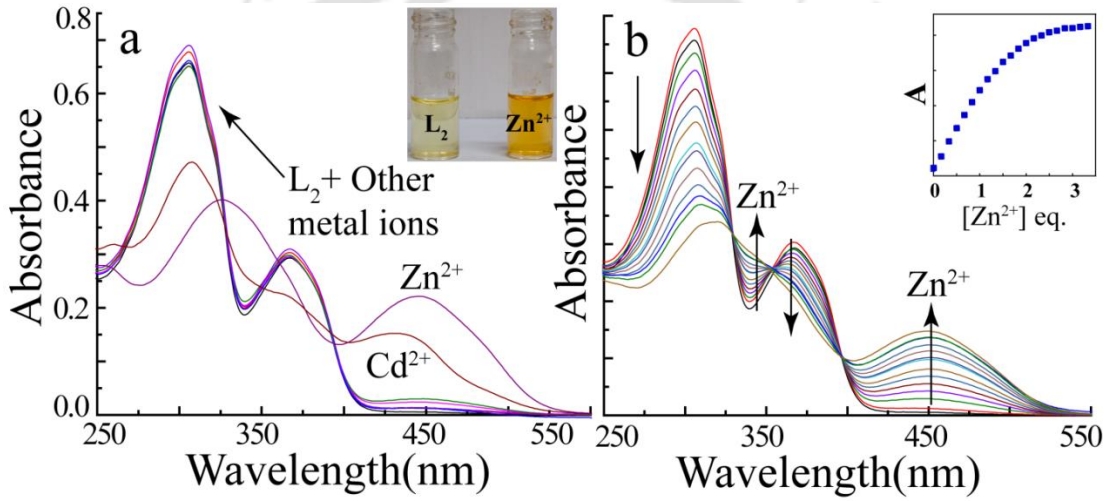

Figure 4.1. Changes in absorption spectroscopy of $\mathbf{L_2}$ (25 μM) with (a) various metal ions (10 eq.) and (b) with incremental addition of Zn^{2+} (0 μM – 60 μM). Inset: Plot of absorbance at 450 nm vs $[Zn^{2+}]$.

nm, 352 nm and 396 nm indicating the transition of the free ligand into metal complex (inset Fig. 4.1a). A visual colour change was observed during the above process from colourless to yellow (Fig. 4.1a). From the absorption titration experiment it was also witnessed that change in the absorption spectra became minimum after the addition of two equivalent of metal ion (Fig. 4.1b inset) which suggested a 1:2 binding stoichiometry between $\mathbf{L_2}$ and Zn^{2+}. Essentially, absorption spectrum indicated that the receptor exhibited high selectivity towards Zn^{2+} with a marginal response to Cd^{2+}.

4.3. Fluorescence spectroscopic studies of L_2 in presence of metal ions

With visible light excitability, when the receptor ($\mathbf{L_2}$) was excited at 470 nm, a weak emission peak was observed at ~530 nm. A set of different metal ions (Na^+, K^+, Mg^{2+}, Ca^{2+}, Co^{2+}, Ni^{2+}, Cu^{2+}, Cd^{2+}, Ag^+, Pb^{2+}, Hg^{2+}, Al^{3+}, Cr^{3+}, Fe^{3+}, Zn^{2+}) were used to ascertain the selectivity of $\mathbf{L_2}$.

Interestingly only Zn^{2+} caused a drastic enhancement in the emission intensity of **L_2** with a prominent peak obtained at 555 nm while Cd^{2+} causes a very small enhancement in the emission intensity (Fig. 4.2a). This observation clearly demonstrated high selectivity of **L_2** towards Zn^{2+} over other metal ions including Cd^{2+}. During titration with Zn^{2+}, **L_2** displayed a linear enhancement in the emission intensity of the free ligand with a progressive red shift (Fig. 4.2b). After the addition of two equivalent of Zn^{2+} ion the change in the emission spectra became

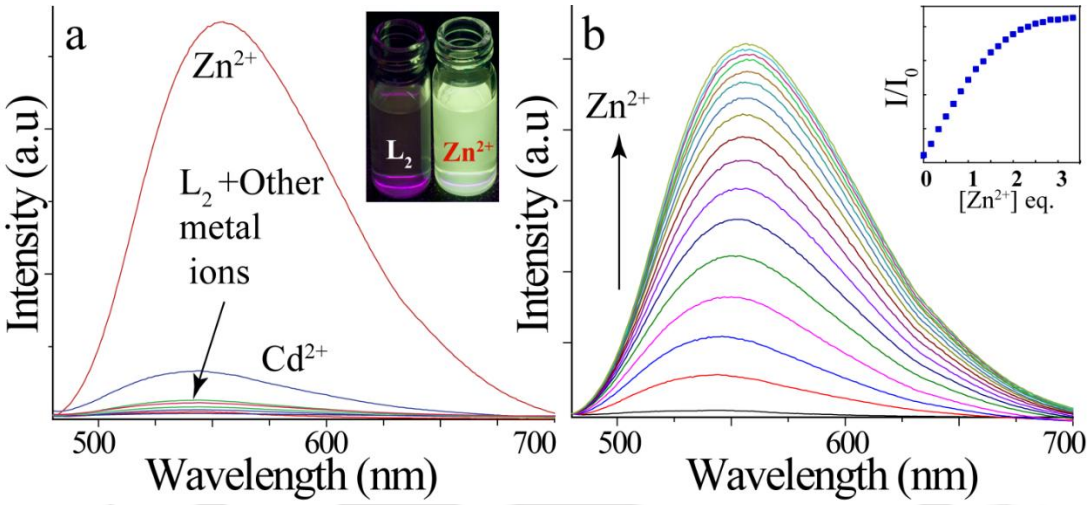

Figure 4.2. Changes in emission spectra of **L_2** (25 μM) in presence of (a) various metal ions (10 eq.) and (b) with incremental addition of Zn^{2+} (0 μM - 60μM). Inset: Change in colour change under UV lamp (λ_{em}= 365nm) upon addition of Zn^{2+} to **L_2**.

minimal supporting the result obtained from UV-Vis experiment (inset Fig. 4.2b). Fluorescence quantum yields of the Zn^{2+} complex was calculated to be 18-times higher than that of the probe alone (0.16 and 0.009, respectively). A change in the fluorescence emission from colourless to yellow was observed under UV-lamp after the addition of Zn^{2+} to the receptor solution (Fig. 4.2a inset). Careful analysis of Job's plot (Fig. A4.1a) obtained from the fluorescence titration experiment established a 1:2 binding stoichiometry between **L_2** and Zn^{2+}. The association constant[4.22] and detection limit of **L_2** for Zn^{2+} were calculated to be 5.58 $\times 10^5$ M^{-1} (Fig. A4.1b) and approximately 69 ppb respectively.

The amplification of fluorescence intensity of the receptor, **L_2** by Zn^{2+} was also confirmed through screening with competing metal cations of interest (Fig. 4.3). Except for Zn^{2+}, only Cd^{2+} among the verified cations triggered the emission enhancement, but it was negligible as compared to that of Zn^{2+}. It is to be noted that even highly abundant intracellular alkali metal ions (Na^+, K^+) and alkaline earth metal ions (Mg^{2+}, Ca^{2+}) did not affect the emission spectra of **L_2** even in the presence of excess amount. The effect of different counter anions of zinc salt was also investigated in the same condition using different zinc salts like Zn $(ClO_4)_2$, Zn $(OAc)_2$, Zn

$(NO_3)_2$, $ZnCl_2$, $ZnBr_2$ and $ZnSO_4$. From the experiment it was found that the counter anions of zinc did not influence the recognition process of Zn^{2+} by **L_2**.

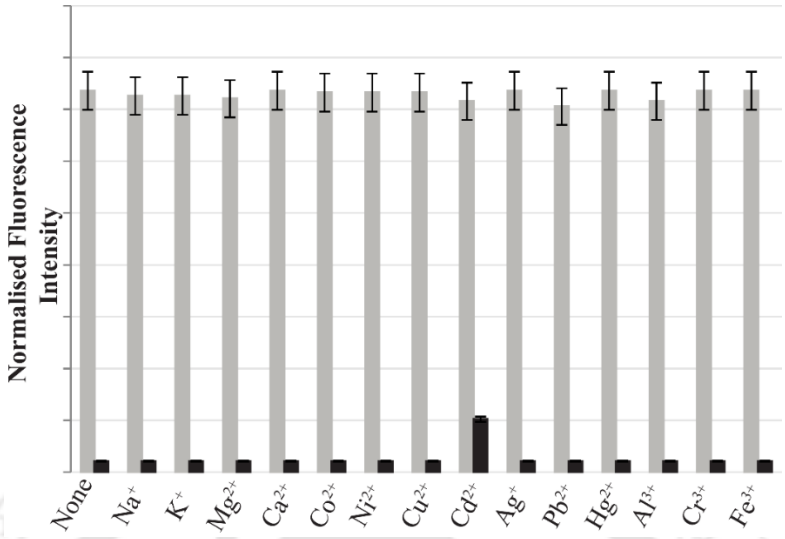

Figure 4.3. Normalized fluorescence responses of **L_2** (10 μM) at 550 nm in presence of various cations in mixed solvent. The black bars represent the emission intensities of **L_2** in the presence of cations of interest (5.0 eq.). The gray bars represent the change of the emission upon subsequent addition of Zn^{2+} to the above solution. Display error bars with 5% values.

4.4. pH Dependent study

The fluorescence property of the receptor, **L_2** was checked at different pH. At lower pH (2-6), the receptor displayed blue fluorescence whereas at higher pH (9 and above) the receptor exhibited a yellow fluorescence with lower intensity. Possibly at lower pH, protonation or hydrolysis of the imine bond may have resulted in a blue fluorescence. On the other hand, at higher pH deprotonation of the hydroxyl group perhaps leads to a weak yellow fluorescence. Interestingly, it was observed that the ligand has stable fluorescence within the pH range of 6.5-9.0. This observation suggested that the ligand could render pH-independent fluorescence measurement in physiological microenvironment. The high selectivity of **L_2** towards Zn^{2+} over other biologically important metal ions, its sensing capability in physiological condition and a lower detection limit enhances the analytical merit of the developed receptor (**L_2**) for the recognition of intracellular Zn^{2+}.

4.5. ^{1}H NMR Titration

We were unsuccessful to get a single crystal of the Zn^{2+} complex of **L_2** suitable for X-ray diffraction even after several attempts. Therefore, in order to understand the mode of interaction between **L_2** and Zn^{2+} or the structural changes in **L_2** after interacting with Zn^{2+}, we acquired ^{1}H-

NMR data. ^{1}H-NMR titration of the receptor, **L_2** with $Zn(ClO_4)_2$ was performed in DMSO-d_6. During ^{1}H-NMR titration of **L_2** with Zn^{2+} significant spectral changes of **L_2** were observed. Reduction in the intensity of the hydroxyl group (-OH) indicated deprotonation as a result of interaction with Zn^{2+} and after the addition of two equivalent of Zn^{2+} ion, the hydroxyl group peak was obliterated. As illustrated in Fig. A4.6, upfield shifts were observed in the case of the pyridyl hydrogen atoms. The Schiff base hydrogen atom and the hydrogen atoms on the DFMP ring also underwent upfield shifts whereas very little change was observed for the amide proton (-NH) as compared to the other protons within the system. Collectively ^{1}H-NMR titration strongly suggested the formation of a hydroxo bridged complex between **L_2** and Zn^{2+} resulting in the deprotonation of the hydroxyl group and the pyridyl nitrogen atom coordinating to Zn^{2+} causing shifts to the pyridyl hydrogen atoms.

4.6. ESI-MS Experiment

The binding mode between **L_2** and Zn^{2+} was also investigated through ESI-MS. A peak at 869.8240 signifies the mass of the ensemble $(\mathbf{L_2}+2Zn+3ClO_4+CH_3CN)^+$ $C_{23}H_{21}Cl_3N_7O_{15}Zn_2$ and another peak at 403.1546 represents the mass of the free receptor. So, the result from ESI-MS experiment also supports the results obtained from the UV-Vis and emission spectroscopy.

4.7. Mechanism of Zn^{2+} Sensing

The enhancement in the fluorescence intensity of the receptor, **L_2** after interacting with Zn^{2+} may be attributed to the CHEF and ICT process. Firstly, the low fluorescence of **L_2** may be due to the free rotation of the imine (-C=N) bond. As illustrated in scheme 4.2, in presence of Zn^{2+}, chelation of the metal ion with the –OH group and with the two imine N-atoms ensues. Consequently, the free rotation around the imine bond gets restricted and the system becomes more rigid. Furthermore, chelation of Zn^{2+} by the hydroxide group and the Schiff base N-atoms leads to the formation a hydroxo bridged binuclear zinc complex in which the conjugation increases drastically resulting in a CHEF effect. On the other hand, due to the binding of Zn^{2+} the ICT is facilitated over the π-system. This also caused sufficient enhancement in the fluorescence. The CHEF phenomenon in conjunction with the ICT process upon interacting with Zn^{2+}, perhaps results in the enhancement the fluorescence intensity of the free receptor along with a red shift of ~25 nm. The proposed CHEF mechanism was verified by conducting control experiments with the receptor **L_{2C}**, which lacked the hydroxyl group. As anticipated, **L_{2C}** did not show any change in its emission spectra after interaction with Zn^{2+} owing to the lack of chelation of Zn^{2+} and a CHEF effect thereof. This result strongly suggested that the di-imine moiety with the hydroxyl group at the core was essentially implicated in the Zn^{2+} sensing phenomenon.

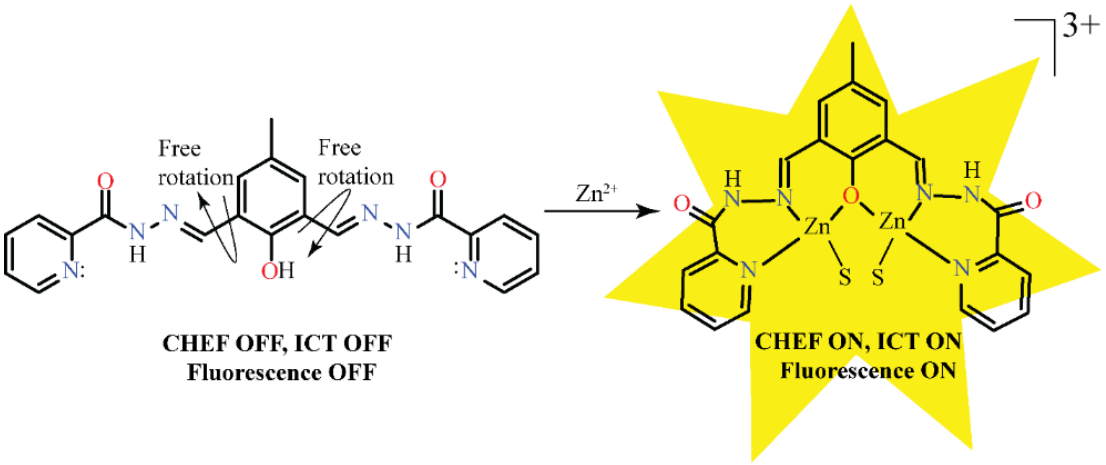

Scheme 4.2. Proposed mechanism of sensing.

4.8. Theoretical Calculations of L_2 and L_2-Zn Complex

Further, the above premise of our proposed sensing mechanism was corroborated with the theoretical calculations of **L_2** and its Zn complex. To understand the relationship between the structural changes of **L_2** and its complex with Zn^{2+} and the optical response of **L_2** to Zn^{2+}, we carried out density functional theory (DFT) calculations with the B3LYP/6-31+G(d,p) method basis set using the Gaussian 03 program. The optimized geometry along with the highest occupied molecular orbital (HOMO) and the lowest unoccupied molecular orbital (LUMO) of **L_2** and its

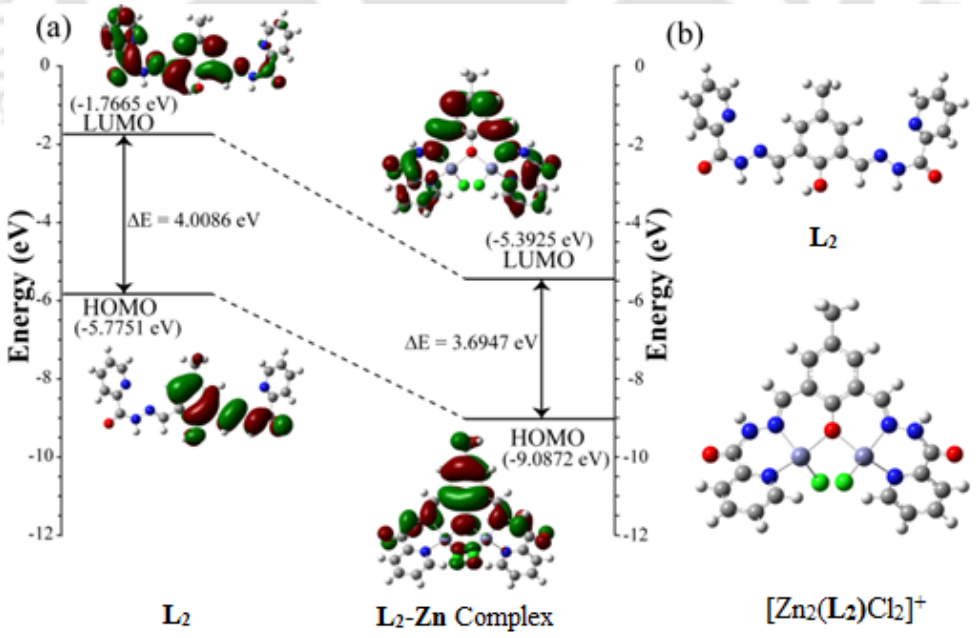

Figure 4.4. (a) Energy diagrams of HOMO and LUMO orbitals of **L_2** and the **L_2**–Zn complex calculated at the DFT level using a B3LYP/6-31+G(d,p) basis set. (b) Optimized structure of **L_2** and its Zn^{2+} complex.

Zn^{2+} complex are presented in Fig. 4.4. These HOMO and LUMO energy diagrams revealed that the energy gap for the di-nuclear Zinc complex of **L_2** (two Zinc ions are linked through the Oxo-bridge) was reduced as compared to the ligand alone (Fig. 4.4(a)). This perhaps led to the occurrence of red shifted (25 nm) fluorescence emission band upon chelation of the ligand with two Zn^{2+} ions in the proposed fashion. Selected orbitals and their corresponding energies for both **L_2** and its Zn complex were provided in supporting information (Table.S1 and S2 in supporting information) which might have been playing vital role in the optical spectral outcome.

4.9. Cellular Sensing of Zn^{2+}

Owing to the promising response of **L_2** towards Zn^{2+} and its intense emission in visible region, it was envisaged that compound **L_2** could be used for detection of intracellular Zn^{2+} by fluorescence-based imaging of live cells. However, to accomplish this target, it was imperative to initially evaluate the cytotoxic potential of compound **L_2** on live cells. The well-established MTT (3-(4,5-dimethylthiazol-2-yl)-2,5-diphenyltetrazolium bromide) assay, which is based on mitochondrial dehydrogenase activity of viable cells, illustrated that neither **L_2** nor its zinc complex was able to exhibit any effect on the viability of HeLa cells (human cervical carcinoma cells), even at concentrations as high as 50 μM (Fig. A4.2.). The results obtained from the *in vitro* cytotoxic assay were encouraging and suggested that a ligand concentration upto 50 μM can perhaps be employed for the fluorescence imaging studies of **L_2** and **L_2**–Zn complex in live cells. Hence, to evaluate the efficiency of compound **L_2** as a chemosensor for intracellular detection of Zn^{2+} by fluorescence microscopy, HeLa cells were treated with 25 μM **L_2** solution for 1 h followed by incubation with 50 μM $Zn(ClO_4)_2$ to promote the formation of **L_2**–Zn complex. Fluorescence microscope analysis revealed that compound **L_2** alone failed to exhibit any fluorescence in HeLa cells (Fig. 4.5). However, when treated with $Zn(ClO_4)_2$, a distinct and strong turn-on green fluorescence was observed which could be attributed to the formation of intracellular **L_2**-Zn complex. This observation is in well agreement with the results observed earlier in solution studies. It may be mentioned here that brightfield images of treated HeLa cells revealed the characteristic morphological attribute of HeLa cells, which also suggested that the cells were viable. The fluorescence microscopic analysis strongly suggested that compound **L_2** could readily traverse the membrane barrier, pervade into HeLa cells, and rapidly sense intracellular Zn^{2+}.

4.10. Conclusion

In brief, we have synthesized and demonstrated the sensing potential of an efficient receptor (**L_2**) for Zn^{2+} in physiological condition (99.7% HEPPES buffer, pH=7.4). The ligand **L_2** can be

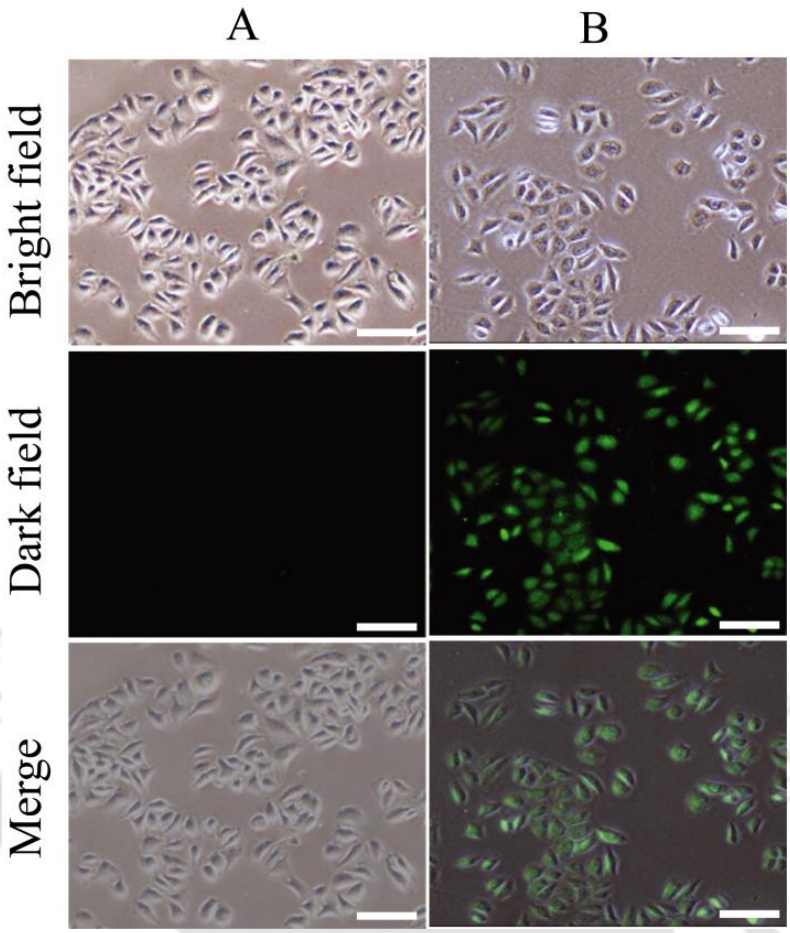

Figure 4.5. Fluorescence microscopic images of HeLa cells after adding 25 μM of $\mathbf{L_2}$ (column A) and after subsequent treatment with 50 μM Zn^{2+} (Column B). Scale bar for the images is 100 μm.

excited by visible light and has high selectivity towards Zn^{2+} over other biologically significant metal ions, even in the presence of higher concentration of competing metal ions. The judicious choice of a DFMP core in the receptor rendered a strong CHEF-based turn-on fluorescence following chelation of Zn^{2+} by the hydroxide group and the Schiff base N-atoms. Theoretical calculations of $\mathbf{L_2}$ and $\mathbf{L_2}$-zn ensemble also support our proposed mechanism. Due to the high selectivity of $\mathbf{L_2}$ towards Zn^{2+} in exclusively physiological medium and non-cytotoxic nature, the newly developed receptor was successful in sensing intracellular Zn^{2+}, wherein immensely intense turn-on green fluorescence was manifested in HeLa cells. The non-cytotoxic behaviour of $\mathbf{L_2}$ and its capability of sensing intracellular Zn^{2+} are well for future *in vivo* biomedical applications of the sensor.

So, coming from $\mathbf{L_1}$ to $\mathbf{L_2}$ i.e; changing the simple Schiff base to a imine-hydrazone receptor, $\mathbf{L_2}$ can sense Zn^{2+} in complete physiological medium whereas in the case of $\mathbf{L_1}$, there was a need of a mixture medium (Buffer: EtOH=7:3) for the sensing process. $\mathbf{L_2}$ was found to be non-toxic in behaviour which encouraged us to employ $\mathbf{L_2}$ for the sensing of intracellular Zn^{2+}. Both $\mathbf{L_1}$ and $\mathbf{L_2}$

recognized Zn^{2+} specifically with turn-on responses but the response of $\mathbf{L_2}$ was at higher wavelength (550 nm, yellow fluorescence) compared to $\mathbf{L_1}$ (480 nm, green fluorescence). Another fact is that $\mathbf{L_1}$-Zn complex has the selectivity towards Ppi but $\mathbf{L_2}$-Zn complex has no selectivity towards any anions.

References

4.1. (a) P. N. Prasad, *Introduction to Biophotonics*, Wiley, NJ, 2003; (b) J. B. Pawley, *Handbook of Biological Confocal Microscopy*, Plenum, New York, 1995; (c) J. W. Lichtman and J.-A. Conchello, *Nat. Methods*, 2005, **2**, 910.

4.2. (a) B. L. Vallee and K. H. Falchuk, *Physiol. Rev.*, 1993, **73**, 79; (b) J. M. Berg and Y. Shi, *Science*, 1996, **271**, 1081; (c) T. V. O'Halloran, *Science*, 1993, **261**, 715; (d) C. J. Frederickson, J. Y. Koh and A. I. Bush, *Nat. Rev. Neurosci.*, 2005, **6**, 449; (e) P. J. Fraker and L. E. King, *Annu. Rev. Nutr.*, 2004, **24**, 277; (f) A. C. Burdette and S. J. Lippard, *Proc. Natl. Acad. Sci. U. S. A.*, 2003, **100**, 3605; (g) Z. C. Xu, J. Y. Yoon and D. R. Spring, *Chem. Soc. Rev.*, 2010, **39**, 1996.

4.3. (a) M. J. Hambidge, *Nutr.*, 2000, **130**, 1344S; (b) J. Y. Koh, S. W. Suh, B. J. Gwag, Y. Y. He, C. Y. Hsu and D. W. Choi, *Science*, 1996, **272**, 1013; (c) H. Bartlett and F. Eperjesi, *Ophthalmic Physiol. Opt.*, 2003, **23**, 383; (d) C. Sindreu, R. D. Palmiter and D. R. Storm, *Proc. Natl. Acad. Sci. U. S. A.*, 2011, **108**, 3366; (e) A. I. Bush, *Alzheimer Dis. Assoc. Disord.*, 2003, **17**, 147; (f) C. L. F. Walker, Z. A. Bhutta, N. Bhandari, T. Teka, F. Shahid, S. Taneja and R. E. Black, *Am. J. Clin. Nutr.*, 2007, **85**, 887.

4.4. A. Voegelin, S. Poster, A. C. Scheinost, M. A. Marcus and R. Kretzsch-mar, *Environ. Sci. Technol.*, 2005, **39**, 6616.

4.5. (a) E. Tomat and S. J. Lippard, *Curr. Opin. Chem. Biol.*, 2010, **14**, 225; (b) Z. Xu, J. Yoon and D. R. Spring, *Chem. Soc. Rev.*, 2010, **39**, 1996; (c) E. L. Que, D. W. Domaille and C. J. Chang, *Chem. Rev.*, 2008, **108**, 1517; (d) P. Jiang and Z. Guo, *Coord. Chem. Rev.*, 2004, **248**, 205.

4.6. (a) E. M. Nolan and S. J. Lippard, *J. Am. Chem. Soc.*, 2003, **125**, 14270; (b) S. Atilgan, T. Ozdemir and E. U. Akkaya, *Org. Lett.*, 2010, **12**, 4792; (c) J. L. Sessler and J. M. Davis, *Acc. Chem. Res.*, 2001, **34**, 989; (d) B. W. Michel, A. R. Lippert and C. J. Chang, *J. Am. Chem. Soc.*, 2012, **134**, 15668.

4.7. (a) H. Giloh and J. W. Sedat, *Science*, 1982, **217**, 1252; (b) D. Sinnecker, P. Voigt, N. Hellwig and M. Schaefer, *Biochemistry*, 2005, **44**, 7085; (c) J. N. Henderson, H.-W. Ai, R. E. Campbell and S. J. Remington, *Proc. Natl. Acad. Sci. U. S. A.*, 2007, **104**, 6672; (d) N. Periasamy, S. Bicknese and A. S. Verkman, *Photochem. Photobiol.*, 1996, **63**, 265.

4.8. (a) T. E. Kaiser, V. Stepanenko and F. Würthner, *J. Am. Chem. Soc.*, 2009, **131**, 6719; (b) K.-R. Wang, D.-S. Guo, B.-P. Jiang, Z.-H. Sun and Y. Liu, *J. Phys. Chem. B*, 2010, **114**, 101; (c) Q. Zhao, S. Zhang, Y. Liu, J. Mei, S. Chen, P. Lu, A. Qin, Y. Ma, J. Z. Sun and B. Z. Tang, *J. Mater. Chem.*, 2012, **22**, 7387.

4.9. (a) F. Qian, C. Zhang, Y. Zhang, W. He, X. Gao, P. Hu and Z. Guo, *J. Am. Chem. Soc.*, 2009, **131**, 1460; (b) T. Hirayama, K. Okuda and H. Nagasawa, *Chem. Sci.*, 2013, **4**, 1250; (c) Y. Qian, J. Karpus, O. Kabil, S.-Y. Zhang, H.-L. Zhu, R. Banerjee, J. Zhao and C. He, *Nat. Commun.*, 2011, **2**, 495; (d) H. S. Jung, P. S. Kwon, J. W. Lee, J. Kim, C. S. Hong, J. W. Kim, S. Yan, J. H. Lee, T. Joo and J. S. Kim, *J. Am. Chem. Soc.*, 2009, **131**, 2008.

4.10. (a) Z. Xu, Y. Xiao, X. Qian, J. Cui and D. Cui, *Org. Lett.*, 2005, **7**, 889; (b) J. B. Wang, X. F. Qian and J. N. Cui, *J. Org. Chem.*, 2006, **71**, 4308.

4.11. (a) T. Gunnlaugsson, A. P. Davis, J. E. O'Brien and M. Glynn, *Org. Lett.*, 2002, **4**, 2449; (b) D. H. Vance and A. W. Czarnik, *J. Am. Chem. Soc.*, 1994, **116**, 9397; (c) S. K. Kim and J. Yoon, *Chem. Commun.*, 2002, 770.

4.12. (a) N. C. Lim, J. V. Schuster, M. C. Porto, M. A. Tanudra, L. Yao, H. C. Freake and C. Bruckner, *Inorg. Chem.*, 2005, **44**, 2018; (b) S. Guha, S. Lohar, A. Banerjee, A. Sahana, A. Chaterjee, S. K. Mukherjee, J. S. Matalobos and D. Das, *Talanta*, 2012, **91**, 18; (c) S. Das, A. Sahana, A. Banerjee, S. Lohar, S. Guha, J. S. Matalobos and D. Das, *Anal. Methods*, 2012, **4**, 2254.

4.13. (a) P. D. Beer, *Acc. Chem. Res.*, 1998, **31**, 71; (b) M. J. Kim, R. Konduri, H. Ye, F. M. MacDonnell, F. Puntoriero, S. Serroni, S. Campagna, T. Holder, G. Kinsel and K. Rajeshwar, *Inorg. Chem.*, 2002, **41**, 2471.

4.14. (a) S. Nishizawa, Y. Kato and N. Teramae, *J. Am. Chem. Soc.*, 1999, **121**, 9463; (b) J.-S. Wu, J.-H. Zhou, P.-F. Wang, X.-H. Zhang and S.- K. Wu, *Org. Lett.*, 2005, **7**, 2133; (c) B. Schazmann, N. Alhashimy and D. Diamond, *J. Am. Chem. Soc.*, 2006, **128**, 8607; (d) A. Banerjee, A. Sahana, S. Guha, S. Lohar, I. Hauli, S. K. Mukhopadhyay, J. S. Matalobos and D. Das, *Inorg. Chem.*, 2012, **51**, 5699; (e) A. Sahana, A. Banerjee, S. Lohar, S. Guha, S. Das, S. K. Mukhopadhyay and D. Das, *Analyst*, 2012, **137**, 3910.

4.15. J.-S. Wu, W.-M. Liu, X.-Q. Zhuang, F. Wang, P.-F. Wang, S.-L. Tao, X.-H. Zhang, S.-K. Wu and S.-T. Lee, *Org. Lett.*, 2007, **9**, 33.

4.16. S. Lohar, A. Sahana, A. Banerjee, A. Banik, S. K. Mukhopadhyay, J. S. Matalobos and D. Das, *Anal. Chem.*, 2013, **85**, 1778.

4.17. X. Peng, Y. Wu, J. Fan, M. Tian and K. Han, *J. Org. Chem.*, 2005, **70**, 10524.

4.18. (a) S. Das, S. Guha, A. Banerjee, S. Lohar, A. Sahana and D. Das, *Org. Biomol. Chem.*, 2011, **9**, 7097.

4.19. (a) J. M. Serin, D. W. Brousmiche and J. M. J. Frechet, *J. Am. Chem. Soc.*, 2002, **124**, 11848; (b) A. E. Albers, V. S. Okreglak and C. J. Chang, *J. Am. Chem. Soc.*, 2006, **128**, 9640; (c) S. H. Lee, S. K. Kim, J. H. Bok, S. H. Lee, J. Yoon, K. Lee and J. S. Kim, *Tetrahedron Lett.*, 2005, **46**, 8163; (d) W. R. Dichtel, J. M. Serin, C. Edder, J. M. J. Frechet, M. Matuszewski, L.-S. Tan, T. Y. Ohulchanskyy and P. N. Prasad, *J. Am. Chem. Soc.*, 2004, **126**, 538; (e) M. Suresh, S. Mishra, S. K. Mishra, E. Suresh, A. K. Mandal, A. Shrivastav and A. Das, *Org. Lett.*, 2009, **11**, 2740; (f) P. Mahato, S. Saha, E. Suresh, R. D. Liddo, P. P. Parnigotto, M. T. Conconi, M. K. Kesharwani, B. Ganguly and A. Das, *Inorg. Chem.*, 2012, **51**, 1769; (g) K. Sreenath, J. Allen, R. M. W. Davidson and L. Zhu, *Chem. Commun.*, 2011, **47**, 11730; (h) R. J. Wandell, A. H. Younes, L. Zhu, *New J. Chem.*, 2010, **34**, 2176.

4.20. (a) X. Peng, T. Wu, J. Fan, J. Wang, S. Zhang, F. Song and S. Sun, *Angew. Chem., Int. Ed.*, 2011, **50**, 4180; (b) Z. Xu, J. Yoon and D. R. Spring, *Chem. Soc. Rev.*, 2010, **39**, 1996; (c) Z.-Q. Guo, W.-H. Zhu, M.-M. Zhu, X.-M. Wu and H. Tian, *Chem. Eur. J.*, 2010, **16**, 14424; (d) Z.-P. Liu, C.-L. Zhang, Y.-L. Li, Z.-Y. Wu, F. Qian, X.-L. Yang, W.-J. He, X. Gao and Z.-J. Guo, *Org. Lett.*, 2009, **11**, 795; (e) C. E. Felton, L.P. Harding, J. E. Jones, B. M. Kariuki, S. J. A. Pope and C. R. Rice, *Chem. Commun.*, 2008, 6185; (f) H.-H. Wang, Q. Gan, X.-J. Wang, L. Xue, S.-H. Liu and H. Jiang, *Org. Lett.*, 2007, **9**, 4995.

4.21. (a) S. Maruyama, K. Kikuchi, T. Hirano, Y. Urano and T. Nagano, *J. Am. Chem. Soc.*, 2002, **124**, 10650; (b) K. Kiyose, H. Kojima, Y. Urano and T. Nagano, *J. Am. Chem. Soc.*, 2006, **128**, 6548; (c) C. C. Woodroofe and S. J. Lippard, *J. Am. Chem. Soc.*, 2003, **125**, 11458; (d) M. Taki, J. L. Wolford and T. V. O'Halloran, *J. Am. Chem. Soc.*, 2004, **126**, 712; (e) C. J. Chang, J. Jaworski, E. M. Nolan, M. Sheng and S. J. Lippard, *Proc. Natl. Acad. Sci. U.S.A.*, 2004, **101**, 1129; (f) M. M. Henary, Y. Wu and C. J. Fahrni, *Chem.−Eur. J.*, 2004, **10**, 3015; (g) N. C. Lim, C. Bruckner, *Chem. Commun.*, 2004, 1094. (h) A. Ajayaghosh, P. Carol and S. Sreejith, *J. Am. Chem. Soc.*, 2005, **127**, 14962; (i) K. Komatsu, Y. Urano, H. Kojima and T. Nagano, *J. Am. Chem. Soc.*, 2007, **129**, 13447; (j) X. Zhang, K. S. Lovejoy, A. Jasanoff and S. J. Lippard, *Proc. Natl. Acad. Sci. U.S.A.*, 2007, **104**, 10780.

4.22. H. A. Benesi and J. H. Hildebrand, *J. Am. Chem. Soc.*, 1949, **71**, 2703.

Appendix

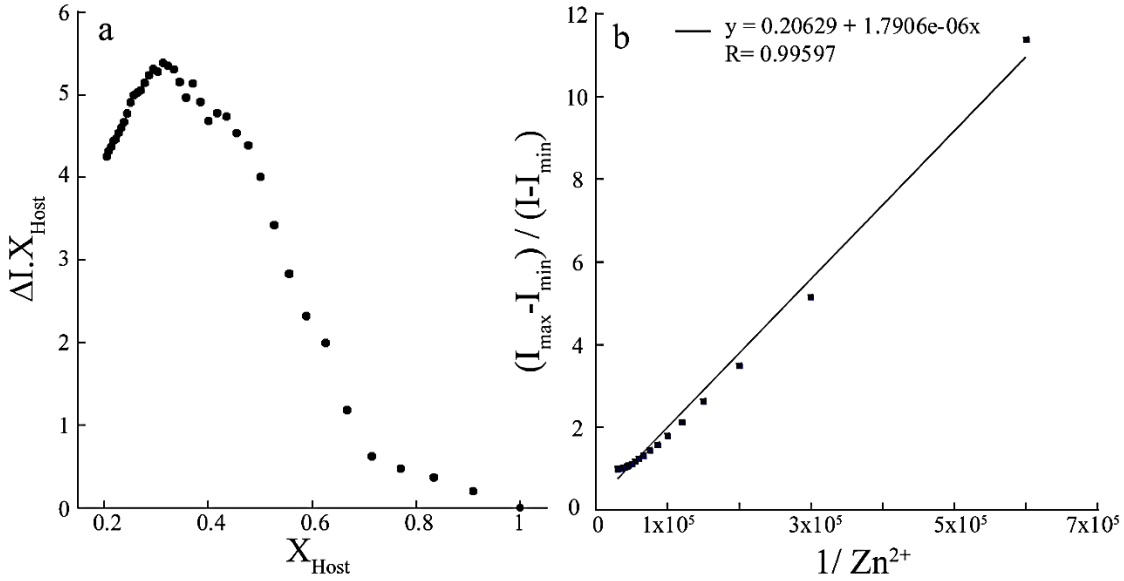

Figure A4.1. (a) Job's plot between $\mathbf{L_2}$ and Zn^{2+}. (b) Benesi–Hildebrand plot between $\mathbf{L_2}$ and Zn^{2+}.

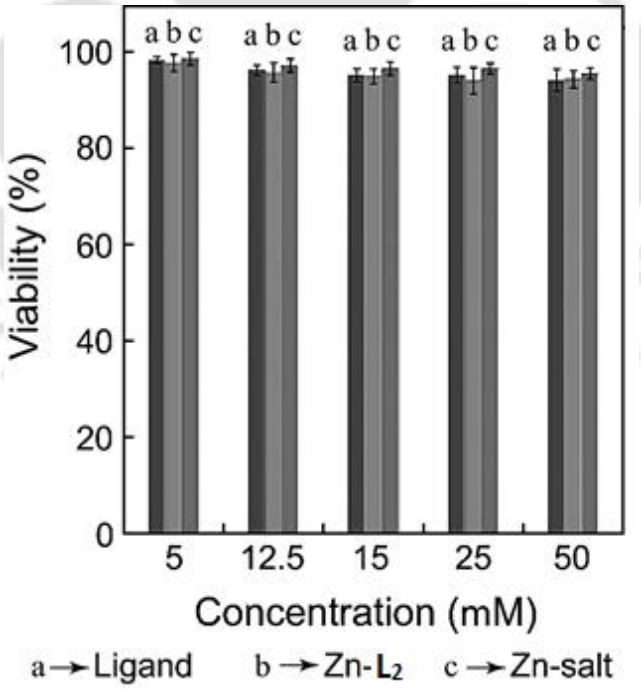

Figure A4.2. MTT assay to determine the cytotoxic effect of compound $\mathbf{L_2}$ and $\mathbf{L_2}$–Zn complex on HeLa cells.

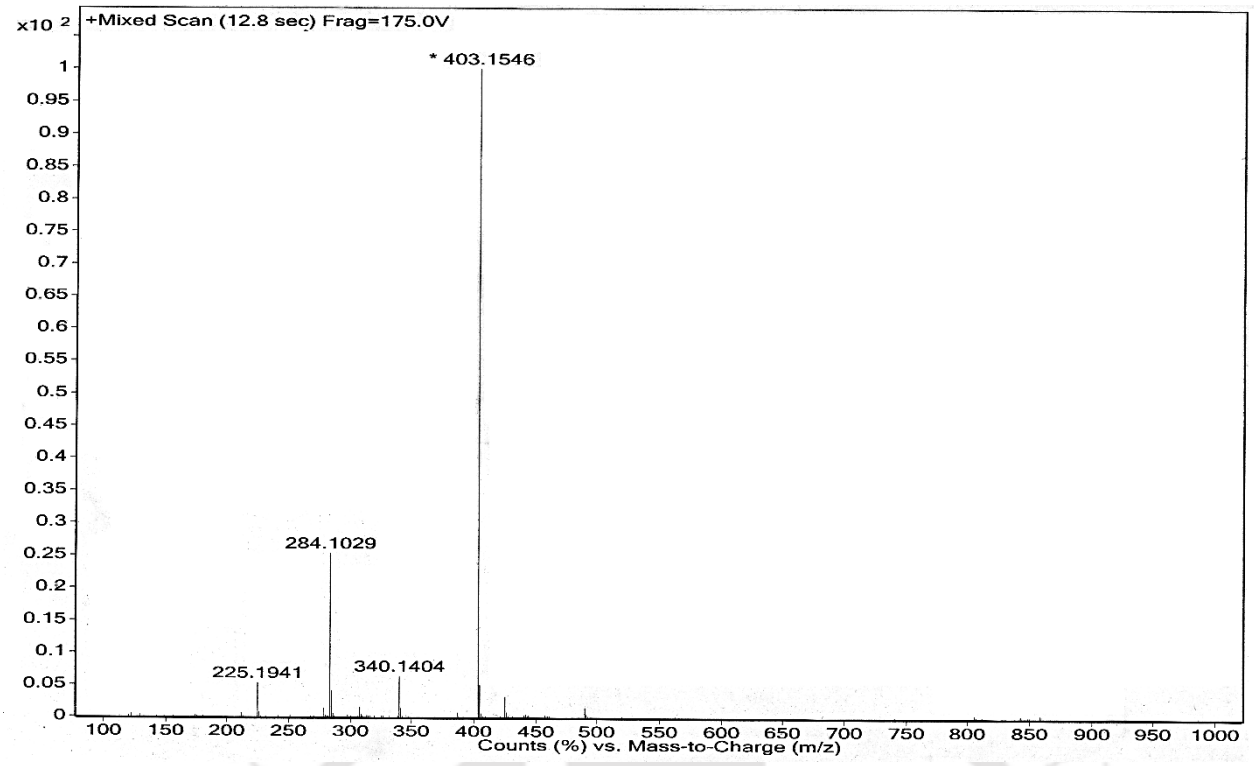

Figure A4.3. Mass spectrum of $\mathbf{L_2}$ (positive mode), Expected *m/z* for $C_{21}H_{19}N_6O_3$ $(\mathbf{L_2}+H)^+$ = 403.1519, Found 403.1546.

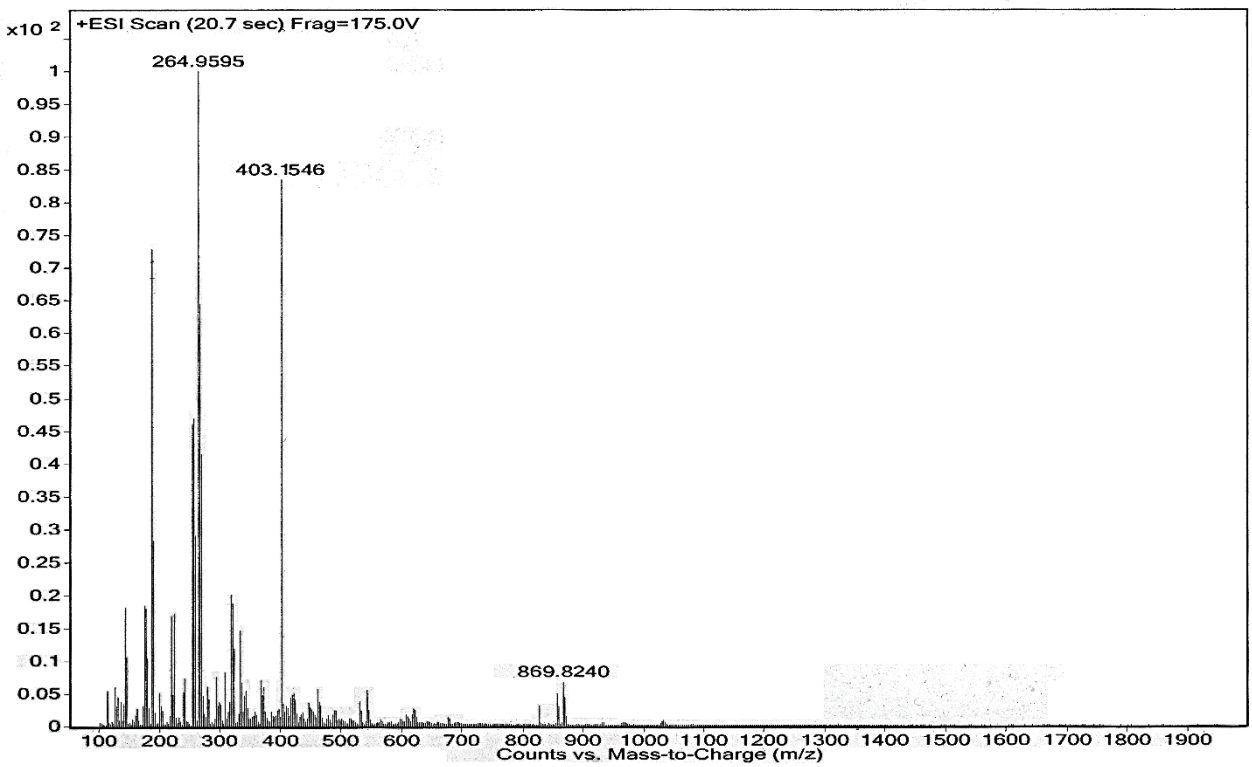

Figure A4.4. Mass spectrum of zinc complex of $\mathbf{L_2}$ (positive mode). Expected *m/z* for $C_{23}H_{21}Cl_3N_7O_{15}Zn_2$ ($\mathbf{L_2}$+2Zn+3ClO_4+CH_3CN) = 869.8713, found 869.8240.

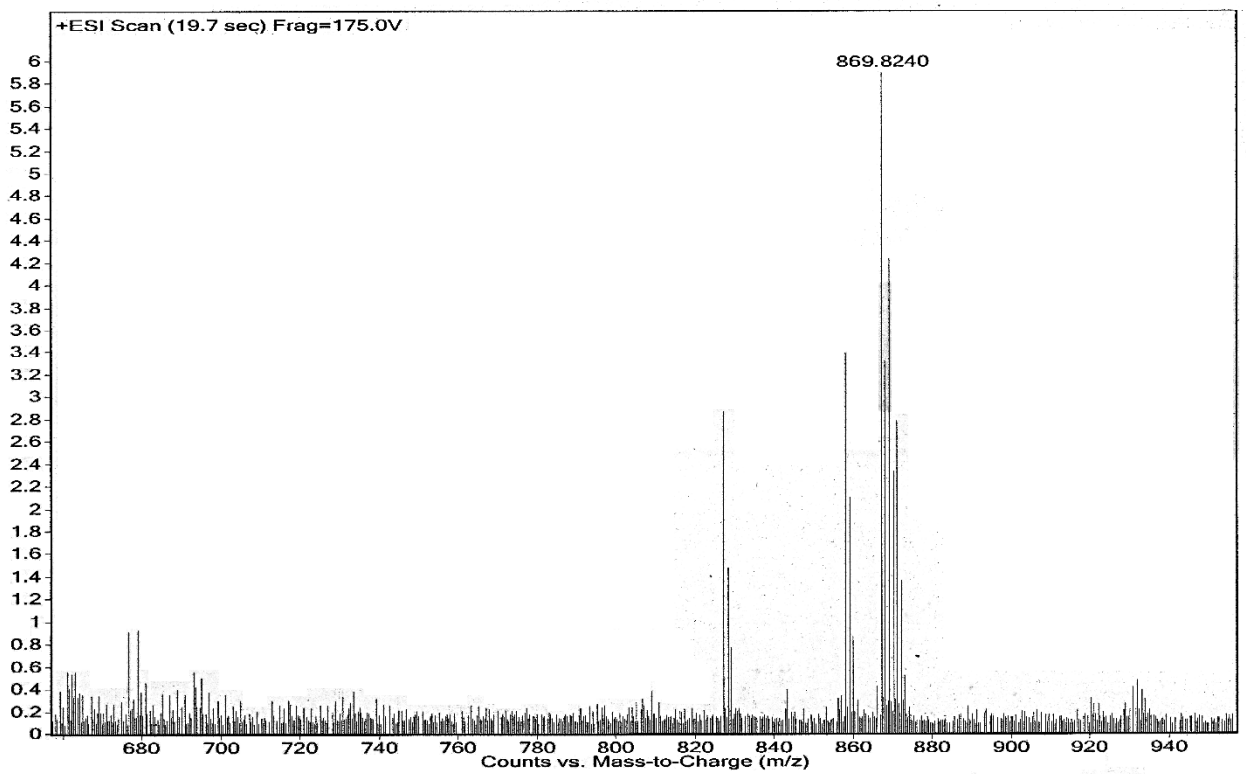

Figure A4.5. Expanded mass spectrum of zinc complex of $\mathbf{L_2}$ (positive mode).

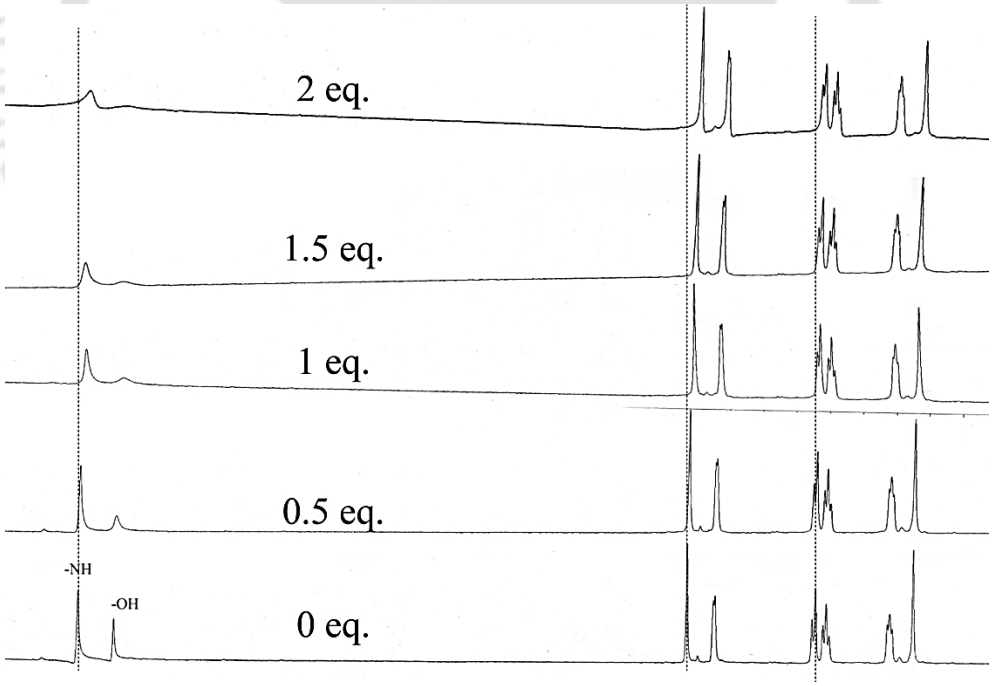

Figure A4.6. ^{1}H-NMR titration of $\mathbf{L_2}$ with Zn^{2+} in DMSO-d_6.

Table S1. Selected orbitals and their energies for $\mathbf{L_2}$ at B3LYP/6-31G(d,p).

Occupied Orbitals	Energy (eV)	Vacant Orbitals	Energy (eV)
HOMO -2 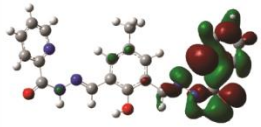	-6.6684	LUMO 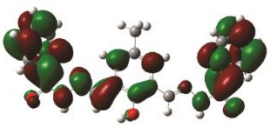	-1.7665
HOMO -1 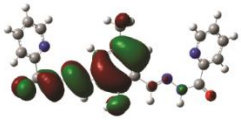	-5.9307	LUMO+1 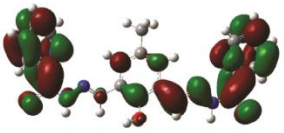	-1.4209
HOMO 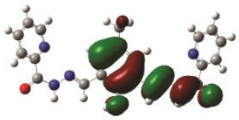	-5.7751	LUMO+2 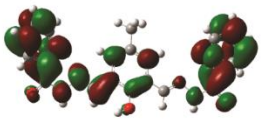	-1.1535

Table S2. Selected orbitals and their energies for $\mathbf{L_2}$-Zn^{2+} complex at B3LYP/6-31G(d,p).

Occupied Orbitals	Energy (eV)	Vacant Orbitals	Energy (eV)
HOMO -2 	-9.9906	LUMO 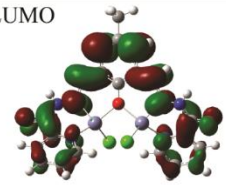	-5.3925
HOMO -1 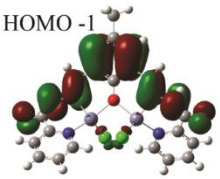	-9.5457	LUMO+1 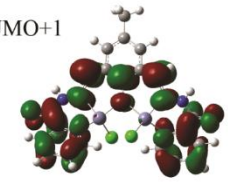	-5.1796
HOMO 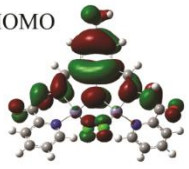	-9.0872	LUMO+2 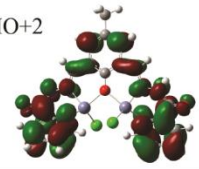	-4.7617

Chapter 5

A lab-on-a-molecule: Traffic signal like sensing of Al^{3+}, Zn^{2+} and F^{-}

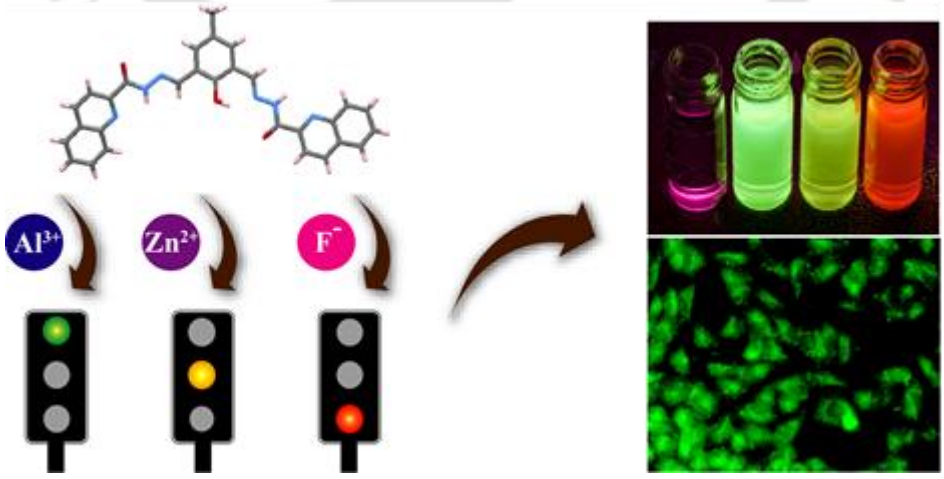

Chapter 5

5.1. Background and Focus of the Chapter

Development of molecular sensors for selective cation or anion sensing is critical for a host of pertinent environmental, biological and diagnostic applications.[5.1] Amongst the cations, zinc plays a critical role in a plethora of biological processes and has significant healthcare implications.[5.2, 5.3, 5.4] Though, there are reports of zinc sensors, [5.5] still there is a need for developing new sensors that render selective detection in presence of analogous analytes such as Cd^{2+} and in biological medium. Chemists have also been actively engaged in developing Al^{3+} sensors, given the profound role of Al^{3+} in neurotoxicity and neurodegenerative diseases[5.6] and its substantial impact on the environment.[5.7] In the context of anions, development of fluoride-specific sensors has gained prominence, owing to its significant role in various human ailments. [5.8] Although, research efforts in recent years has yielded some progress in developing fluoride sensors[5.9] sensing the anion in a competitive and aqueous system still remains a formidable challenge for analytical chemists.[5.10] With regard to the detection of environmental and biologically relevant ions, fluorescence-based tools are conceived to be efficient as they significantly enhance the capabilities for rapid and specific sensing of target analytes.[5.11, 5.1C] However, the analytical merit of fluorescent sensors developed against selective ions is limited in case of multi-analyte mixtures. To address this challenge, design and application of a single probe that renders multi-analyte sensing in various formats has been reported in recent times. [5.12] To develop an efficient multi-analyte sensor, it is critical to enhance the sensing repertoire of a single probe. This necessitates judicious design of the sensing ligand in order to achieve a discriminating response for various analytes.

The design principle of the reported ligand encompasses (i) incorporation of a strong fluorophore, (ii) suitable chelating ligand for binding metal ions and (iii) amide functionality for anion binding (Scheme 5.1). Dialdehyde derivatives are well known for their strong metal binding properties through two Schiff's base –N atoms with the hydroxyl group present at the centre of the binding cleft.[5b,11e,11f] The hydroxyl group readily deprotonates on binding with metal ions, which switch-on the ICT process and the CHEF process. Now, in order to ensure efficient anion binding, the presence of H-bonding donor is critical. Hence, in the present study, quinoline hydrazide residue has been chosen for binding both cation and anion. Quinoline has high affinity for Al^{3+}, whereas the –NH and the –OH will offer binding site to the anions. Based on this rationale, herein, we report a single dialdehyde-based fluorescent probe, which can differentially sense Al^{3+}, Zn^{2+} and

F^- ions and its distinct spectral properties upon target interaction and its application in live cell imaging studies are also reported.

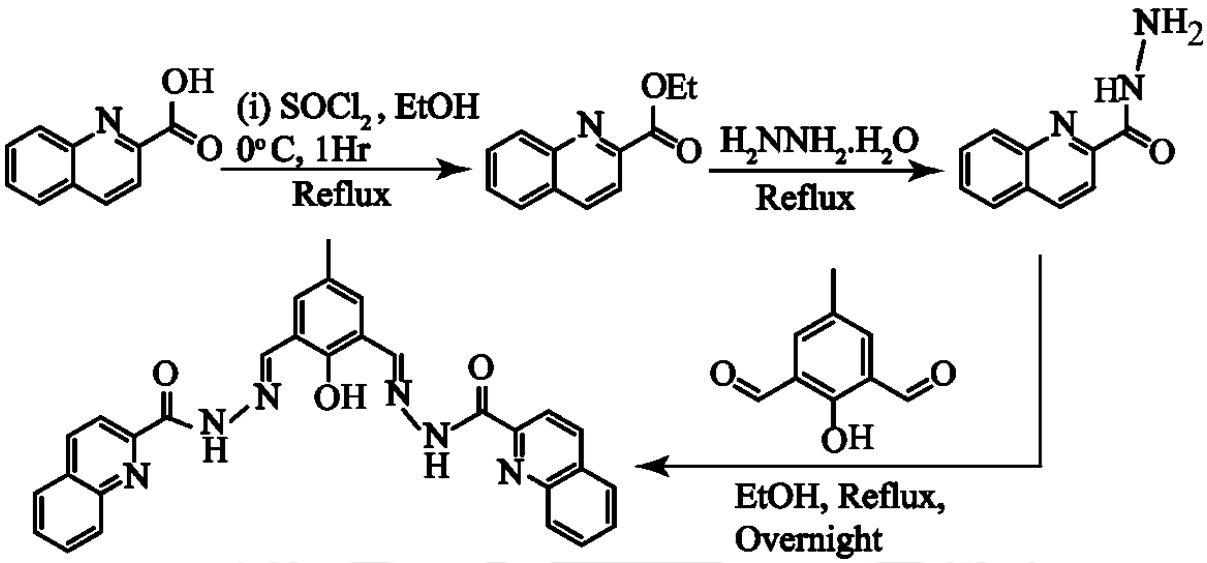

Scheme 5.1. Synthetic route for $\mathbf{L_3}$.

5.2. Crystal structure of L_3

Block shaped single crystals of $\mathbf{L_3}$ were grown from slow evaporation of its propanol solution. It crystallizes in monoclinic system with P21/c space group (Z = 8). The ligand $\mathbf{L_3}$ crystallizes in monoclinic system of space group $P2_1/c$. Crystal structure shows two arms are not planer and stay little above the plane of central benzene ring. Close inspection in interaction pattern indicates a intramolecular H-bonding between phenolic OH and imine N-atom (O6···N8 = 2.624 Å) is present in each asymmetric unit which possibly holds the arm tightly. We have observed a dimeric interaction between two ligand *via* carbonyl C=O and aromatic C−H H-bond (Fig. 5.1 and Fig. A5.9). Noticeably the only crystalline water molecule connects two ligand perpendicularly by donating hydrogen to quinoline N-atom atom and carbonyl C=O.

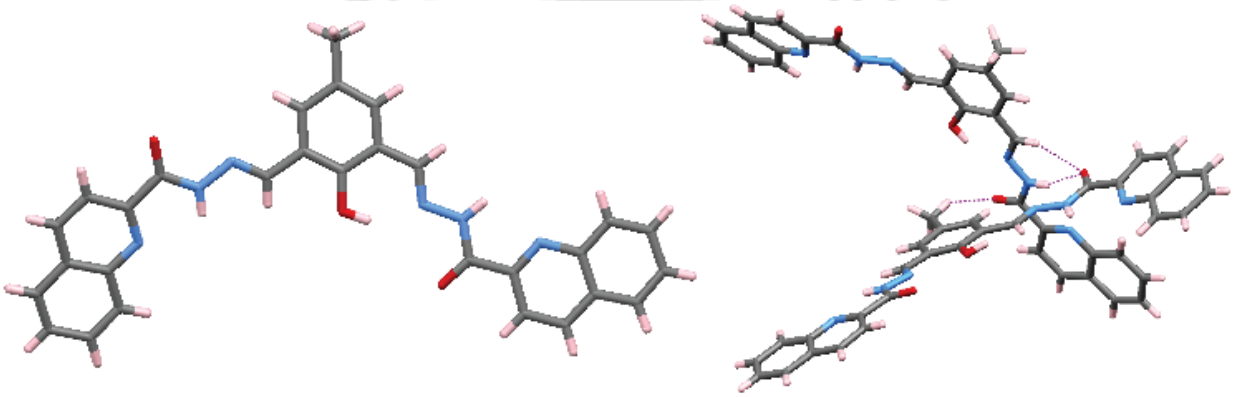

Figure 5.1. (a) Crystal structure of $\mathbf{L_3}$. (b) Various non-covalent interactions in the crystal.

5.3. UV-Vis spectroscopic studies of L_3 in the presence of metal ions

Interaction of **L_3** with various metal ions (Na^+, K^+, Mg^{2+}, Ca^{2+}, Co^{2+}, Ni^{2+}, Cu^{2+}, Cd^{2+}, Ag^+, Pb^{2+}, Hg^{2+}, Al^{3+}, Cr^{3+}, Fe^{3+}, Zn^{2+}) was pursued in a HEPES buffer medium (5 mM, pH 7.4) containing 0.33% of DMSO. The receptor exhibited three characteristic peaks at 289 nm ($\varepsilon = 4.67 \times 10^4\ M^{-1}\ cm^{-1}$), 315 nm ($\varepsilon = 3.96 \times 10^4\ M^{-1}\ cm^{-1}$) and at 368 nm ($\varepsilon = 2.65 \times 10^4\ M^{-1}\ cm^{-1}$), originating from $\pi-\pi^*$ transitions and the long conjugation present in the free ligand system. Amongst various metal ions (10 equivalent of each), interaction with Al^{3+}, Zn^{2+}, and Cu^{2+} only resulted in a change in the absorption spectra of **L_3**, with the maximum change observed with Zn^{2+} (Fig. 5.2a). Titration experiment with gradual addition of Al^{3+} ions resulted in diminishing of the peaks at 289 nm, 315 nm and 368 nm along with the emergence of a new peak at 430 nm ($\varepsilon = 1.97 \times 10^3\ M^{-1}\ cm^{-1}$ for Al^{3+} and $\varepsilon = 1.51 \times 10^4\ M^{-1}\ cm^{-1}$ for Zn^{2+}) (Fig. 5.2b), which can be attributed to the strong ligand-to-metal charge-transfer (LMCT). Presence of isosbestic points at 337 nm and 395 nm established the transformation of free receptor in its aluminium complex (Fig. 5.2b). Titration experiment with Zn^{2+} yielded analogous results as in the case of Al^{3+}, albeit a change of higher magnitude (Fig. 5.2c). Interestingly, a visual colour change from colourless to light yellow and deep yellow were observed with Al^{3+} and Zn^{2+}, respectively (Fig. 5.2b inset).

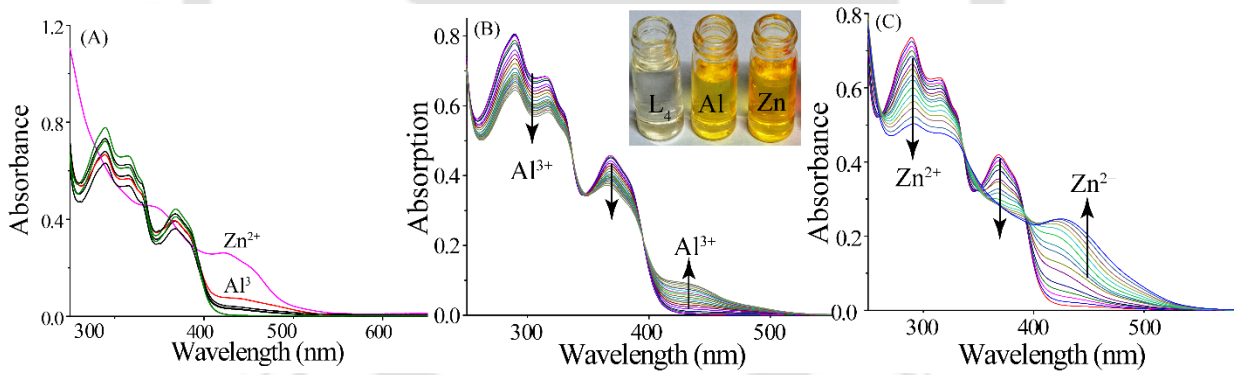

Figure 5.2. Changes in absorption spectra of **L_3** (25 μM) with (A) different metal ions (B) the incremental addition of Al^{3+}. Inset: colour change upon the addition of Al^{3+} and Zn^{2+} to **L_3**, (C) the incremental addition of Zn^{2+}.

5.4. Fluorescence spectroscopic studies of L_3 in the presence of metal ions

When excited at 395 nm, **L_3** displayed a weak emission peak at 520 nm. In presence of a set of metal ions (Na^+, K^+, Mg^{2+}, Ca^{2+}, Co^{2+}, Ni^{2+}, Cu^{2+}, Cd^{2+}, Ag^+, Pb^{2+}, Hg^{2+}, Al^{3+}, Cr^{3+}, Fe^{3+}, Zn^{2+}) in a buffered solution, a remarkable enhancement in the emission spectra of **L_3** was observed only with Al^{3+} and Zn^{2+} at two distinct wavelengths corresponding to 500 nm and 550 nm, respectively (Fig. 5.3a). These results validated the selectivity of **L_3** towards Al^{3+} and Zn^{2+}. Consequently, green fluorescence was observed in case of Al^{3+} whereas greenish yellow fluorescence was

observed upon interaction with Zn^{2+} (Fig. 5.3a inset). Titration experiments were also performed with gradual addition of Al^{3+} and Zn^{2+} to the solution of **L_3**. In both the cases, a systematic increment in the emission intensity of **L_3** was observed (Fig. 5.3b and Fig. 5.3c). It may be mentioned that in both cases, enhancement in emission intensity of **L_3** became minimal after the addition of two equivalents of the target metal ions (Fig. 5.3a, b, insets). Job's plot obtained from the titration experiments yielded 1:2 stoichiometry for both Al^{3+} and Zn^{2+} (Fig. A5.1a, A5.2a). The association constant of **L_3** for Al^{3+} and Zn^{2+} derived from Bensei-Hildebrand plot[5.13, 5.11f] (Fig. A5.1b, A5.2b) was observed to be 1.07 x 10^5 M^{-2} and 1.75x 10^5 M^{-2}, respectively. The detection limit of **L_3** for Al^{3+} and Zn^{2+} was 32 ppb and 35 ppb, respectively. The quantum yield of the free receptor was 0.002 whereas quantum yields for **L_3**-Al and L-Zn complexes were found to be 0.42 and 0.54 respectively. The selectivity of **L_3** towards Al^{3+} and Zn^{2+} was also established through experiments in the presence of competing metal ions (Fig. A5.3a, A5.3b).

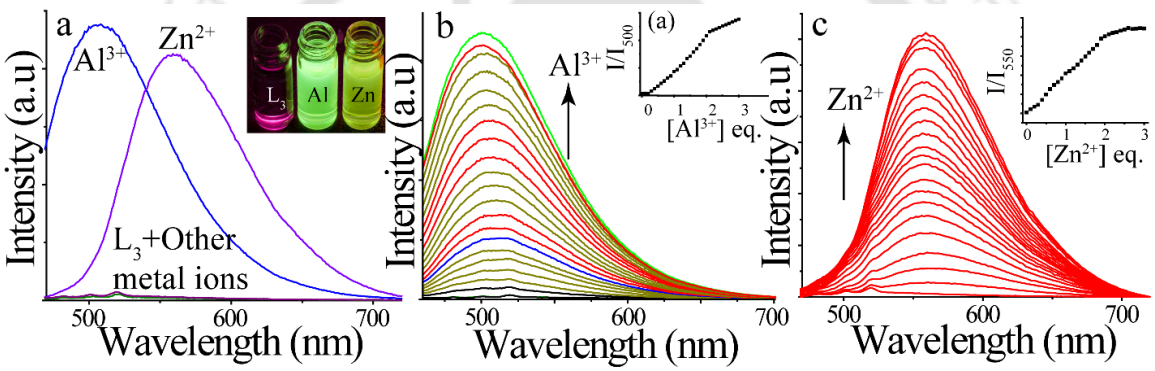

Figure 5.3. Changes in emission spectra of **L_3** (25 μM) (a) with different metal ions; Inset: Visual colour change upon the addition of Al^{3+} and Zn^{2+} to **L_3** under UV lamp (λ_{ex}= 365 nm). (b) with the incremental addition of Al^{3+}. Inset: (b) Intensity at 500 nm vs [Al^{3+}] plot, (b) (B) with incremental addition of Zn^{2+}, Inset: Intensity at 550 nm vs [Zn^{2+}] plot.

5.5. UV-Vis spectroscopic studies of L_3 in the presence of anions

To ascertain the sensing potential of **L_3** towards multi-target analyte, spectroscopic studies in presence of different anions were performed in an acetonitrile medium with 0.33% DMSO as a co-solvent. Among a set of different anions (F^-, Cl^-, Br^-, OH^-, I^-, NO_3^-, HSO_3^-, SO_4^{2-}, ClO_4^-, ClO_3^-, CN^-, S_2^-, $H_2PO_4^-$, PO_4^{3-}), a prominent change in the absorption spectra of **L_3** was manifested only upon addition of F^- (Fig. 5.4a). Titration of **L_3** with incremental amount of F^- resulted in a systematic decrease in the absorption peak at 368 nm and emergence of a new peak at 506 nm (Fig. 5.4b). Two distinct isosbestic points at 340 nm and 395 nm in the titration spectra indicated the formation of a new species. Interestingly, the colour of the solution changed from colourless to orange during the titration process (Fig. 5.4b, inset).

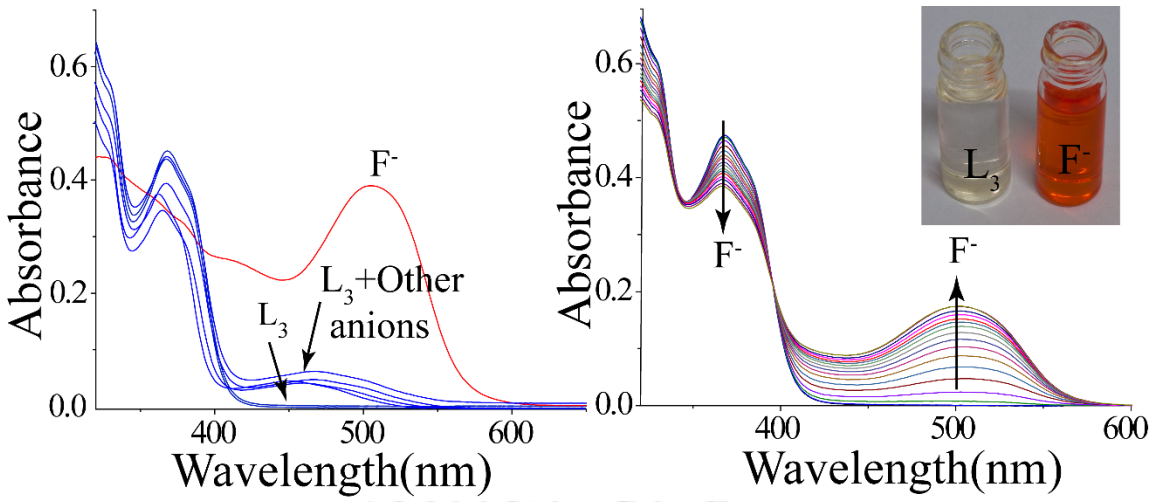

Figure 5.4. Changes in absorption spectra of **L_3** (25 μM) with (a) the addition of different anions (b) the incremental addition of F^-. Inset: Visual colour change upon the addition of F^- to **L_3**.

5.6. Fluorescence spectroscopic studies of L_3 in the presence of anions

When a set of various anions was used as target analyte, only F^- imparted a change in the emission spectra of **L_3** while other anions failed to induce any variation (Fig. 5.5a). Titration of **L_3** with fluoride triggered a distinct enhancement in the emission intensity at 575 nm (Fig. 5.5b) and the

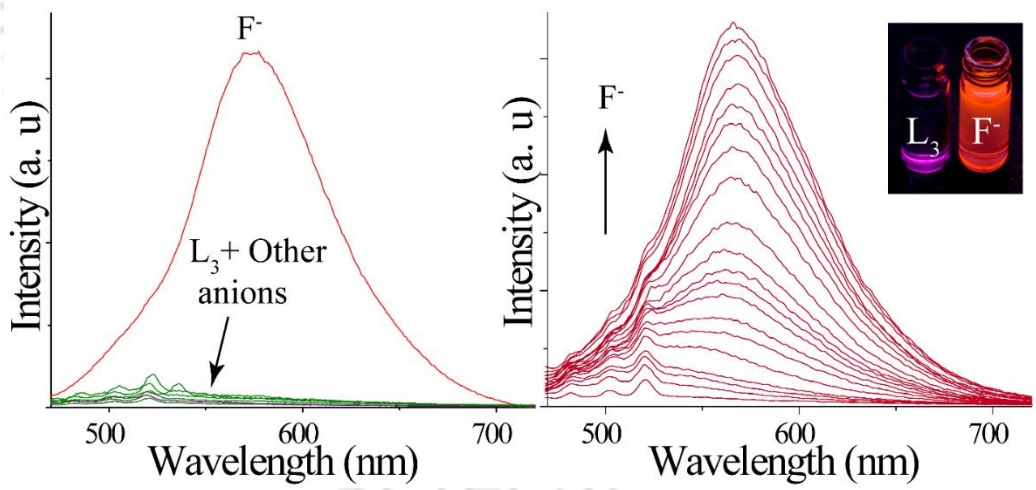

Figure 5.5. Changes in the emission spectra of **L_3** (25 μM) (a) with the addition of different anions (b) with the incremental addition of F^-. Inset: Visual colour change upon the addition of F^- to **L_3** under UV lamp (λ_{ex}= 365 nm).

fluorescence of the solution also changed to bright orange (Fig. 5.5a, inset). Jobs plot derived from the titration process revealed a 1:1 stoichiometry between **L_3** and F^-. The receptor **L_3** could detect F^- as low as 40 ppb. The quantum yield of the free receptor was 0.002 whereas quantum yield for **L_3**-F ensemble was calculated to be 0.40. The spectral and colour change were due to the

formation of receptor−fluoride H-bonded complex. This phenomenon was validated by addition of a small volume of water/methanol, which yielded a colourless solution.

5.7. pH dependent study

At lower pH (2-5), **L_3** was unable to sense any of the metal ions due to the protonation of the receptor. In the pH range of 5.5-9.5, the sensing behaviour of **L_3** towards both the metal ions was robust. At pH greater than 10, **L_3** could only recognize Zn^{2+} through a turn-on response. Interestingly, the receptor displayed stable fluorescence at physiological pH (Fig. 5.6), which suggested that the receptor is likely to be amicable for sensing in the physiological microenvironment and cellular milieu.

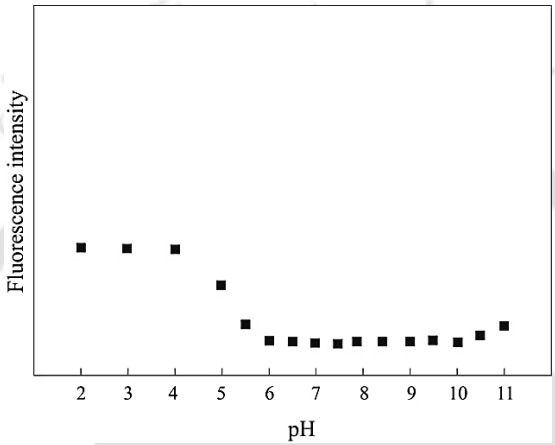

Figure 5.6. Effect of pH on the fluorescence intensity of **L_3**.

5.8. ^{1}H-NMR titration experiment of L_3 in presence of Al^{3+}, Zn^{2+} and F^-

To probe the interaction between **L_3** with Al^{3+} and Zn^{2+}, ^{1}H-NMR titration experiment was performed for both the metal ions. Titration of **L_3** with Al^{3+} resulted in upfield shift for –NH (0.020 ppm), -OH (0.049 ppm) and the Schiff base protons (0.056 ppm) (Fig. A5.4). In case of titration with Zn^{2+} similar trends of lesser magnitude were observed (Fig. A5.5). With the gradual addition of Zn^{2+}, the reduction in the intensity of –OH group peak was accompanied by an upfield shift, which indicated deprotonation of **L_3**. The above results strongly indicated that the phenolic –OH group and the Schiff base N-atoms bind with both the metal ions along with the deprotonation of the phenolic –OH group. Involvement of the quinoline ring in binding with Al^{3+} was clear from the shifts of the quinoline ring protons whereas in the case of Zn^{2+}, quinoline ring did not participate in binding which was also evident from the ^{1}H-NMR experiment. The changes in the ^{1}H-NMR spectra of **L_3** were observed up to the addition of two equivalents of Zn^{2+} ions, which supported the results obtained from the absorption and emission spectroscopy. ^{1}H- NMR titration of **L_3** with tetra-butyl salt of fluoride yielded prominent changes in comparison with the metal ions (Fig. A5.6). Deprotonation of both the phenolic –OH group and the –NH group was

observed on the addition of excess of F^- ion. Initially the phenolic –OH group, was deprotonated and a downfield shift along with reduction in the intensity of the –NH proton was observed ($\Delta\delta$=0.055 ppm). The imine proton also confronted downfield shift of $\Delta\delta$=0.116 ppm, whereas the quinoline ring protons were shifted upfield but the shifts ($\Delta\delta$) were miniscule compared to the other changes. So, due to deprotonation of both the phenolic –OH and the –NH groups, sharp changes were observed in the case of fluoride in both absorption and emission spectroscopy.

5.9. Plausible Mechanism of sensing

The low fluorescence of the free receptor may be attributed to the absence of intramolecular charge transfer (ICT) and the free rotation around the imine bond. Upon interaction with the target analytes, the free rotation around the imine bonds got restricted, which resulted in the formation of a rigid platform. Hence, a chelation enhanced fluorescence enhancement (CHEF) process occurred in the presence of the analytes. Further, in all cases, deprotonation triggers the ICT process, which leads to the turning-on of the fluorescence of the receptor.

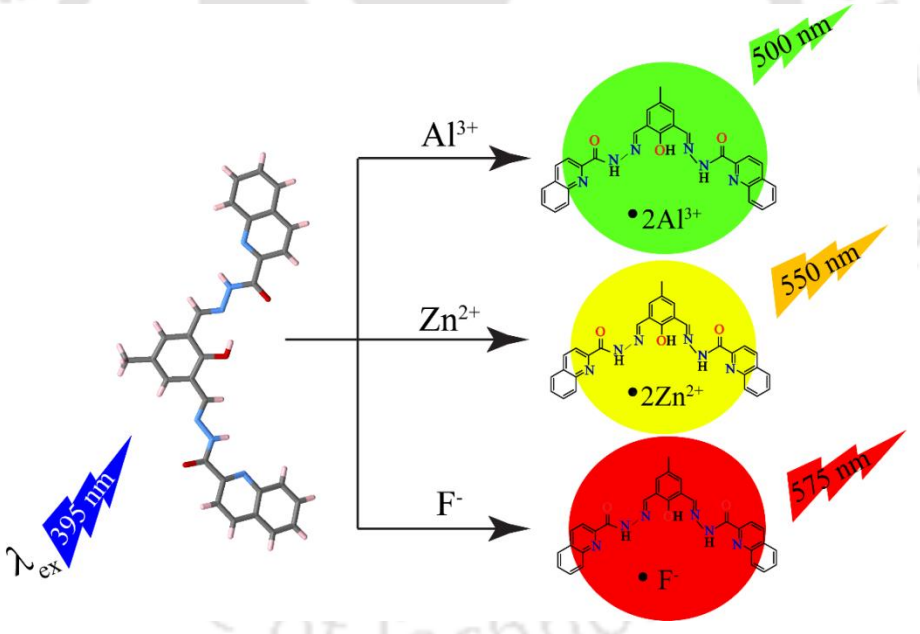

Scheme 5.2. Schematic representation of sensing of Al^{3+}, Zn^{2+} and F^- by $\mathbf{L_3}$.

5.10. Biological studies of L_3 in the presence of metal ions

On the basis of the excellent response of $\mathbf{L_3}$ towards Al^{3+} and Zn^{2+} in solution mimicking the physiological condition, we anticipated that $\mathbf{L_3}$ could be explored for the sensing of these target metals in live cells. To accomplish this goal, it was significant to probe the cytotoxic effect of $\mathbf{L_3}$ and its metal complexes on live cells. A conventional MTT assay, which is based on the mitochondrial dehydrogenase activity of viable cells illustrated that $\mathbf{L_3}$ as well as the metal

complexes failed to affect the viability of the HeLa cells even at a concentration as high as 50 μM (Fig. A5.7.). Subsequently, sensing of Al^{3+} and Zn^{2+} was pursued in HeLa cells by cell imaging studies, wherein the cells were initially incubated with 10 μM of **L_3** followed by addition of 20 μM each of either Al^{3+} or Zn^{2+} in separate sets. HeLa cells incubated with only **L_3** failed to exhibit any fluorescence, while bright green fluorescence manifested in the cells upon addition of the target metals (Fig. 5.7.). It was noted that the fluorescence was well spread in the cell, which suggested that the ligand could traverse across the cell membrane and diffuse throughout the cell. It was also evident that the HeLa cells retained their morphological trait during the cell imaging studies (Fig. 5.7), which reiterated the non-toxic nature of the developed receptor.

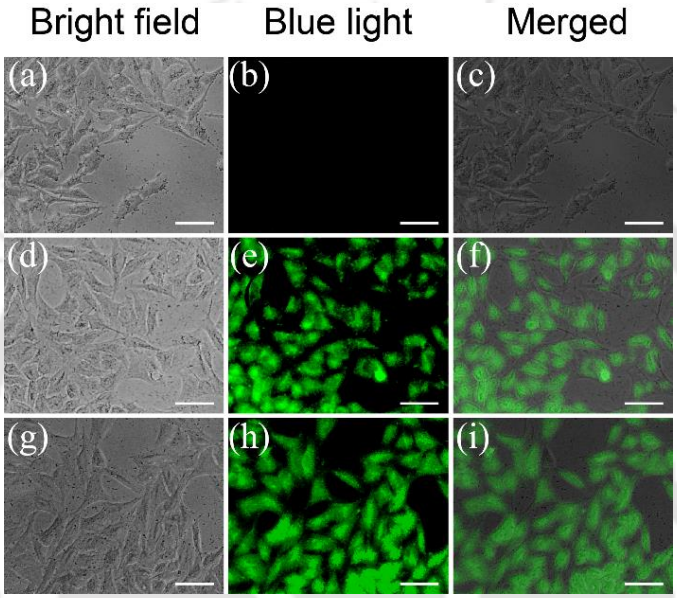

Figure 5.7. Fluorescence microscopic images of HeLa cells treated with (A-C) 5.0 μM of **L_3**, (D-F) pre-treated with 5.0 μM of **L_3** followed by addition of 50 μM Al^{3+} solution, (G-I) pre-treated with 5.0 μM of **L_3** followed by addition of 50 μM Zn^{2+} solution. Scale bar for the images is 100 μM.

5.11. Conclusion

In brief, we have designed and synthesized a new di-aldehyde-based sensor, which facilitates distinctive sensing of Al^{3+}, Zn^{2+} and F^-. The present work is a judicious illustration of developing a single fluorescence-based probe for multi-analytes, which may render useful applications in environmental and diagnostic regime.

After receiving encouraging results by altering simple imine (**L_1**) to an imine-hydrazone (**L_2**), herein we have designed **L_3** by just altering the pyridyl ring (**L_2**) to a quinoline ring (**L_3**) keeping rest of the surroundings unchanged and investigated its properties. From the above results, it was evident that **L_3** behaved differently from **L_2**. When **L_2** can sense only Zn^{2+}, **L_3** can sense Al^{3+} and Zn^{2+} both in complete physiological medium at two different wavelengths (500 nm and 550 nm

respectively). In addition to that, **L_3** was also selective towards F^- in acetonitrile medium at 575 nm. **L_3** was established to be non-toxic in nature which encouraged us to employ **L_3** for the sensing of intracellular Al^{3+} and Zn^{2+}. So, **L_3** acted as a lab-on-a-molecule which can sense Al^{3+}, Zn^{2+} and F^- at three different wavelengths (500 nm, 550 nm nad 575 nm respectively) with three different fluorescence (green, yellow and orange fluorescence) producing a traffic signal like sensing.

References

5.1. D. Astruc, E. Boisselier and C. Ornelas, *Chem. Rev.*, 2010, **110**, 1857- 1959; (b) J. Wu, W. Liu, J. Ge, H. Zhang and P. Wang, *Chem. Soc. Rev.*, 2011, **40**, 3483- 3495. (c) A. P. de Silva, H. Q. N. Gunaratne, T. Gunnlaugsson, A. J. M. Huxley, C. P. McCoy, J. T. Rademacher and T. E. Rice, *Chem. Rev.*, 1997, **97**, 1515-1566.

5.2. (a) K. M. Hambidge and N. F. Krebs, *J. Nutr.*, 2007, **137**, 1101-1105; (b) J. M. Berg and Y. Shi, *Science*, 1996, **271**, 1081-1085; (c) A. C. Burdette and S. J. Lippard, *Proc. Natl. Acad. Sci. U. S. A.*, 2003, **100**, 3605–3610.

5.3. (a) S. Y. Assaf and S. H. Chung, *Nature*, 1984, **308**, 734−736; (b) C. J. Frederickson and A. I. Bush, *BioMetals*, 2001, **14**, 353-366; (c) P. Molnar, J. V. Nadler, *Brain Res.*, 2001, **910**, 205-207; (d) A. M. Hosie, E. L. Dunne, R. J. Harvey and T. G. Smart, *Nat. Neurosci.*, 2003, **6**, 362–369.

5.4. (a) J. Y. Koh, S. W. Suh, B. J. Gwag, Y. Y. He, C. Y. Hsu and D. W. Choi, *Science*, 1996, **272**, 1013-1016; (b) C. Sindreu, R. D. Palmiter and D. R. Storm, *Proc. Natl. Acad. Sci. U. S. A.*, 2011, **108**, 3366–3370; (c) A. I. Bush, *Alzheimer Dis. Assoc. Disord.*, 2003, **17**, 147–150; (d) C. J. Frederickson, J. Y. Koh and A. I. Bush, *Nat. Rev. Neurosci.*, 2005, **6**, 449–462.

5.5. (a) Z. Xu, J. Yoon and D. R. Spring, *Chem. Soc. Rev.*, 2010, **39**, 1996-2006; (b) B. K. Datta, S. Mukherjee, C. Kar, A. Ramesh and G. Das, *Anal. Chem.*, 2013, **85**, 8369–8375; (c) Y. Mikata, A. Yamashita, K. Kawata, H. Konno, S. Itami, K. Yasuda and S. Tamotsu, *Dalton Trans.*, 2012, **41**, 4976–4984; (d) J. E. Kwon, S. Lee, Y. You, K.-H. Baek, K. Ohkubo, J. Cho, S. Fukuzumi, I. Shin, S. Y. Park and W. Nam, *Inorg. Chem.*, 2012, **51**, 8760–8774.

5.6. (a) A. Salifoglou, *Coord. Chem. Rev.*, 2002, **228**, 297–317; (b) M. E. Percy, T. P. A. Kruck, A. I. Pogue and W. J. Lukiw, *J. Inorg. Biochem.*, 2011, **105**, 1505–1512; (c) G. D. Fasman, *Coord. Chem. Rev.*, 1996, **149**, 125–165; (d) D. Krewski, R. A. Yokel, E. Nieboer, D. Borchelt, J. Cohen, J. Harry, S. Kacew, J. Lindsay, A. M. Mahfouz and V. Rondeau, *J. Toxicol. Environ. Health, Part B.*, 2007, **10(S1)**, 1-269.

5.7. (a) E. Altschuler, *Med. Hypotheses*, 1999, **53**, 22-23; (b) S. Polizzi, E. Pira, M. Ferrara, M. Bugiani, A. Papaleo, R. Albera and S. Palmi, *NeuroToxicology*, 2002, **23**, 761–774; (c) H. E. Witters, S. VanPuymbroeck, A. H. X. Stouthart and S. E. W. Bonga, *Environ. Toxicol. Chem.*, 1996, **15**, 986–996; (d) L. V. Kochian, O. A.

Hoekenga and M. A. Piñeros, *Annu. Rev. Plant Biol.*, 2004, **55**, 459-493; (e) A. B. S. Poléo, K. Østbye, S. A. Øxnevad, R. A. Andersen, E. Heibo and L. A. Vøllestad, *Environ. Pollut.*, 1997, **96**, 129-39.

5.8. (a) E. Gazzano, L. Bergandi, C. Riganti, E. Aldieri, S. Doublier, C. Costamagna, A. Bosia and D. Ghigo, *Curr. Med. Chem.*, 2010, **17**, 2431–2441; (b) B. Spittle, Neurotoxic effects of fluoride, *Fluoride*, 2011, **44,** 117-124; (c) P. Grandjean and P. J. Landrigan, *Lancet.*, 2006, **368**, 2167-2178.

5.9. (a) M. Cametti and K. Rissanen, *Chem. Commun.*, 2009, 2809-2829; (b) S.-D. Jeong, A. Nowak-Krol, Y. Kim, S.-J. Kim, D. T. Gryko and C.-H. Lee, *Chem. Commun.*, 2010, **46**, 8737–8739; (c) T. Mizuno, W.-H. Wei, L. R. Eller and J. L. Sessler, *J. Am. Chem. Soc.*, 2002, **124**, 1134–1135; (d) J. Wang, L. Yang, C. Hou and H. Cao, *Org. Biomol. Chem.*, 2012, **10**, 6271-6274; (e) I.-S. Ke, M. Myahkostupov, F. N. Castellano and F. P. Gabbai, *J. Am. Chem. Soc.*, 2012, **134,** 15309–15311.

5.10. (a) J. L. Sessler, P. A. Gale and W. S. Cho, *Anion Receptor Chemistry;* Royal Society of Chemistry: Cambridge, UK, 2006. (b) W. J. Marshall and S. K. Bangert, *Clinical Chemistry*, Elsevier: Edinburgh, 5th ed.; 2004.

5.11. (a) G. Aragay, J. Pons and A. Merkoc, *Chem. Rev.*, 2011, **111,** 3433–3458; (b) K. M. Dean, ,Y. Qin and A. E. Palmer, *Biochim. Biophys. Acta*, 2012, **1823**, 1406–1415; (c) S. Samanta, S. Goswami, A. Ramesh and G. Das, *Sens. Actuators, B*, 2014, **194,** 120-126; (d) C. Kar, M. D. Adhikari, A. Ramesh and G. Das, *Inorg. Chem.*, 2013, **52,** 743–752; (e) B. K. Datta, D. Thiyagarajan, C. Kar, A. Ramesh and G. Das, *Org. Biomol. Chem.*, 2014, **12,** 4975-4982; (f) C. Kar, M. D. Adhikari, B. K. Datta, A. Ramesh and G. Das, *Sensor. Actuators, B.*, 2013, **188,** 1132-1140.

5.12. (a) D. C. Magri, G. J. Brown, G. D. McClean and A. P. de Silva, *J. Am. Chem. Soc.*, 2006, **128,** 4950–4951; (b) A. P. de Silva and S. Uchiyama, *Nat. Nanotechnol.*, 2007, **2,** 399–410; (c) D. Margulies, C. E. Felder, G. Melman, A. Shanzer, *J. Am. Chem. Soc.*, 2007, **129,** 347–354; (d) M. Dong, Y. Peng, Y.-M. Dong, N. Tang and Y.-W. Wang, *Org. Lett.*, 2012, **14,** 130–133; (e) L. E. Santos-Figueroa, M. E. Moragues, E. Climent, A. Agostini, R. Martinez-Manez, F. Sanceno´n, *Chem. Soc. Rev.*, 2013, **42,** 3489-3613.

5.13. H. A. Benesi and J. H. Hildebrand, *J. Am. Chem. Soc.*, 1949, **71,** 2703–2707.

5.14. *Saint, Smart and XPREP*, Siemens Analytical X-ray Instruments Inc., Madison, Wisconsin, USA, 1995.

5.15. G. M. Sheldrick, *SADABS: software for Empirical Absorption* Correction, University of Gottingen, Institute fur Anorganische Chemieder Universitat, Tammanstrasse 4, D- 3400 Gottingen, Germany, 1999–2003.

5.16. (a) G. M. Sheldrick, *SHELXS-97*, University of Gottingen, Germany, 1997; (b) G. M. Sheldrick, *SHELXL-97, Program for Crystal Structure Refinement*, University of Gottingen, Germany, 1997.

5.17. *Mercury 1.3 Supplied with Cambridge Structural Database, CCDC*, Cambridge, U.K., 2003–2004.

Appendix

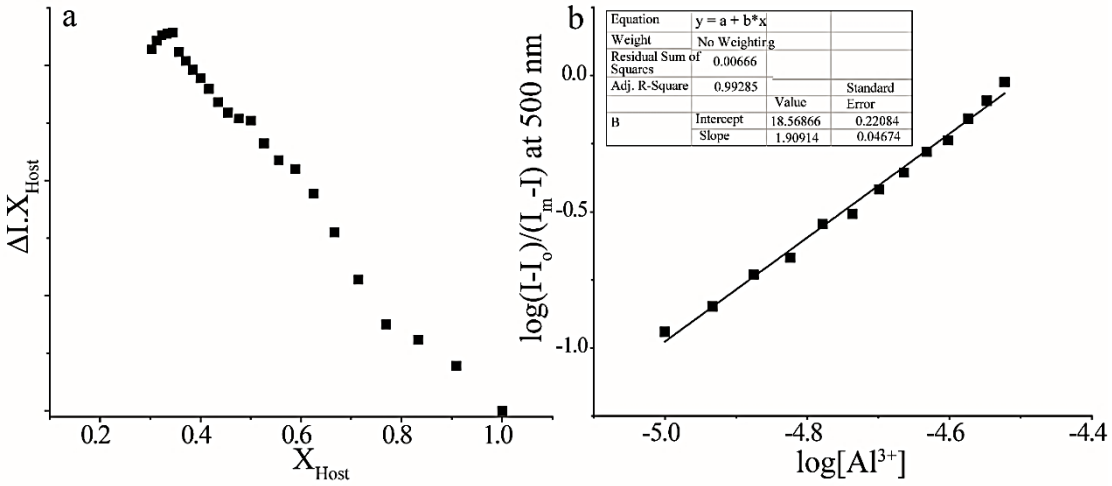

Figure A5.1. (a) Job's plot between $\mathbf{L_3}$ and Al^{3+} ions. X_{Host} is the mole fraction of $\mathbf{L_3}$ and ΔI is the change $(I-I_0)$ in the intensity of the emission spectra in presence of guest i.e; Al^{3+}, (b) Bensei-Hildebrand plot obtained for Al^{3+} from the emission experiment (emission intensity calculated from 500 nm) studies.

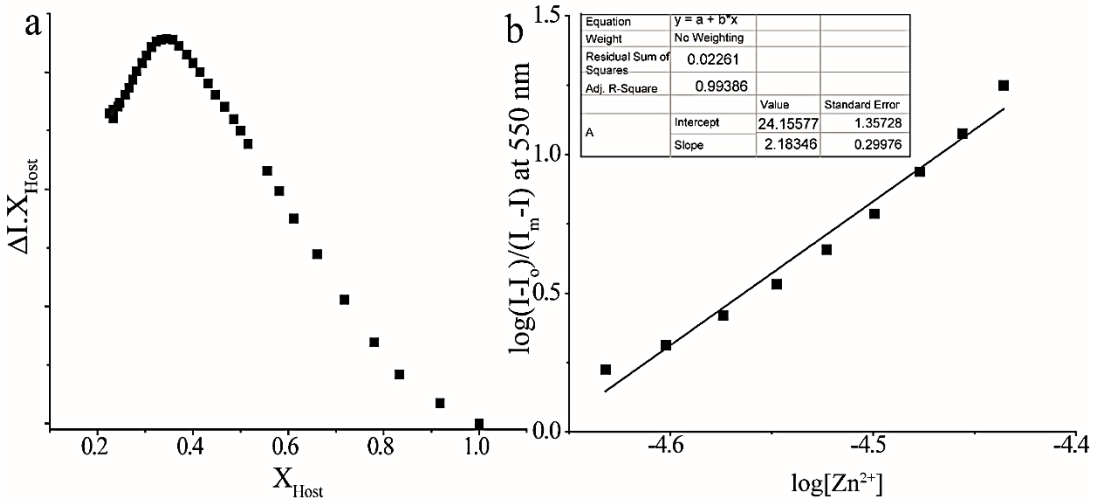

Figure A5.2. (a) Job's plot between $\mathbf{L_3}$ and Zn^{2+} ions. X_{Host} is the mole fraction of $\mathbf{L_3}$ and ΔI is the change $(I-I_0)$ in the intensity of the emission spectra in presence of guest i.e; Zn^{2+}, (b) Bensei-Hildebrand plot obtained for Zn^{2+} from the emission experiment (emission intensity calculated from 550 nm) studies.

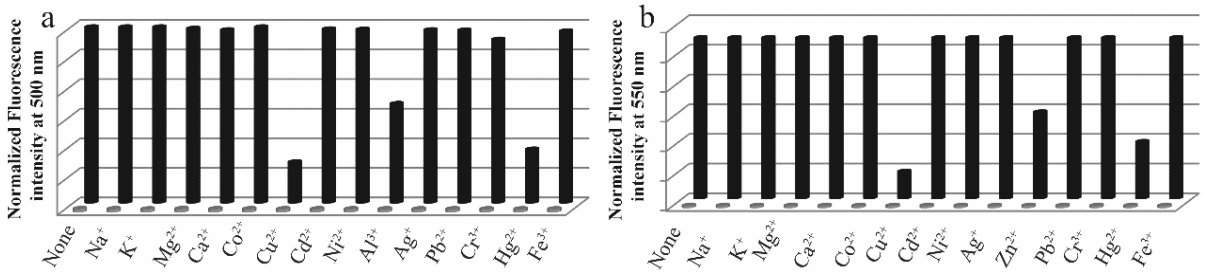

Figure A5.3. (a)Normalized fluorescence responses of $\mathbf{L_3}$ (10 μM) to various cations in mixed solvent. The gray bars represent the emission intensities of $\mathbf{L_3}$ in the presence of cations of interest (5 eqv.). The black bars represent the change of the emission that occurs upon the subsequent addition of Al^{3+} to the above solution. (b) Normalized fluorescence responses of $\mathbf{L_3}$ (10 μM) to various cations in mixed solvent. The gray bars represent the emission intensities of $\mathbf{L_3}$ in the presence of cations of interest (5 eqv.). The black bars represent the change of the emission that occurs upon the subsequent addition of Zn^{2+} to the above solution.

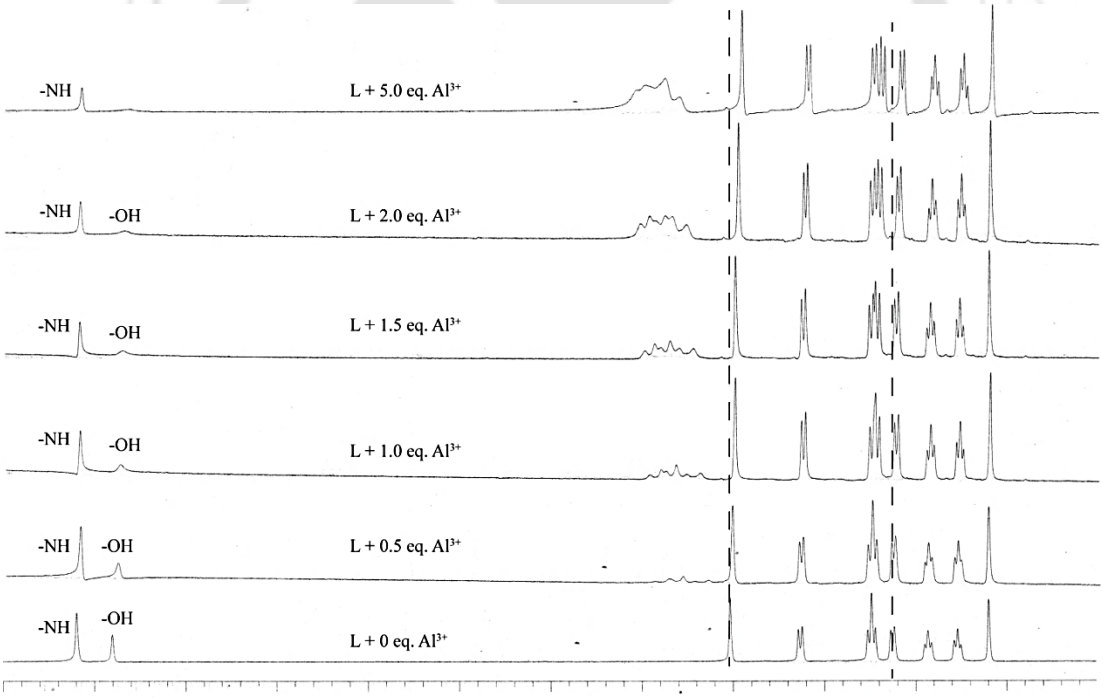

Figure A5.4. ^{1}H-NMR titration spectras of $\mathbf{L_3}$ with Al^{3+} in DMSO-d_6.

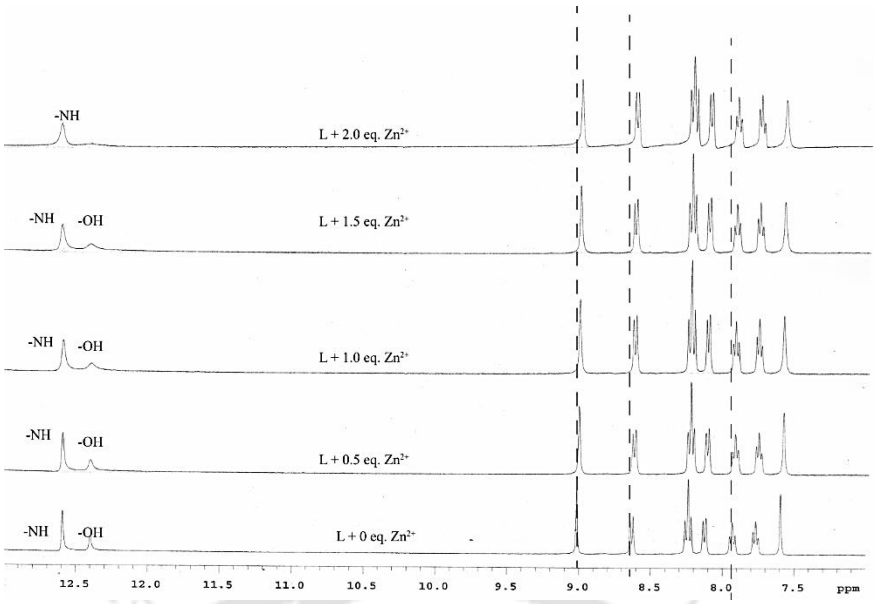

Figure A5.5. ^{1}H-NMR titration spectras of $\mathbf{L_3}$ with Zn^{2+} in DMSO-d_6.

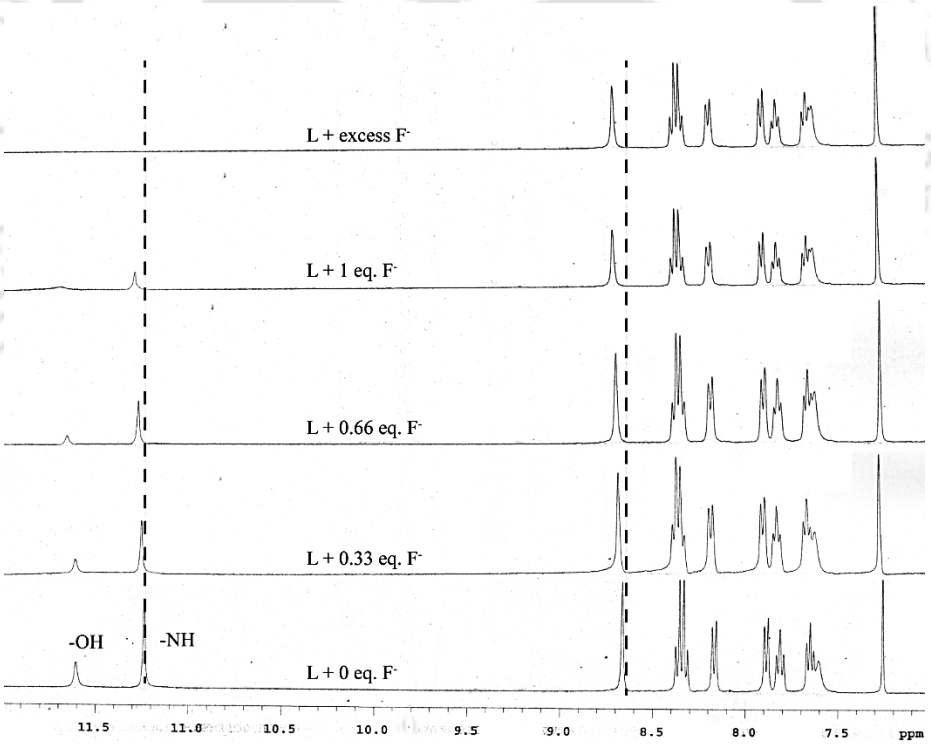

Figure A5.6. ^{1}H-NMR titration spectras of $\mathbf{L_3}$ with F^{-} in $CDCl_3$.

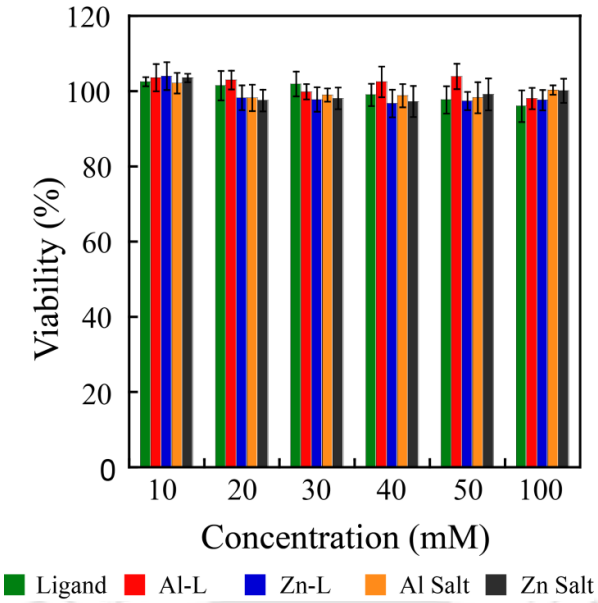

Figure A5.7. MTT assay to determine the cytotoxic effects of compounds $\mathbf{L_3}$, $\mathbf{L_3}$–Al and $\mathbf{L_3}$–Zn complex on HeLa cells.

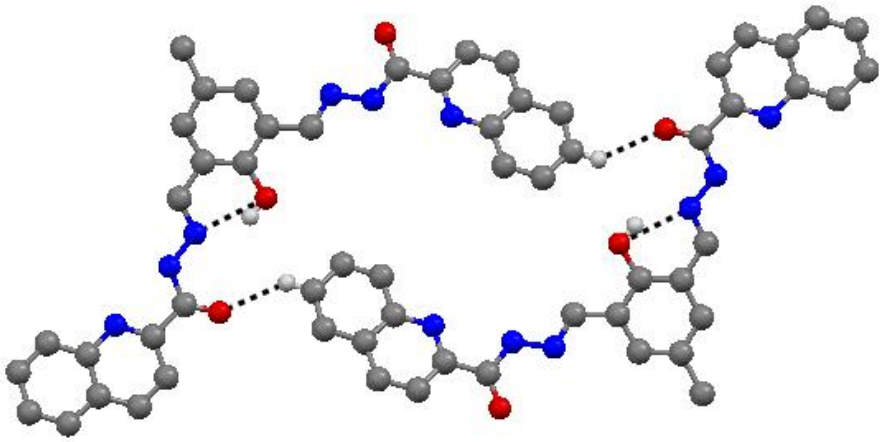

Figure A5.8. Crystal structure of $\mathbf{L_3}$ and various interactions presents in it.

Chapter 6

A Near-Infrared emissive Al^{3+} sensing platform for specific detection in solution, cells and probing DNase activity

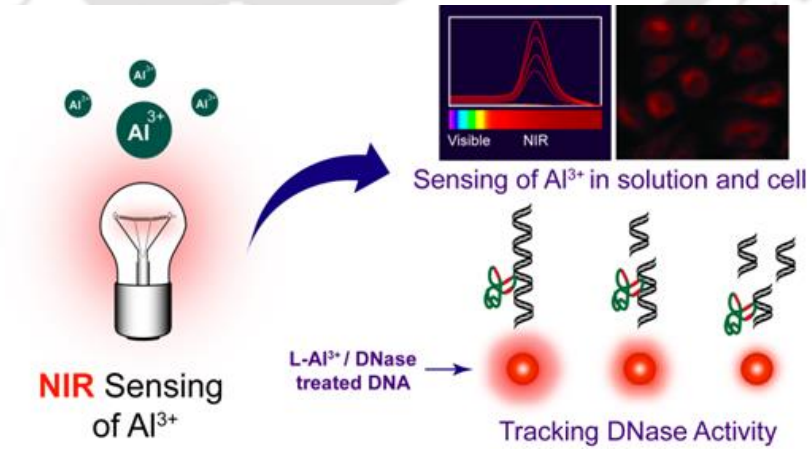

Chapter 6

6.1. Background and Focus of the Chapter

Aluminium has the distinction of being the third most abundant metal on earth's crust and its overriding influence on environment and human health is a cause of serious concern. Aluminium is a neurotoxic agent, which is potentially involved in perturbations of the central nervous system and grave neurodegenerative ailments such as Alzheimer's.[6.1-6.3] Apart from its potential role in neuro-disorders, aluminium toxicity is considered to induce a number of other healthcare concerns such as gastrointestinal problems, intervention with calcium metabolism, impaired liver and kidney function and others. [6.4-6.5] Given the germane role of aluminium in human health, there is considerable motivation amongst analytical chemists working in the regime of biomedical diagnostics to generate potent sensors that would enable selective detection of Al^{3+} in solution as well as in biological samples.

General methods for the detection of aluminum are graphite furnace atomic absorption spectroscopy and inductively coupled plasma atomic emission spectroscopy. However, these techniques are generally arduous and expensive. With regard to detection of biologically relevant ions, it has been demonstrated that fluorescence-based and electrochemical sensors are suitable platforms to achieve high selectivity and sensitivity.[6.6-6.16] Amongst the biologically relevant cations, sensing of Al^{3+} is especially challenging owing to the lack of spectroscopic signatures and poor coordination potential of the metal.[6.17] Hence, in comparison with transition metals, only a limited number of fluorescent chemosensors have been reported for Al^{3+}.[6.18-6.31] Furthermore, these probes display absorption and emission in the ultraviolet-visible (UV/Vis) light range, which can be a major bottleneck in biomedical applications since the high absorption and auto-fluorescence of biomolecules in this region can significantly interfere with signal acquisition. To circumvent this impediment, it is envisaged that Al^{3+}-selective fluorescent probes with absorption and emission in the near infrared (NIR) region (650–900 nm) are highly desirable due to the reduced propensity of photo-damage to biological samples, increased sample penetration and minimum background auto-fluorescence, which would significantly abet bioimaging studies. [6.32-6.40] As discussed earlier, we were unable to reach the near-IR region with the previous ligands, so in this chapter we choose a tricarbocyanine core which have its absorption and emission at the NIR region. Based on this premise, herein we report a novel tricarbocyanine-based NIR fluorescent probe for Al^{3+}. The receptor can selectively detect Al^{3+} among other trivalent and biologically relevant cations through a remarkable fluorescence emission signal captured in the

NIR region. The potential of the developed sensor is validated by sensing Al^{3+} in imaging studies using a cell culture model and probing of DNase activity in solution.

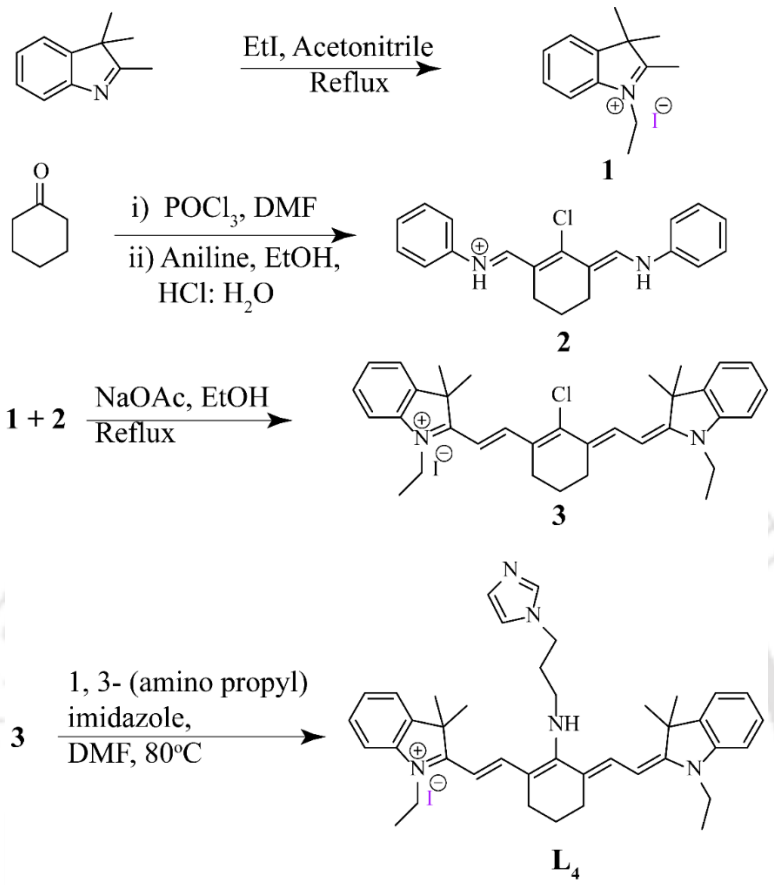

Scheme 6.1. Synthetic route to $\mathbf{L_4}$.

6.2. Absorption spectroscopic studies of L_4 in presence of metal ions

The sensing behavior of $\mathbf{L_4}$ was explored in a mixed solvent system of 5.0 mM HEPES buffer: methanol (3:2), pH 7.2. UV-visible absorbance spectroscopy of $\mathbf{L_4}$ indicated a characteristic absorption peak at 410 nm (Fig. 6.1a). When the receptor was interacted with a set of metal ions (Na^+, K^+, Ca^{2+}, Mg^{2+}, Al^{3+}, Cd^{2+}, Co^{2+}, Cr^{3+}, Fe^{3+}, Hg^{2+}, Mn^{2+}, Ni^{2+}, Pb^{2+}, Zn^{2+} and Ag^+, Ga^{3+} and In^{3+}), virtually no change in the absorption peak could be observed except for Al^{3+} and Fe^{3+} (Fig. 6.1a). The high selectivity of $\mathbf{L_4}$ for Al^{3+} could be readily captured in the striking change in the absorption spectra. Interaction of $\mathbf{L_4}$ with Al^{3+} resulted in the emergence of three new peaks at 343 nm, 539 nm and at 710 nm, while the signature absorption peak of the receptor at 410 nm decreased (Fig. 6.1a). The development of the three new peaks in the absorption spectra may be ascribed to the switching-on of the internal charge transfer (ICT) process. A similar response was also observed with Fe^{3+}, albeit of a lesser magnitude. Titration of $\mathbf{L_4}$ with incremental addition of Al^{3+} lead to the steady emergence of the three new absorption peaks (at 343 nm, 539 nm and at

710 nm) and a gradual diminution of the peak at 410 nm (Fig. 6.1b). Manifestation of two isosbestic points at 378 nm and 448 nm evidently indicated the conversion of free receptor into the metal complex (Fig. 6.1b). From the titration experiments, it was also noted that the change in the absorption spectra was marginal after addition of one equivalent metal ion, which may perhaps be attributed to a 1:1 stoichiometry of interaction between **L₄** and Al^{3+}. It may also be mentioned here that a visual change in the color of a solution of **L₄** from colorless to violet was observed during the titration experiment (Fig. 6.1b, inset), which rendered naked eye detection of Al^{3+} in solution.

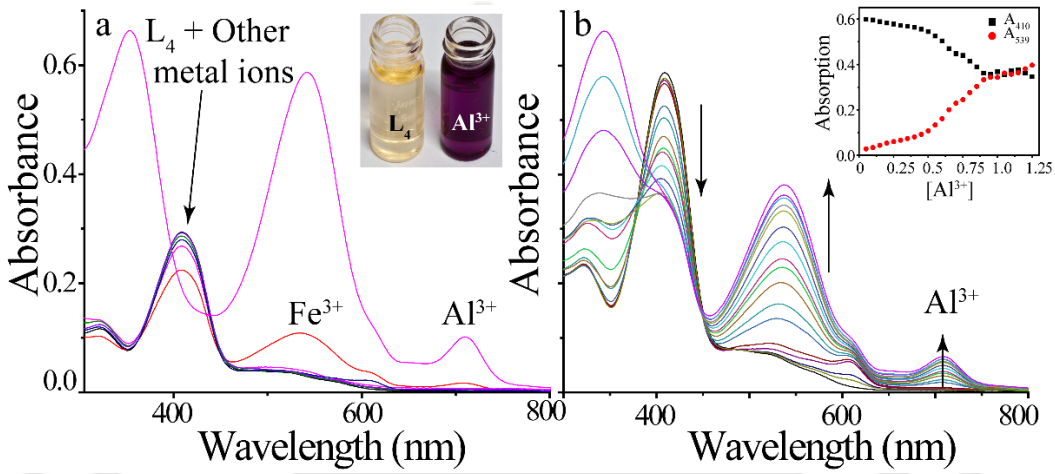

Figure 6.1. Changes in absorption spectra of **L₄** (in mixed solvent medium methanol: HEPES buffer (2:3) medium (5 mM, pH 7.4) containing 0.33% of DMSO) (a) upon the addition of different metal ions and (b) upon gradual addition of Al^{3+}. Inset (b): Visual color change on the addition of Al^{3+} to **L₄**. Inset (b) Changes in absorbance of **L₄** at the wavelengths 410 nm and 539 nm vs [Al^{3+}] plot.

6.3. Fluorescence spectroscopic studies of L_4 in presence of metal ions

Encouraged by the results obtained in UV-visible absorption spectroscopy, our next endeavour was to pursue fluorescence-based sensing of Al^{3+}. Upon excitation at 640 nm, the receptor **L₄** did not exhibit any fluorescence (Fig. 6.2a). However, when the receptor was treated separately with 10 equivalents of various metal ions (Na^+, K^+, Ca^{2+}, Mg^{2+}, Al^{3+}, Cd^{2+}, Co^{2+}, Cr^{3+}, Fe^{3+}, Hg^{2+}, Mn^{2+}, Ni^{2+}, Pb^{2+}, Zn^{2+} Ag^+, Ga^{3+} and In^{3+}), only Al^{3+} triggered a noteworthy turn-on response with an emission peak distinctly residing in the NIR region of around 730 nm (Fig. 6.2a). Among the other tested metal ions, Ga^{3+} was able to mark slight enhancement in the fluorescence, but the change in the fluorescence spectra of **L₄** by Ga^{3+} was very minute compared to that of the Al^{3+}. It was also noted that the fluorescence emission spectra of the receptor **L₄** remained unaffected in the presence of Fe^{3+} (Fig. 6.2a), although a marginal change in the absorption spectra of **L₄** could be observed upon interaction with Fe^{3+} (Fig. 6.1a). This result highlighted the high selectivity of **L₄** towards Al^{3+} over other metal ions including trivalent cations (Fe^{3+}, Cr^{3+}, Ga^{3+} and In^{3+}). Titration of **L₄** with the gradual addition of Al^{3+} resulted in a linear enhancement in the emission

intensity of **L_4** upto one equivalent of Al^{3+} (Fig. 6.2b). Upon further addition of Al^{3+}, the enhancement was negligible.

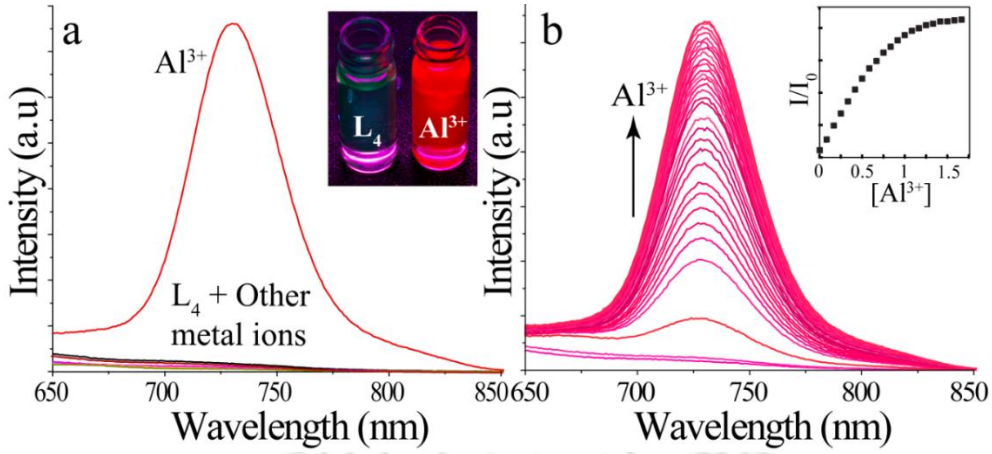

Figure 6.2. Changes in emission spectra of **L_4 (**in mixed solvent medium methanol: HEPES buffer (2:3) medium (5 mM, pH 7.4) containing 0.33% of DMSO) upon the addition of (a) different metal ions and (B) upon gradual addition of Al^{3+}. Inset (A): Intensity at 730 nm vs. [Al^{3+}] plot. Inset (b): Visual color change on the addition of Al^{3+} to **L_4** under UV lamp.

In order to ascertain the sensing potential of **L_4**, it was imperative to determine the selectivity of the probe in a complex media having competing analytes. To this end, the probe, **L_4** was treated with five equivalent of Al^{3+} in the presence of five equivalents of other metal ions. Interestingly, the receptor **L_4** could selectively detect Al^{3+} without any interference from other metal ions even in a complex mixture (Fig. 6.3).

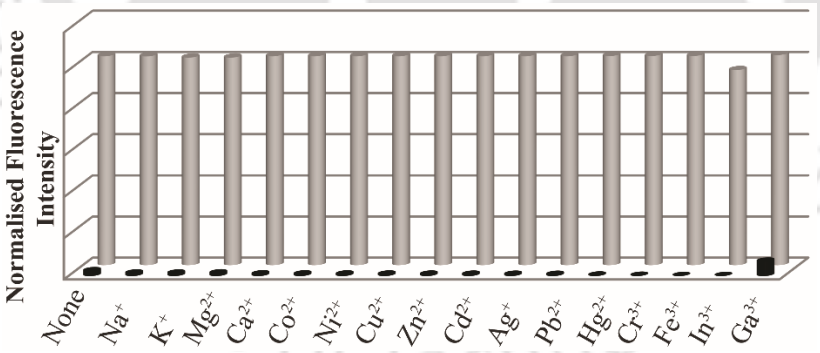

Figure. 6.3. Normalized fluorescence responses of **L_4** (10 μM) to various cations in mixed solvent medium methanol: HEPES buffer (2:3) medium (5 mM, pH 7.4) containing 0.33% of DMSO. The gray bars represent the emission intensities of **L_4** in the presence of cations of interest (5 eqv.). The black bars represent the change of the emission that occurs upon the subsequent addition of Al^{3+} to the above solution.

The 1:1 binding stoichiometry between **L_4** and Al^{3+} was also established from a Job's plot derived from the fluorescence titration experiment (Fig. A6.1a.). Interestingly a change in the fluorescence emission of **L_4** from colorless to bright red was conspicuous during the titration experiment with Al^{3+}. The detection limit of the probe for Al^{3+} was determined as 1.95×10^{-8} M,

which is lower than the reported ones[6.18, 6.20, 6.21] and the association constant was calculated to be 8.4 x 10^5 M^{-1} using Benesi-Hildebrand equation.[6.41]

6.4. ESI-MS Experiment

The 1:1 binding mode between **L_4** and Al^{3+} was also corroborated by ESI-MS experiment. A peak at 357.1794 indicated the mass of the ensemble $[\mathbf{L_4}+Al+2Cl+H_2O]^{2+}$ (Fig. A6.5). The quantum yield of the **L_4**-Al complex was found to be 0.54 whereas the quantum yield of the free probe was found to be 0.006.

A comparative appraisal of the sensing properties of the reported probe indicated that Al^{3+} detection could be achieved in the NIR region and was thus better as compared to many previously described fluorophores, wherein sensing was mostly accomplished in the visible region.[6.18-6.21, 6.26-6.31] Further, the detection limit (1.95x10^{-8} M) reported in this study is at par with other reported fluorophores used for Al^{3+} sensing. [6.18-6.31]

6.5. pH dependent study

Fluorescence-based sensing of Al^{3+} by **L_4** was also pursued at various pH. At lower pH (2.0-4.5), the receptor exhibits higher fluorescence intensity and a marginal enhancement in the emission intensity in the presence of Al^{3+} (Fig. A6.1b). This is due to the protonation of the imidazole ring in lower pH, which stops the PET process present in the free receptor resulting in the turn-ON fluorescence intensity of the receptor. As the imidazole ring was already protonated in this pH range, the binding to Al^{3+} will not be possible, hence only marginal enhancement in the fluorescence intensity of **L_4** is observed in presence of Al^{3+} in this pH range. However, in the pH range of 5.0-12.0, the receptor have stable fluorescence intensity and a significant increase in the fluorescence emission intensity of **L_4** upon interaction with Al^{3+} was evident, which suggested that the developed sensor was robust and rendered selective sensing of Al^{3+} over a wide range of pH, including biologically relevant pH.

6.6. Plausible mechanism of Al^{3+} sensing

The plausible mechanism of fluorescence-based Al^{3+} is as follows: The low fluorescence of the free receptor **L_4** is attributed to the photo-induced electron transfer (PET) process occurring from the imidazole N-atoms to the fluorophoric unit, which results in the quenching of fluorescence of the receptor. In presence of Al^{3+}, the imidazole N-atoms bind with the metal ion resulting in engagement of the free lone pair on the N-atom of the imidazole ring. Consequently, the PET process is hindered leading to enhancement in the fluorescence intensity in the NIR region

(Scheme 2). On the other hand, the visual color change may be attributed to the switching-on of the ICT process.

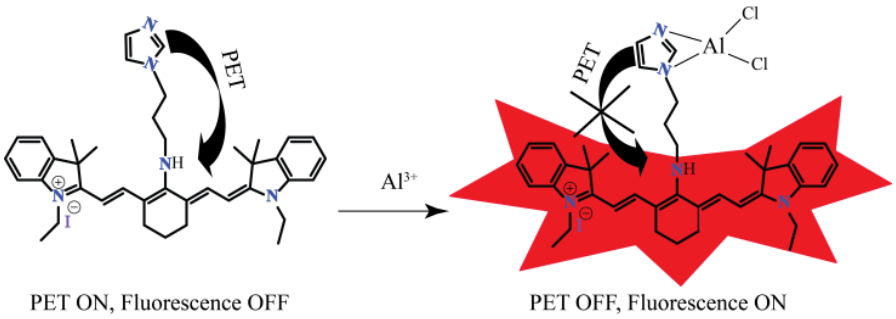

Scheme 6.2. Plausible mechanism of NIR-based sensing of Al^{3+}.

6.7. Cellular sensing of Al^{3+}

Given the role of aluminium in imparting neurotoxicity, there is a significant interest in developing sensors that facilitate intracellular detection of the metal. In this context, it was envisaged that the NIR-emitting attribute of probe **L_4** would be pertinent in pursing fluorescence-based Al^{3+} sensing in live cells through imaging studies, with minimum interference from autofluorescence of biomolecules. However, in this endeavor, it was imperative to ascertain the cytotoxic potential of the probe and the Al^{3+} complex. Interestingly, an MTT assay indicated that the viability of cultured HeLa cells (human cervical carcinoma cells) were not affected in presence of the probe **L_4** and **L_4**-Al^{3+} complex at varying concentrations (Fig. A6.2a), which suggested the non-toxic nature of the sensor as well as the metal complex. This finding motivated us to determine the potential of the probe **L_4** in detecting intracellular Al^{3+} by fluorescence-based

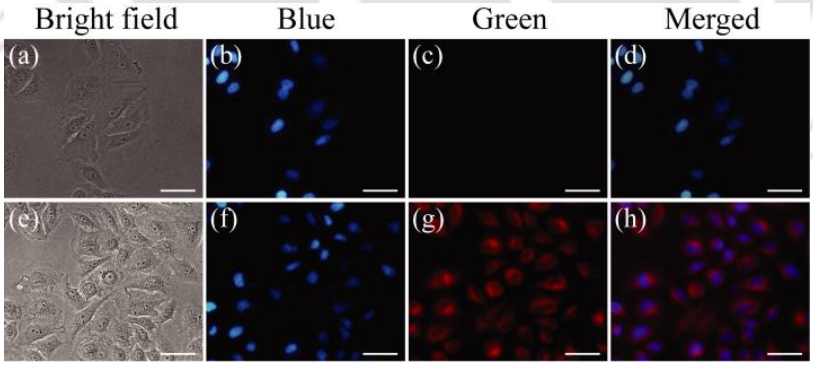

Figure 6.4. Fluorescence microscope images of (a-d) HeLa cells treated with 5.0 μM of **L_4** and (e-h) HeLa cells pre-treated with 5.0 μM of **L_4** followed by addition of 10 μM Al^{3+} solution. Scale bar for the images is 50 μ. Blue light excitation reveals nuclear staining in HeLa cells by DAPI and green light excitation demonstrates NIR-sensing of **L_4**-Al^{3+} complex in HeLa cells.

cell imaging studies. To this end, the essential observation was that HeLa cells incubated with only the sensor **L_4** failed to exhibit any fluorescence apart from the prominent nucleus-associated fluorescence manifested due to DAPI staining (Fig. 6.4, panel b-d). Interestingly, when HeLa cells pre-treated with **L_4** were incubated with Al^{3+}, a bright red fluorescence emission was

conspicuous in the cells (Fig. 6.4, panel g). Further, upon merging of the DAPI-stained and **L_4**-Al^{3+} stained images, it was evident that the red fluorescence emission originating from **L_4**-Al^{3+} complex was essentially restricted to the cytoplasm of the cells (Fig. 6.4, panel g-h). It is significant to mention that the characteristic morphology of HeLa cells was conserved during the imaging studies, which reiterated the non-toxic nature of the probe **L_4**.

6.8. Interaction with DNA and tracking DNase activity by L_4-Al^{3+} complex

The selective sensing Al^{3+} by **L_4** was encouraging and we envisioned that the NIR-emissive **L_4**-Al^{3+} ensemble could perhaps be explored as a handle to pursue interaction studies with DNA in solution on the basis of the strong interaction of Al^{3+} with phosphate groups in DNA. Further, it was envisaged that the solution-based interaction of the ensemble with DNA could be subsequently explored in developing important applications in biomedical diagnostics such as assessment of nuclease activity and DNA footprinting. Nucleases are considered to be vital in various biological processes involving DNA replication, recombination, DNA repair, genotyping, and mapping analysis. Literature reports also highlight the merit of developing sensing platforms for nuclease assay.[6.42-6.44] In order to pursue this goal, **L_4**-Al^{3+} complex was interacted in solution

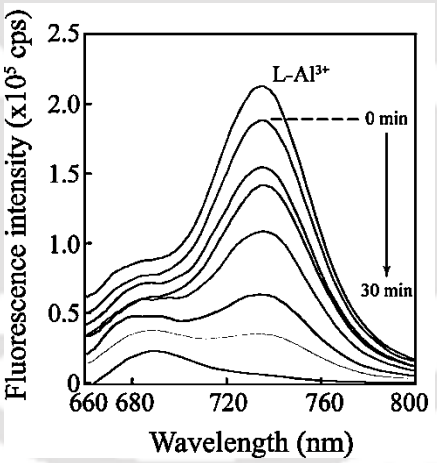

Figure 6.5. Change in emission spectra of **L_4**-Al^{3+} (2.5 μM) complex upon interaction with DNase I-treated CT-DNA fragments generated at various time periods (0-30 minutes). 500 ng of CT-DNA was interacted with 2.0 units of DNase I at 37°C for various time periods.

with calf thymus DNA (CT-DNA). Interaction with CT-DNA resulted in nominal reduction in the fluorescence intensity of **L_4**-Al^{3+} complex (Fig. 6.5). Interestingly, the utility of **L_4**-Al^{3+} complex in monitoring activity of DNase I enzyme on CT-DNA in solution could be demonstrated as there was a systematic reduction in the fluorescence emission intensity of the complex with time (Fig. 6.5). It may be mentioned here that interaction with other biologically relevant phosphate-based

analytes such as ATP, ADP and AMP yielded negligible changes in the fluorescence emission intensity of the ensemble (Fig. A6.2b).

6.9. Conclusion

In the present study, a judiciously designed fluorophoric probe based on a tricarbocyanine dye was developed that displayed a prominent and selective turn-on response in the NIR region upon interaction with Al^{3+}. To the best of our knowledge this study is the first report on an NIR emitting sensor specific for Al^{3+} alone. The developed probe could also be readily deployed in fluorescence-based imaging studies for non-invasive and spatial sensing of Al^{3+} in live HeLa cells. Given its non-toxic nature and NIR-emissive trait, it is envisaged that the sensor can perhaps be explored in future as a non-destructive imaging toolkit in *in vivo* cellular studies that investigate the toxic basis of Al^{3+}. The $\mathbf{L_4}$-Al^{3+} ensemble also rendered interaction with CT-DNA in solution and could also be explored for label-free and time-dependent tracking of nuclease activity. The encouraging results obtained in the present study strongly indicate the future possibility of using this NIR-emissive sensing tool for *in vivo* diagnostic as well DNA-based bioanalytical applications.

References

6.1. A. Salifoglou, *Coord. Chem. Rev.*, 2002, **228**, 297.

6.2. G. D. Fasman, *Coord. Chem. Rev.*, 1996, **149,** 125.

6.3. D. Krewski, R. A. Yokel, E. Nieboer, D. Borchelt, J. Cohen, J. Harry, S. Kacew, J. Lindsay, A. M. Mahfouz, V. J. Rondeau, *Toxicol. Environ. Health, Part B: Crit. Rev.*, 2007, **10**, Suppl 1:1-269.

6.4. G. Berthon, *Coord. Chem. Rev.*, 2002, **228**, 319.

6.5. A. M. Pierides, W. G. Edwards Jr, U. X. Cullum Jr, J. T. McCall, H. A. Ellis, *Kidney Int.*, 1980, **18**, 115.

6.6. G. Aragay, J. Pons, A. Merkoc, *Chem. Rev.*, 2011, **111**, 3433.

6.7. M. K. Bojdi, M. H. Mashhadizadeh, M. Behbahani, A. Farahani, S. S. H. Davarani, A. Bagheri, *Electrochimica Acta*, 2014, **136**, 59.

6.8. M. K. Bojdi, M. Behbahani, A. Sahragard, B. G. Amin, A. Fakhari, A. Bagheri, *Electrochimica Acta*, 2014, **149**, 108.

6.9. K. M. Dean, Y. Qin, A. E. Palmer, *Biochim. Biophys. Acta.*, 2012, **1823**, 1406.

6.10. B. K. Datta, C. Kar, A. Basu, G. Das, *Tetrahedron Lett.*, 2013, **54**, 771.

6.11. C. Kar, A. Basu, G. Das, *Tetrahedron Lett.*, 2012, **53**, 4754.

6.12. C. Kar, M. D. Adhikari, A. Ramesh, G. Das, *Inorg. Chem.*, 2013, **52**, 743.

6.13. B. K. Datta, S. Mukherjee, C. Kar, A. Ramesh, G. Das, *Anal. Chem.*, 2013, **85**, 8369.

6.14. C. Kar, M. D. Adhikari, B. K. Datta, A. Ramesh, G. Das, *Sens. Actuators, B.*, 2013, **188**, 1132.

6.15. S. Samanta, S. Goswami, A. Ramesh, G. Das, *Sensor. Actuators, B.*, 2013, **194**, 120.

6.16. B. K. Datta, D. Thiyagarajan, S. Samanta, A. Ramesh, G. Das, *Org. Biomol. Chem.*, 2014, **12**, 4975.

6.17. K. Soroka, R. S. Vithanage, D. A. Phillips, B. Walker, P. K. Dasgupta, *Anal. Chem.*, 1987, **59**, 629.

6.18. S. Kim, J. Y. Noh, K. Y. Kim, J. H. Kim, H. K. Kang, S. Nam, S. H. Kim, S. Park, C. Kim, J. Kim, *Inorg. Chem.*, 2012, **51**, 3597.

6.19. X. Sun, Y. W. Wang, Y. Peng, *Org. Lett.*, 2012, **14**, 3420.

6.20. S. Samanta, S. Goswami, M. N. Hoque, A. Ramesh, G. Das, *Chem. Commun.*, 2014, **50**, 11833.

6.21. S. Goswami, A. Manna, S. Paul, K. Aich, A. K. Das, S. Chakraborty, *Dalton Trans.*, 2013, **42**, 8078.

6.22. B. Sen, S. Pal, S. Lohar, M. Mukherjee, S. K. Mandal, A. R. Khuda-Bukhsh, P. Chattopadhyay, *RSC Adv.*, 2014, **4**, 21471.

6.23. A. Sahana, A. Banerjee, S. Lohar, B. Sarkar, S. K. Mukhopadhyay, D. Das, *Inorg. Chem.* 2013, **52**, 3627.

6.24. J. Y. Jung, S. J. Han, J. Chun, C. Lee, J. Yoon, *Dyes Pigm.*, 2012, **94**, 423.

6.25. Hau, F. K.-W.; He, X.; Lam, W. H.; Yam, V. W.-W. *Chem. Commun.*, 2011, **47**, 8778.

6.26. Y. Lu, S. Huang, Y. Liu, S. He, L. Zhao, X. Zeng, *Org. Lett.*, 2011, **13**,5274.

6.27. D. Maity, T. Govindaraju, *Inorg. Chem.*, 2010, **49**, 7229.

6.28. K. K. Upadhyay, A. Kumar, *Org. Biomol. Chem.*, 2010, **8**, 4892.

6.29. L. Wang, W. Qin, X. Tang, W. Dou, W. Liu, Q. Teng, X. Yao, *Org. Biomol. Chem.*, 2010, **8**, 3751.

6.30. A. Sahana, A. Banerjee, S. Das, S. Lohar, D. Karak, B. Sarkar, S. K. Mukhopadhyay, A. K. Mukherjee, D. Das, *Org. Biomol. Chem.*, 2011, **9**, 5523.

6.31. S. A. Lee, G. R. You, Y. W. Choi, H. Y. Jo, A. R. Kim, I. Noh, S.-J. Kim, Y. Kim, C. Kim, *Dalton Trans.* 2014, **43**, 6650.

6.32. D. D. Nolting, J. C. Gore, W. Pham, *Curr. Org. Synth.*, 2011, **8**, 521.

6.33. R. Weissleder, *Nat. Biotechnol.*, 2001, **19**, 316.

6.34. J. O. Escobedo, O. Rusin, S. Lim, R. M. Strongin, *Curr. Opin. Chem. Biol.*, 2010, **14**, 64.

6.35. S. A. Hilderbrand, R. Weissleder, *Curr. Opin. Chem. Biol.*, 2010, **14**, 71.

6.36. G. Qian, Z. Y. Wang, *Chem.–Asian J.*, 2010, **5**, 1006.

6.37. C. Tung, Y. Lin, W. Moon, R. Weissleder, *ChemBioChem.*, 2002, **3**, 784.

6.38. R. Weissleder, V. Ntziachristos, *Nat. Med.*, 2003, **9**, 123.

6.39. L. Yuan, W. Lin, K. Zheng, L. He, W. Huang, *Chem. Soc. Rev.*, 2013, **42**, 622.

6.40. D. C. Williams, S. A. Soper, *Anal. Chem.*, 1995, **67**, 3427.

6.41. H. A. Benesi, J. H. Hildebrand, *J. Am. Chem. Soc.*, 1949, **71**,2703.

6.42. G. L. Liu, Y. Yin, S. Kunchakarra, B. Mukherjee, D. Gerion, S. D. Jett, D. G. Bear, J. W. Gray, A. P. Alivisatos, L. P. Lee, F. F. Chen, *Nature nanotechnology.*, 2006, **1**, 47.

6.43. F. Pu, D. Hu, J. Ren, S. Wang, X. Qu, *Langmuir.*, 2010, **26**, 4540.

6.44. A. M. Rush, M. P. Thompson, E. T. Tatro, N. C. Gianneschi, *ACS Nano.*, 2013, 7, 1379.

Appendix

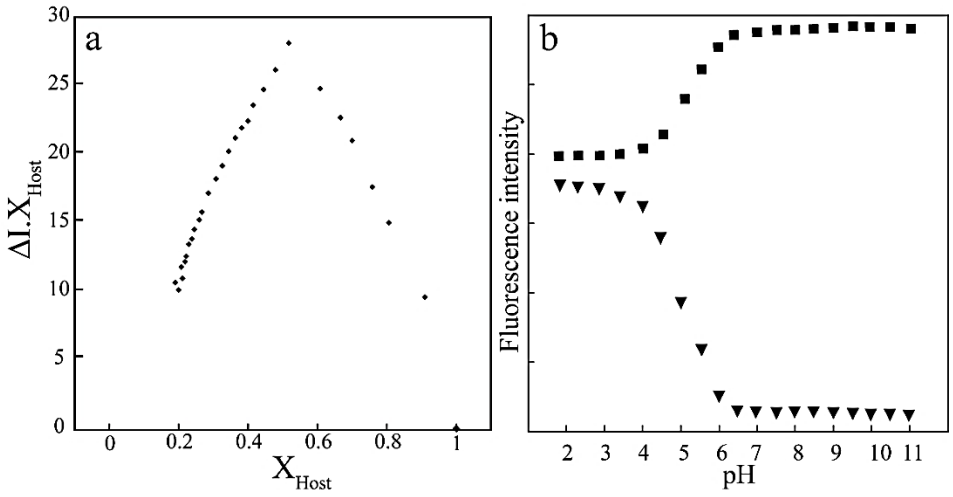

Figure A6.1. (a) Jobs plot between $\mathbf{L_4}$ and Al^{3+}, (b) Effect of pH on the sensing behaviour of $\mathbf{L_4}$. The black triangles are the fluorescence intensities of $\mathbf{L_4}$ at different pH whereas the black square blocks are the fluorescence intensities of $\mathbf{L_4}$ upon the addition of Al^{3+}.

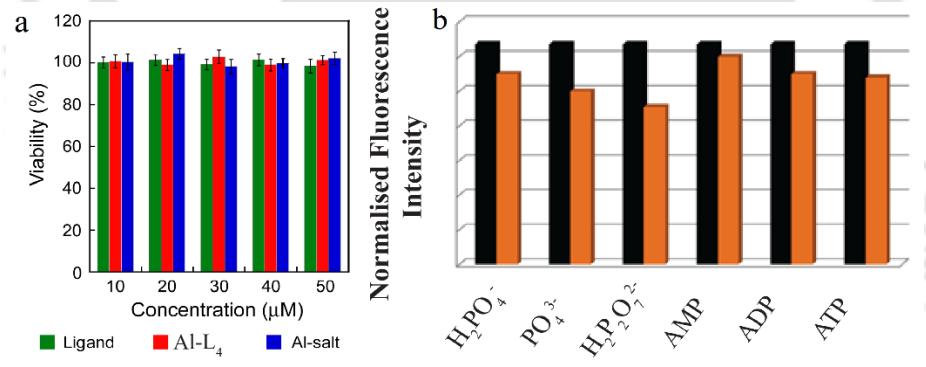

Figure A6.2. (a) MTT assay to determine the cytotoxic effect of compound $\mathbf{L_4}$ and $\mathbf{L_4}$–Al complex on HeLa cells. (b) Normalized fluorescence responses of $\mathbf{L_4}$-$\mathbf{Al^{3+}}$ complex (10 μM) to various phosphate anions (5 equivalents) in mixed solvent medium ethanol: HEPES buffer (2:3) medium (5 mM, pH 7.4) containing 0.33% of DMSO. The black bars represent the emission intensities of $\mathbf{L_4}$-$\mathbf{Al^{3+}}$ in mixed solvent. The orange bars represent the changes in the emission intensities of $\mathbf{L_4}$-$\mathbf{Al^{3+}}$ complex upon the subsequent addition of different phosphates to the above solution.

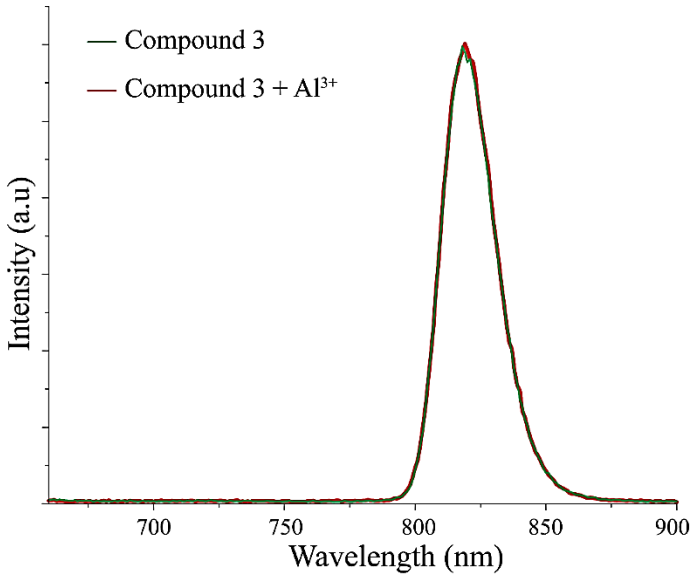

Figure A6.4. Emission spectra of compound **3** before and after interaction with Al^{3+}.

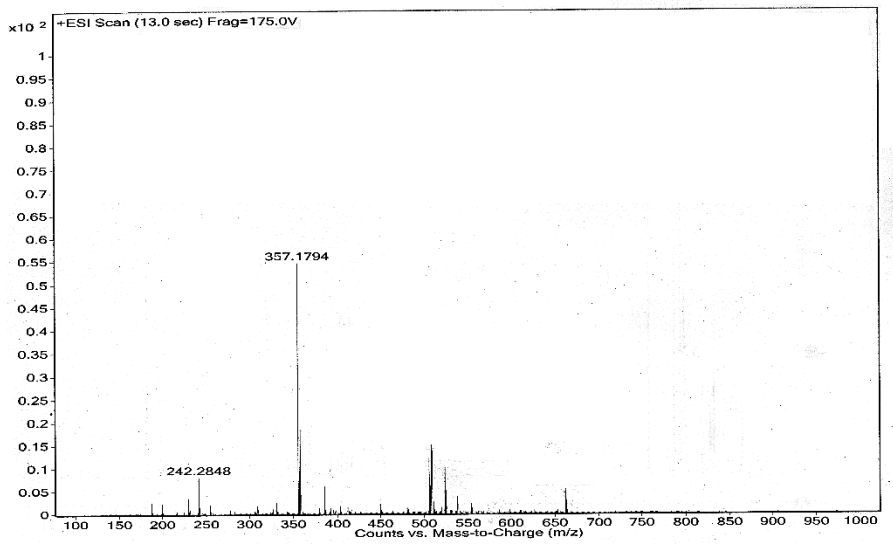

Figure A6.5. ESI-MS spectra of **L_4-Al** complex.

Conclusion and Future Perspective

In conclusion, the overall thesis elucidates some important results in the field of chemosensor for biologically and environmentally important analytes in solution and in biological medium. We have designed, synthesized and investigated some unique receptor systems (**L_1-L_4**) ranging from simple to complex structures and also spectral responses ranging from UV-region to near-IR region which can detect various analytes in aqueous solution and inside living cells.

Receptor **L_1** can selectively sense Zn^{2+} in physiological condition with a turn-on (green fluorescence) response. The *in situ* formed complex, **L_1**.2Zn can selectively and specifically sense PPi among all the other biologically important anions. The unique selectivity of the PPi by **L_1**-Zn ensemble could be used as an analytical tool to probe PPi generation in a prototype PCR setup and track DNA amplification with higher sensitivity as compared to conventional agarose gel electrophoresis. Interestingly, the principle of PPi estimation in PCR rendered rapid estimation of bacterial cell numbers of *E.coli* MTCC 43. Receptor **L_2** can also specifically sense Zn^{2+} in complete physiological medium with a turn-on response (yellow fluorescence). The receptor was non-toxic and sense Zn^{2+} in HeLa cells. **L_3** can sense Al^{3+}, Zn^{2+} and F^- ions (green, yellow and orange fluorescence respectively) with three distinctive emission spectra. The ligand can work in a wide pH range including the physiological pH and was also applied for sensing intracellular Al^{3+} and Zn^{2+} in live HeLa cells. In chapter 6, we have discussed about **L_4** which can selectively and specifically recognize Al^{3+} among all other cations with turn-on responses (red fluorescence). Both the absorption (710 nm) and emission (730 nm) responses were in the NIR region. Interestingly, upon interaction with DNA in solution, the **L_4**-Al^{3+} ensemble rendered tracking of DNase activity in solution through a systematic reduction in the fluorescence emission intensity.

Fluorescence and colorimetric chemo-sensorial chemistry has grown considerably since the pioneering work of Sousa with the naphthalene compounds. After the Nobel Prize in supramolecular chemistry in 1987 to Charles J. Pedersen, Jean-Marie Lehn and Donald J. Cram, the design and application of fluorescent molecular devices increased exponentially. The possibility of a precise molecular recognition between a chemosensor and their guests has many applications in analytical chemistry, supramolecular science, biochemistry, physical chemistry, medicinal chemistry, toxicology, forensic sciences and applicable disciplines even to the modern nanosciences. However, for these applications to reach their prospective basic work is in tuning the receptor molecule in such a way that it is easily soluble in aqueous media and the spectral response is vivid and at longer end of the spectra. Although the results included in this thesis are

extremely useful from a fundamental viewpoint, there is other challenging aspects in supramolecular chemistry that need to be developed, basically from an applicative approach. Research in these areas with a focus on technological and biomedical applications, based upon the remarkable cation, anion and neutral molecular sensing appear to be forthcoming.

Barun Kumar Datta

Academic Summary

2011-present: Ph.D. student at Indian Institute of Technology Guwahati, India.
(Thesis has been submitted)
Thesis title: "**Design and synthesis of Fluorogenic and Chromogenic probes for the Detection of Ionic Guests in Solution and Biological medium**".

2008-2010: Masters in Chemistry (Specialization: Inorganic Chemistry)
Visva-Bharati University, West Bengal, India.

2005-2008: Graduation (Chemistry), Burdwan Raj College, Burdwan, West Bengal, India.

2005: 12th (Science), WBCHSE, 81.8%.

2003: 10th, WBBSE, 78.375%.

Honours and awards

- Qualified CSIR-National Eligibility Test (NET) for Junior Research Fellowship, 2010.
- Qualified GATE, 2011.

Research Interests

- Design and synthesis of fluorescent probes
- Fluorescence sensing of biologically important ions and molecules
- Applications of new sensor technologies in biotechnology and environmental analysis

Expertise

- Spectroscopic techniques (UV, Fluorescence, FT-IR, Atomic absorption), Optical and fluorescence microscopy, NMR spectroscopy, mass spectrometry, DLS, single crystal x-ray diffraction

Publications

1. Selective Fluorescence Sensor for Al^{3+} and Pb^{2+} in physiological condition by a benzene based tripodal receptor, **B. K. Datta**, C. Kar, A. Basu and G. Das, *Tetrahedron Lett.,* 2013, **54**, 771.

2. Zn^{2+} and Pyrophosphate Sensing: Selective Detection in Physiological Conditions and Application in DNA-based Rapid Estimation of Bacterial Cell Numbers, **B. K. Datta,** S. Mukherjee, C. Kar, A. Ramesh and G. Das, *Anal. Chem.,* 2013, **85,** 8369.
3. A novel chemosensor with visible light excitability for sensing Zn(II) in physiological medium and in HeLa cells, **B. K. Datta**, D. Thiyagarajan, S. Samanta, A. Ramesh, G. Das, *Org. Biomol. Chem.*, 2014, **12**, 4975.
4. A novel C_{3v}-symmetric completely water soluble turn-on chemo sensor for Cd^{2+} and the resultant complex for iodide anion in aqueous medium, **B. K. Datta,** C. Kar and G. Das, *Sensor. Actuators, B. Chem*, 2014, **204**, 474.
5. A fluorescent naphthalene based benzene tripod for the selective recognition of fluoride in physiological condition, **B. K. Datta,** C. Kar and G. Das, *J. Chem. Sci.,* 2015, **127**, 337.
6. A Near-Infrared emissive Al^{3+} sensing platform for specific detection in solution, cells and probing DNase activity, **B. K. Datta**, D. Thiyagarajan, C. Kar, A. Ramesh and G. Das, *Anal. Chim. Acta,* 2015, **882**, 76.
7. A Sole Multi-Analyte receptor responds with three distinct fluorescence signals: Traffic signal like sensing of Al^{3+}, Zn^{2+} and F^-, **B. K. Datta,** D. Thiyagarajan, A. Ramesh and G. Das, *Dalton Trans.,* 2015, **44**, 13093.
8. Binding discrepancy of fluoride in quaternary ammonium and alkali salts by a tris(amide) receptor in solid and solution-states, S. Dey, **B. K. Datta**, G. Das, *CrystEngComm,* 2012, **14**, 3306.
9. A CHEF-based Biocompatible Turn ON Ratiometric Sensor for Sensitive and Selective Probing of Cu^{2+}, C. Kar, M. D. Adhikari, **B. K. Datta**, A. Ramesh and G. Das, *Sens. Actuators, B,* 2013, **188,** 1132.
10. A simple and efficient Fluorophoric probe for dual sensing of Fe^{3+} and F^-: Application to bioimaging in native cellular iron pool and live cell, C. Kar, S. Samanta, S. Mukherjee, **B. K. Datta**, A. Ramesh and G. Das, *New J. Chem.,* 2014, **38**, 2660.

Conference Attended

- "MTIC-XV" 2013, IIT Roorkee, Uttarakhand, India (Poster presented).
- "MTIC-XVI" 2015, Jadavpur University, West Bengal, India (Poster Presented).
- Delivered Young Scientist Presentation in Modern Trends in Inorganic Chemistry (MTIC-XVI) held on December 3-5, 2015, Jadavpur University, India.